The Unique Role of the Domain IV Voltage-Sensor in Sodium Channel Inactivation and Gating

by

Deborah L. Capes

A dissertation submitted in partial fulfillment

of the requirements for the degree of

Doctor of Philosophy

(Molecular and Cellular Pharmacology)

at the

UNIVERSITY OF WISCONSIN-MADISON

2012

Date of final oral examination: 06/15/12

The dissertation is approved by the following members of the Final Oral Committee:

Baron Chanda, Associate Professor, Neuroscience
Cynthia Czajkowski, Professor, Neuroscience
Robert Fettiplace, Professor, Neuroscience
Arnold Ruoho, Professor, Neuroscience
Hector Valdivia, Professor, Cellular and Regenerative Biology

ACKNOWLEDGEMENTS

I have to thank all of my lab mates (past and present) from the Chanda lab. For the last few years, you have been like a second family to me. I have really enjoyed all of the good natured teasing that goes on in our lab and it's always a pleasure to go out for a few drinks will all of you. I'll miss you all!

I would also like to thank those of our wonderful staff who have helped me during my time here. They worked hard to make sure that everything went smoothly and without a hitch. To Sue Krey, Rebecca Welch, Mary Walker, Diane Beuchner, Barbara Weitz, Lynn Squire, and Ravi Kochar: I am really grateful to have worked with you.

I would also like to thank my MCP and Physiology classmates. I had a lot of fun talking with you (science and otherwise) and I really have enjoyed going through the program alongside you all. Special thanks to the classmates in my year: Elaine Morlock, Andrew Peterson, and Joe Esquibel – it's been great!

A special thank you to all of my committee members: Cindy Czajkowski, Robert Fettiplace, Arnold Ruoho, and Héctor Valdivia. I have truly appreciated your mentoring throughout the years and I know that you have helped me to see many things in a new and interesting light. Thank you all so much!

Baron, thank you for taking a chance with me as your first graduate student. I have been honored to work with you during this time. You have great advice and you are genuinely excited about science. I really appreciate that. At the end of it all, I can definitely say that I made the right choice in choosing your lab. Thank you for making me a scientist!

Thanks to my fantastic family! Your love and support has meant so much to me throughout the years! Thank you to my parents for always being the cheering squad backing me up. Thanks also are due to Grandma, Peggy, and Lisa – thanks for being so supportive and thanks for all of the cards and letters. Thank you also to Sue, John, Heath, Steven, Jesse, Marcus, Daniel, and Carl. You are all so great!

A very special thank you goes to my sister Michelle. You were there for me every step of the way! You made me leave the lab bench to experience the life outside of grad school (and therefore kept me sane – and much better fed). You were always available for me to ask advice from and you're great to bounce science ideas off of. Thank you also for checking through my thesis. I love you Shell!

Abstract

The Unique Role of the Domain IV Voltage-Sensor in Sodium Channel Inactivation and Gating

Deborah L. Capes

Under the supervision of Dr. Baron Chanda

At the University of Wisconsin-Madison

The opening of the voltage-gated sodium (Nav) channel is responsible for the generation of the upstroke of the action potential. Following the depolarization of the membrane that occurs with an action potential, it is necessary for the Nav channel to inactivate so that the membrane is able to hyperpolarize and return to the resting potential. Defects in inactivation can lead to a plethora of diseases ranging from arrhythmogenic disorders in the heart to epilepsy in the brain. Therefore, it is crucial to obtain a better understanding of the processes underlying both fast and slow inactivation. This study characterizes the role of individual voltage-sensors in the processes of both fast and slow inactivation. This work identifies the voltage-sensor of domain IV as a potential source of the voltage-dependence of slow inactivation. Furthermore, this study identifies domain IV S4 as the crucial voltage-sensor involved in fast inactivation.

TABLE OF CONTENTS

CHAPTER 1

BACKGROUND AND SIGNIFICANCE

1.1 Cellular Communication and the Action Potential

1.1.1 Reflex Arcs (the Anatomy of a Knee-Jerk Reaction)

The body is composed of a complex array of tissues and organ systems. At any given time, these organ systems must work in concert, integrating signals and adapting appropriately to external stimuli. One of the most critical aspects in the functioning of a complex system is to have rapid and efficient communication between the disparate elements. In the case of the body, this communications system is multi-part, consisting of a complex melody of chemical notes including neurotransmitters and mechanisms by which cells can communicate via direct contact (as in juxtacrine signaling)(Anklesaria, Teixido et al. 1990), over short distances (paracrine signaling)(Papadopoulos, Kamtchouing et al. 1987), and over long distances (endocrine signaling).

Though chemicals play a crucial role in the intricate system to system communication, arguably the most important form of rapid signaling is electrical signaling in neurons and excitable tissue. For example, it has been shown that the reflex action of withdrawing the hand from a painful stimuli precedes the actual sensation of pain. Many elements are responsible for this rapid withdrawal reflex, firstly, receptors that detect noxious stimuli (believed to be the transient receptor potential, TRP, channel) depolarize the cell membrane of the sensory neuron (Greffrath, Schwarz et al. 2009). Next, once the membrane potential raises above threshold, voltage-gated sodium ion (Nav) channels open, allowing sodium ions to enter the cell and further depolarizing the membrane (Hodgkin and Huxley 1952). All along the neuron, the wave of depolarization

activates further sodium channels, propagating the action potential. At the synapse, the electrical signal is converted into a chemical signal via the release of neurotransmitters. The neurotransmitters bind to receptors on the postsynaptic neuron and cause local depolarization of the cell membrane. The signal moves from spinal neurons to motor neurons rapidly, bypassing the central nervous system, and finally proceeds to the neuromuscular junction, where the release of acetylcholine opens nicotinic acetylcholine receptors (nAChRs), and causes a localized depolarization of the muscle cell. This localized depolarization triggers an action potential wave in which the muscle Nav channels propagate the signal and it is this electrical message which causes the muscle cells to contract and results in withdrawal of the hand (see Fig. 1).

1.1.2 Selective Permeability: a Building Block for the Action Potential

From the simplest organism to a complex vertebrate, one of the most critical components for viability is the selective permeability of the cell membrane, that is the ability of the cell to keep harmful elements out of the cell and essentials in. The lipid bilayer of the membrane with its hydrophobic interior is also sufficient to halt the permeation of charged ions such as sodium (Na^+), potassium (K^+), and calcium (Ca^{2+}). Specialized leak channels and pumps such as the Na^+/K^+-ATPase maintain specific concentration gradients of these ions inside and outside the cell (Hodgkin and Keynes 1955; Hilden and Hokin 1975).

Differences in ion concentrations inside and outside of the cell enable the cell to do work by funneling ions along their concentration gradients. Cells even use differences in ion concentrations (hydrogen ions, H^+) to form adenosine triphosphate (ATP), the energetic currency of the cell (Mitchell 1961; Hille 2001). Additionally, differences in the

ionic concentrations across the cell membrane result in the charge difference that is an essential ingredient for the action potential - the electrical signal that triggers everything from the firing of neurons to the contraction of muscle cells in the heart.

When the cell is at its resting membrane potential, the concentration of Na^+ inside the cell is much lower than that outside the cell. Additionally, the concentration of K^+ inside the cell is much higher than that outside the cell. The equilibrium potential for K^+ is much more hyperpolarized than that of Na^+ (+ 67 mV vs -98 mV for K^+ in skeletal muscle) (Hille 2001). In the resting state, the cell membrane is more permeable to K^+ than to Na^+ and therefore, the resting membrane potential is much closer to the K^+ equilibrium potential (ranging anywhere from -40 to -95 mV) (Hille 2001). However, when selective ion channels in the membrane open in response to stimuli, these ions (and others) will proceed down their electrochemical gradients. Because there is more sodium outside the cell than inside, when the membrane becomes more permeable to sodium (via the opening of specialized channels), the sodium will rush into the cell and bring the membrane potential closer to its own equilibrium potential. This initial localized depolarization of the membrane activates the Nav channels which open and form the upstroke of an action potential.

1.2 The Voltage-Gated Sodium Channel: Structure and Gating Behavior

1.2.1 Structure and Topology

Nav channels consist of a pore-forming α subunit and an accessory β subunit. The β subunit modulates gating behavior of the channels and also regulates expression (Isom, De Jongh et al. 1992). The pore-forming subunit of the channel is called the α subunit and it consists of four homologous, but non-identical, domains, each with six

transmembrane segments designated S1-S6. Both the amino-(N)-terminal and the carboxy-(C)-terminal tails are located intracellularly (Noda, Shimizu et al. 1984; Thomsen and Catterall 1989). In each domain, the S5 and S6 helices come together to form the central pore of the channel, with the re-entrant p-loop forming the selectivity filter (Heinemann, Terlau et al. 1992; Chiamvimonvat, Perez-Garcia et al. 1996; Favre, Moczydlowski et al. 1996; Perez-Garcia, Chiamvimonvat et al. 1997; Huang, Favre et al. 2000) (See Fig. 2A). The S1-S4 helices form the voltage-sensors of the channel with the S4 helices acting as the principal voltage-sensors. The S4 voltage-sensors contain stretches of positively charged basic residues every three residues (Noda, Shimizu et al. 1984; Tempel, Papazian et al. 1987; Stühmer W 1989; Aggarwal and MacKinnon 1996; Seoh, Sigg et al. 1996) (See Fig. 2B) and it is these charges which provide the ability to sense voltage jumps (Noda, Shimizu et al. 1984; Tempel, Papazian et al. 1987; Stühmer W 1989; Aggarwal and MacKinnon 1996; Seoh, Sigg et al. 1996).

Though a crystal structure for a eukaryotic voltage-gated sodium channel is not yet available, structures have been obtained for the closely related voltage-gated potassium (Kv) channel as well as for a prokaryotic voltage-gated sodium channel NavAB (Long, Campbell et al. 2005; Payandeh, Scheuer et al. 2011)(see Fig. 3A and B). As can be seen from these crystal structures, the predicted structure of the sodium channel is propeller-like with the four voltage-sensing domains radiating off of the central pore axis. Another key feature to note about these crystal structures is that the voltage-sensing domains which actuate the pore gates are relatively far from the pore itself. The voltage-sensors are linked to the pore helices via the S4-S5 linkers which are known to transduce the voltage-sensor behavior to the pore gates (Bezanilla 2000; Long,

Campbell et al. 2005; Payandeh, Scheuer et al. 2011). Also of importance is the DIII-DIV loop, an intracellular loop believed to be the inactivation particle (Armstrong, Bezanilla et al. 1973; West, Patton et al. 1992; Kirsch, Alam et al. 1994). These elements are among the most critical for normal sodium channel function.

1.2.2 The Normal Gating Behavior of the Voltage-Gated Sodium Channel

When an excitable cell is at rest, the pore gates of the Nav channel are closed and the voltage-sensors are in their resting positions. As the membrane depolarizes, the extracellular side of the membrane becomes increasingly negative relative to the intracellular side. This change results in the movement of the voltage-sensors toward the extracellular side. Since the voltage-sensors are charged, the movement of the voltage-sensors can be recorded as non-linear capacitive transients called gating currents (Armstrong and Bezanilla 1973; Bezanilla and Armstrong 1975). When the voltage-sensors activate, they actuate the pore gates and open the channel. Sodium fluxes down its electrochemical gradient and into the cell, depolarizing the membrane and generating the upward stroke of the action potential.

Next, the channels must inactivate in order for the potassium channels to be able to hyperpolarize the membrane. The fast inactivation process, sometimes referred to as 'ball-and-chain' or 'hinged lid' inactivation is thought to occur when the DIII-DIV loop binds to its docking site and blocks the channel (Armstrong, Bezanilla et al. 1973; Stühmer W 1989; West, Patton et al. 1992; Kirsch, Alam et al. 1994). The inactivation process is responsible for the refractory period, an interval in which action potentials cannot be initiated or are inhibited. The refractory period is a safeguard against aberrant

excitability and therefore, improper inactivation can be a common mechanism of diseases ranging from epilepsy to cardiac arrhythmia (Goldin 2003).

Though fast inactivation is itself a voltage-sensitive process, there appears to be no charge movement associated with the movement of the inactivation loop itself.. Therefore, the voltage-dependence of fast inactivation must arise from either its coupling to the activation process or from a voltage-sensor associated with inactivation. Currently, it is suspected that the DIV and perhaps the DIII voltage-sensors may contribute the voltage-dependence to this process, however, the evidence is not conclusive (Chahine, George et al. 1994; Chen 1996; Kontis and Goldin 1997; Cha 1999; Horn, Ding et al. 2000).

Finally, the channels recover from inactivation, a process during which the inactivation loop pops out of its binding site and the channels return to their fully resting conformation. Recovery from inactivation is also a voltage-dependent process and a reasonable hypothesis would be that perhaps one or more of the voltage-sensors must return to their resting conformation(s) prior to pore gate closure and inactivation particle unbinding. Following recovery from inactivation, the sodium channels are again able to respond to changes in membrane potential and to trigger another wave of action potentials.

Yet another gating process called slow inactivation occurs in sodium channels. Slow inactivation occurs after periods of long and high frequency activity and also when the membrane is depolarized for long periods of time. This process is thought to occur through the collapse of the selectivity filter region, blocking conduction (Balser, Nuss et al. 1996; Townsend and Horn 1997; Benitah, Chen et al. 1999; Todt, Dudley et al. 1999;

Ong, Tomaselli et al. 2000; Hilber, Sandtner et al. 2001; Vilin, Fujimoto et al. 2001; Xiong, Li et al. 2003; Xiong, Farukhi et al. 2006). As are the processes above, slow inactivation is a voltage-dependent process, however, the source of this voltage-dependence remains uncertain and is widely thought to derive solely from the coupling of slow inactivation to the activation process.

Slow inactivation is most commonly known for its role in spike frequency adaptation, an important step in determining the pattern of brain waves (Fleidervish, Friedman et al. 1996). Additionally, slow inactivation is also a natural brake to terminate aberrant activity in disease situations. For example, when tissue becomes ischemic, the membranes become depolarized and slow inactivation occurs in that tissue, preventing spontaneous action potential generation in the diseased tissue. Certain anti-epileptic drugs like Lacosamide operate via enhancing the slow inactivation of sodium channels and thus decreasing the number of channels that are able to respond to stimuli (Jo and Bean 2011; Wang, Park et al. 2011).

1.2.3 A closer look at the voltage-sensor and voltage-sensor movement

Evidence supporting the S4 helices as the principal voltage-sensors primarily came from experiments in which charges in the S4 segments were neutralized one at a time. When comparing the gating currents collected after these mutations to those of the WT channel, it was discovered that the total charge of the gating currents had reduced (Aggarwal and MacKinnon 1996; Seoh, Sigg et al. 1996). Additionally, it was observed that the largest reduction in the total charge of the potassium channel was observed for the first four positive charges. This data suggests that, at least in the potassium channel, the first four charges are the most important.

Others made neutralizations of single charges in the DIV S4 of the sodium channel. Next, they used a toxin, anthopleurin-A, known to bind to DIV and also known to reduce the total gating charge of the channel on each of these mutants. Using this toxin as a tool to determine the contributions of each of the first three charges of DIV S4, they determined that the charges in the DIVS4 contributed differently to the total charge of the channel. When a neutralization was made of the first charge in the DIV voltage-sensor, the toxin caused much less of a reduction in the total charge of that channel. The third charge was found to make little contribution to the total charge of the channel while the second charge was intermediate (Sheets, Kyle et al. 1999).

Later studies in the sodium channel (Sheets and Hanck 2002) determined that it was the first three charges of the sodium channel voltage-sensors which were the most important, with the fourth charge making little contribution to the total charge of the channel. In the case of this study, only the voltage-sensor of DIII was examined. Cysteine mutagenesis studies done by the Yang group showed that the first three charges in the DIV voltage-sensor were accessible to cysteine modifying reagents applied on the extracellular side of the membrane when at depolarized voltages. However, this was not true for the fourth charge, an observation which suggests that it's possible that not all charges in the voltage-sensors may move through the membrane electric field (Yang, George et al. 1996).

The voltage-sensors of the sodium channel were originally speculated to be alpha helices, however, the recent crystal structure of a functionally related channel provided by the Catterall group suggests that the voltage-sensors may in fact be at least partially 3-10 helices (Payandeh, Scheuer et al. 2011). A long standing controversy in the field of

ion channel research is how the voltage-sensors of the sodium channel - or any voltage-sensitive protein move through the membrane. Various mechanisms have been suggested, ranging from a large paddle-like motion of the voltage-sensors through the membrane (acting as levers on the pore gates) to a smaller primarily vertical motion of the voltage-sensors in the membrane.

Much of the original 'Paddle Model' resulted from study of the crystal structure gleaned from the Kv1.2/2.1 potassium channel chimera (Long, Campbell et al. 2005). Additionally, MacKinnon's group found that a Biotin molecule tethered to a voltage-sensor could be dragged across the membrane (Jiang, Ruta et al. 2003). However, the original paddle model makes few allowances for the difficulty of moving such a highly charged segment of the protein through the unfriendly terrain of the lipid bilayer.

Other groups theorized that the membrane electric field could become focused in the region of an ion channel. This focusing of the electrical field would intensify the effects of membrane potential changes on the voltage-sensors such that fewer gating charges might be needed to produce the same reactions one would expect in a less focused electrical field. Such focusing of the membrane electric field would enable the voltage-sensors to actuate the pore gates with much less of a movement than that proposed by the paddle model (Chanda, Asamoah et al. 2005).

Other evidence arising from mutagenesis studies in the potassium channel Suggests that there must be an aqueous or proteinaceous pathway that the voltage-sensors move through. This ‘gating pore’ theory first arose from a study in which the topmost charge of the potassium channel voltage-sensor was mutated to a histidine. It was observed that this particular mutation resulted in a proton current at hyperpolarized

potentials. This data led the experimenters to theorize that the protons were able to flux through the voltage-sensor itself at hyperpolarized potentials. They further stated that the aqueous internal and external environments at the membrane must be separated by a narrow barrier in the channel (Starace and Bezanilla 2004).

Further evidence supporting the gating pore model arose from studying a human pathological condition, hypokalemic periodic paralysis (hypoPP). In these patients, low concentrations of potassium in the blood lead to episodes of muscle paralysis. One of the mutations known to cause hypoPP is an arginine (R) to histadine (H) mutation. This particular charge mutation was seen to allow the development of a proton current that passed through the voltage-sensor itself. In the case of this mutation there emerged a hyperpolarizing proton leak current that is thought to alter the intracellular pH and to destabilize the resting membrane potential (Struyk and Cannon 2007). These data suggest that the voltage-sensor likely moves through an aqueous or proteinaceous pathway within the protein.

It remains to be seen exactly how the voltage-sensors move in the sodium channel, and therefore, it is necessary to reconcile many data sets with these multiple hypotheses, however, barring the arrival of crystal structures of a eukaryotic sodium channel in multiple states, it will be difficult to speculate with any degree of confidence on the mechanism by which voltage-sensors translocate their charge. Indeed, it is possible that the environment around the voltage-sensors shifts while the voltage-sensors themselves remain stationary.

1.3 Sodium Channel Diseases

1.3.1 Types of sodium channel based channelopathies and the location of α subunit mutations

Malfunctioning sodium channels are known to cause a whole array of human diseases ranging from the moderate to the severe. These conditions affect various systems throughout the body and can affect basically any of the excitable tissues in which sodium channels can be found.

In the heart, two well known and severe conditions have their roots in a sodium channel dysfunction. These conditions are: Long QT syndrome (LQT3) and Brugada syndrome (Grant 2005; Jones and Ruben 2008; Chopra and Knollmann 2011). These arrhythmogenic conditions result in the sudden cardiac death of many affected people.

In the central nervous system, mutations in the sodium channel are known to be responsible for certain types of epilepsy including generalized epilepsy with febrile seizures (GEFS). Also in the nervous system, sodium channel mutations are known to result in extremely painful conditions such as paroxysmal extreme pain disorder (PEPD) and erythromelalgia (Catterall, Dib-Hajj et al. 2008).

In the musculoskeletal system, mutations in the sodium channel can trigger several disorders of paralysis and myotonia. Some of the more well known diseases tied to the skeletal muscle sodium channel are congenital myotonia, hypokalemic periodic paralysis and hyperkalmic periodic paralysis. Even a specific myasthenic syndrome has been previously tied to the sodium channel (Jurkat-Rott, Holzherr et al. 2010).

Interestingly, the mutations responsible for this array of human diseases may be found scattered throughout the channel (see Fig. 4 for examples of mutation locations).

However, there are two locations that these disease causing mutations commonly fall into: DIV (previously suggested to be important in inactivation) and the inactivation loop (between DIII and DIV). The placement of these mutations points to an important role in pathogenesis for sodium channel inactivation.

1.3.2 Mechanistically speaking: the importance of inactivation in sodium channel disease

Across multiple forms of sodium channel diseases, one of the most prevalent mechanisms of sodium channel dysfunction is through an altered inactivation process. These inactivation-linked disorders fall into two categories: loss of function, and gain of function mutations. While these two groups may also be caused by effects on the activation process of the sodium channel, it is hard to miss the relevance of fast inactivation in the production of the disease phenotype.

Loss of function mutations, as the name suggests, cause a reduction in sodium current at physiologically relevant potentials (at least in the case of a mutant with a phenotype). This reduction can be caused through multiple mechanisms including a rightward shift of the G-V curve, a shift in the selectivity of the channel, or altered inactivation (either fast or slow). For example, Brugada syndrome precipitated by the E1784K mutation results in a leftward shift in the steady state inactivation curve (Wei, Wang et al. 1999). This means that the affected sodium channels tend to inactivate at voltages that are more hyperpolarized than in the WT channel (Zimmer and Surber 2008).

All of these loss of function mutations cause a reduction of sodium currents in physiologically relevant conditions. This means that there are either less sodium channels available to drive an action potential or that less sodium current penetrates the cell for each channel that opens. In the specific case of Brugada syndrome, the reduction in

sodium current results in an imbalance between the depolarizing sodium current, and the hyperpolarizing currents (such as potassium current) during the cardiac action potential. This results in a characteristically shorter cardiac action potential (see Fig. 5). Arrhythmias in this case are generated via a process called reentry (Yan and Antzelevitch 1999; Antzelevitch, Brugada et al. 2002). Inactivated sodium channels result in patches of non-excitable tissue and new action potentials must go around these places. However, the sodium channels in those patches eventually recover from inactivation and can be excited by a previously rerouted action potential, generating a new, aberrant wave of depolarizations. Additionally, the mixture of inactivated and reactive channels tends to create a conduction delay. A conduction delay is a necessary component for a reentrant arrhythmia (Wit, Hoffman et al. 1972).

Gain of function mutations, on the other hand, result in an increase in sodium current at physiologically relevant voltages. Again, multiple mechanisms might be behind the gain of function - or a mixture. A leftward shift in the conductance-voltage (G-V) curve of the sodium channel would allow the sodium channel to open at voltages more hyperpolarized than in the WT condition. Accelerated kinetics of activation would also present as a gain of function. On the other hand, as with the loss of function mutations, gain of function can result from altered inactivation. For example, the LQT3 mutation A1330P results in a rightward shift of the steady state fast inactivation curve (Wedekind, Smits et al. 2001).

Arrhythmias result from LQT3 mutations because the interval between ventricular depolarization and repolarization (the QT interval) is extended. In this case, the QT interval is lengthened due to a flux of sodium current that continues beyond the point

where most of the WT sodium channels are inactivated. Therefore, the depolarizing sodium current acts to counter the hyperpolarizing potassium current. The lengthening of the QT interval increases the window of time during which the cardiac tissue is depolarized and also increases the probability of developing triggered arrhythmias (see Fig. 5). For example, potentially deadly arrhythmias can arise when the repolarization of cardiac tissue is delayed enough to allow for the recovery of a fraction of L-type calcium channels. Because the cardiac tissue is still depolarized, L-type calcium channels that have recovered from inactivation can open again, allowing a further depolarizing influx of calcium into the cell and forming an early afterdepolarization (EAD) which, if propagated through the ventricle, can lead to the development of arrhythmia (Davidenko, Cohen et al. 1989).

Due to the undeniable importance of the process of inactivation in pathological conditions, it is important to better understand the elements and steps involved in inactivation. Through a better understanding of inactivation, new disease mechanisms and potential treatment target sites may be elucidated. However, determining the role of different structural elements of the channel may prove difficult due to the complexity inherent in a heterotetrameric channel such as the sodium channel.

1.4 Heterotetrameric Complexity

1.4.1 Different domain, different function?

As stated above, the four domains of the sodium channel are homologous but not identical. This concept of domains with similar but distinct sequences extends as well into the S4 voltage-sensors. As the voltage-sensors themselves are not identical, different domains may (and probably do) contribute differentially to the total gating charge of the

channel. Such dissimilarity creates an opportunity for much more complex features in channel gating behavior than might be seen in a homotetramer.

If a voltage-sensor were to carry a larger fraction of the gating charge than any of the other domains, it would follow that this particular voltage-sensor may have different kinetics of motion or an altered voltage-dependence. Additionally, with voltage-sensors that have different kinetics or voltage-dependencies, it is also possible that each of the voltage-sensors may play a slightly different role in the gating of the sodium channel. There may even be a predominant sequence of voltage-sensor activation in response to a voltage jump.

The concept of differential voltage-sensor behavior is not a new one. Several lines of evidence have pointed to the possibility of different voltage-sensor roles in the past. For example others determined that the site-3 toxin Anthopleurin-A (Ap-A) specifically inhibited inactivation. Furthermore, Ap-A was found to reduce the gating charge by approximately 33% at depolarized potentials, a reduction which the authors believed was due to the effects of the toxin on inactivation (Hanck and Sheets 1995; Sheets and Hanck 1995). Interestingly, Ap-A binds primarily to DIV, strengthening the argument that this domain is involved in inactivation (Benzinger, Drum et al. 1997).

Additionally, there was a study in which either the first or third voltage-sensor charge in one domain was neutralized. This study showed that most of the neutralizations (13 out of 15) caused a decrease in the voltage-dependence of peak sodium current and that 9 out of the 15 neutralizations caused a shift in the conductance-voltage relationship, results consistent with the S4 voltage-sensors being involved in the activation process.

However, it was determined that out of all of the voltage-sensors, only when neutralizations were made in the DIV S4 was inactivation affected (Chen 1996).

More support for the argument of different roles for the voltage-sensors arrives from a study that locked the voltage-sensor of either DII or DIV into one conformation utilizing a photo-activatable crosslinker. This particular study found that when the DII S4 was locked into one position, there was a reduction of ionic currents at every potential, but little effect on inactivation. Conversely, the locking of DIV S4 had a profoundly inhibitory effect on the inactivation of the channel and an *increase* in ionic currents at all potentials (likely due to defective inactivation)(Horn, Ding et al. 2000).

When placing an environmentally sensitive fluorescent probe on the top of a specific voltage-sensor, it was determined that the voltage-sensors behave differently. The DI, DII, and DIII voltage-sensors have rapid kinetics of movement in response to a depolarization and when comparing these kinetics to those of macroscopic channel opening, the movement of the DI-DIII voltage-sensors was found to precede channel opening - as would be expected for a process crucial for activation. On the other hand, the DIV S4 had much slower kinetics of movement and these kinetics matched closely with the decay of current - a finding which seems to tie the DIV voltage-sensor to inactivation (Chanda and Bezanilla 2002).

Additionally, when a toxin interacts specifically with the DIV of the voltage-gated sodium channel, that toxin tends to have an effect solely on channel inactivation. Alternatively, if a toxin interacts with the first three domains, whether or not it targets DIV, that toxin tends to alter the channel opening (Bosmans, Martin-Eauclaire et al. 2008).

Though there are a large number of papers supporting the existence of different roles for the voltage-sensors, some of that information is contradictory. The papers listed above primarily support the role of the DIV S4 in inactivation. However, a paper in which charges were replaced in the voltage-sensors of individual domains found that most of the mutations in the DI and DII voltage-sensors resulted in leftward shifts in fast inactivation, while most mutations in DIV resulted in no significant effects on fast inactivation. In their two paired papers, the Goldin group made the argument that all of the voltage-sensors were involved in activation and inactivation (Kontis 1997; Kontis and Goldin 1997).

Further complicating our ability to delineate specific roles for individual voltage-sensors is the fact that much of the data that we have is difficult to interpret. For example, though the results gleaned from mutations of single gating charges are interesting, they are rather difficult to unravel in light of experiments in the potassium channel suggesting that neutralizations of even numbered charges can shift the open probability to the left whereas neutralizations of odd numbered charges can shift the open probability right (Papazian, Timpe et al. 1991). Furthermore, different charges in a particular voltage-sensor may contribute differently to the total charge of the channel, rendering the effects of the mutations hard to interpret. Additionally, experimental approaches utilizing mutagenesis must take into account the possibility of compensatory changes. For example, the lack of effect of a mutation does not necessarily mean that this residue is unimportant, rather, this may be due to a compensatory mechanism. Thus, one should not assign too much weight to data sets making single charge neutralizations.

A further complication of many of these data sets is that they are observing macroscopic currents. Placing too much weight on changes in the kinetics of macroscopic currents is unwise. The processes of activation and inactivation are closely linked and therefore, the properties of inactivation shape the kinetics of activation as well. In macroscopic currents, there is a rapid rise to the peak of current and then a decay phase. However, the time to the peak of current may appear to be much shorter than it actually is because inactivation begins to set in and causes the current to decrease. This presents an obvious caveat to any experiments looking only at the kinetics of macroscopic currents.

Therefore, while it is reasonably clear that the voltage-sensors of different domains may play different roles, at this point in time, it is difficult to determine exactly what those roles may be. In order to better determine the involvement of a voltage-sensor in the processes of activation and inactivation, a systematic study must be performed in which the voltage-sensors may be functionally isolated from the others so that the behavior of the channel may be studied in the 'absence' of one voltage-sensor at a time. Due to the critical nature of inactivation in sodium channel disease processes, this work aims at specifically elucidating the role of each voltage-sensor in the processes of both fast and slow inactivation.

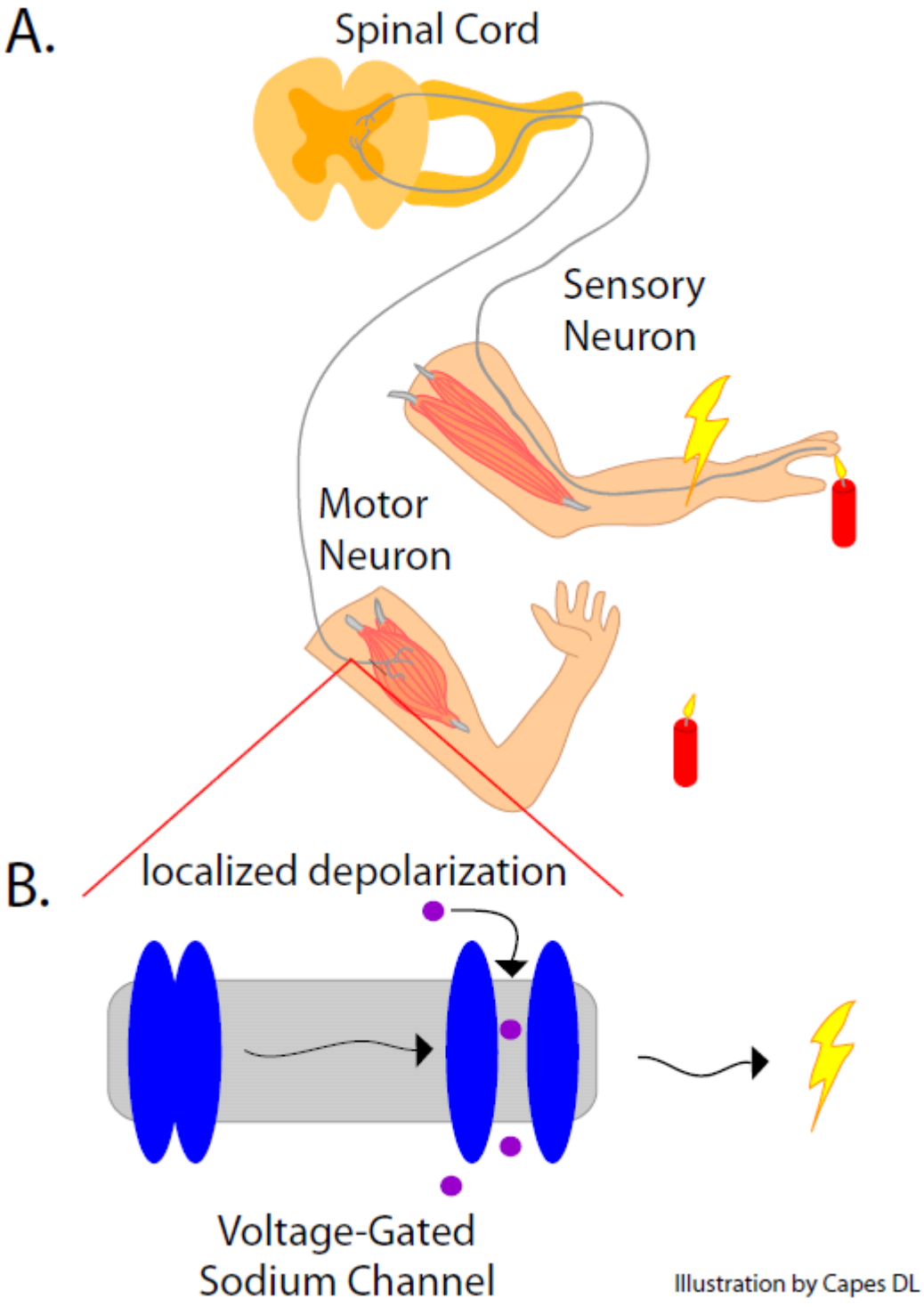

Figure 1: The sodium channel drives the reflex arc. (A) A diagram showing a simple reflex arc. Following a painful stimulus, a wave of depolarizations is initiated that passes through the spinal neurons and to a motor neuron. The motor neuron triggers contraction

of the muscle and withdrawal of the hand. **(B)** An enlarged portion of the membrane of neuron. After a localized depolarization past threshold, sodium channels open, allow sodium ions to enter the cell, and propagate the action potential.

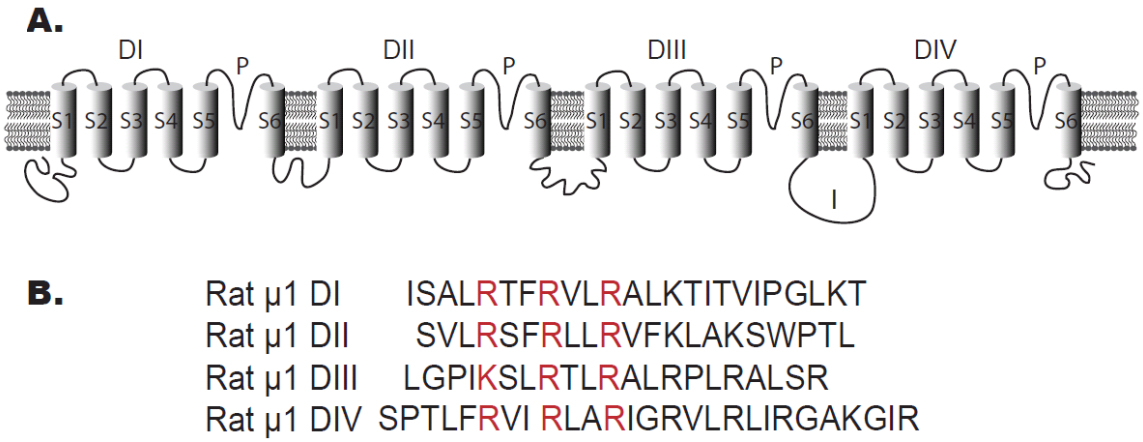

Figure 2: The transmembrane topology of the sodium channel and the sequence of the muscle Nav channel voltage-sensors. (A) The transmembrane topology of the voltage-gated sodium channel is shown. Domain (D) numbers are marked above. The transmembrane helices are labeled as S, the inactivation loop is labeled as I, and the reentrant P loops as P. **(B)** The sequence of the S4 voltage-sensors of the Nav1.4 rat skeletal muscle sodium channel is shown. The positively charged gating charges are marked in red.

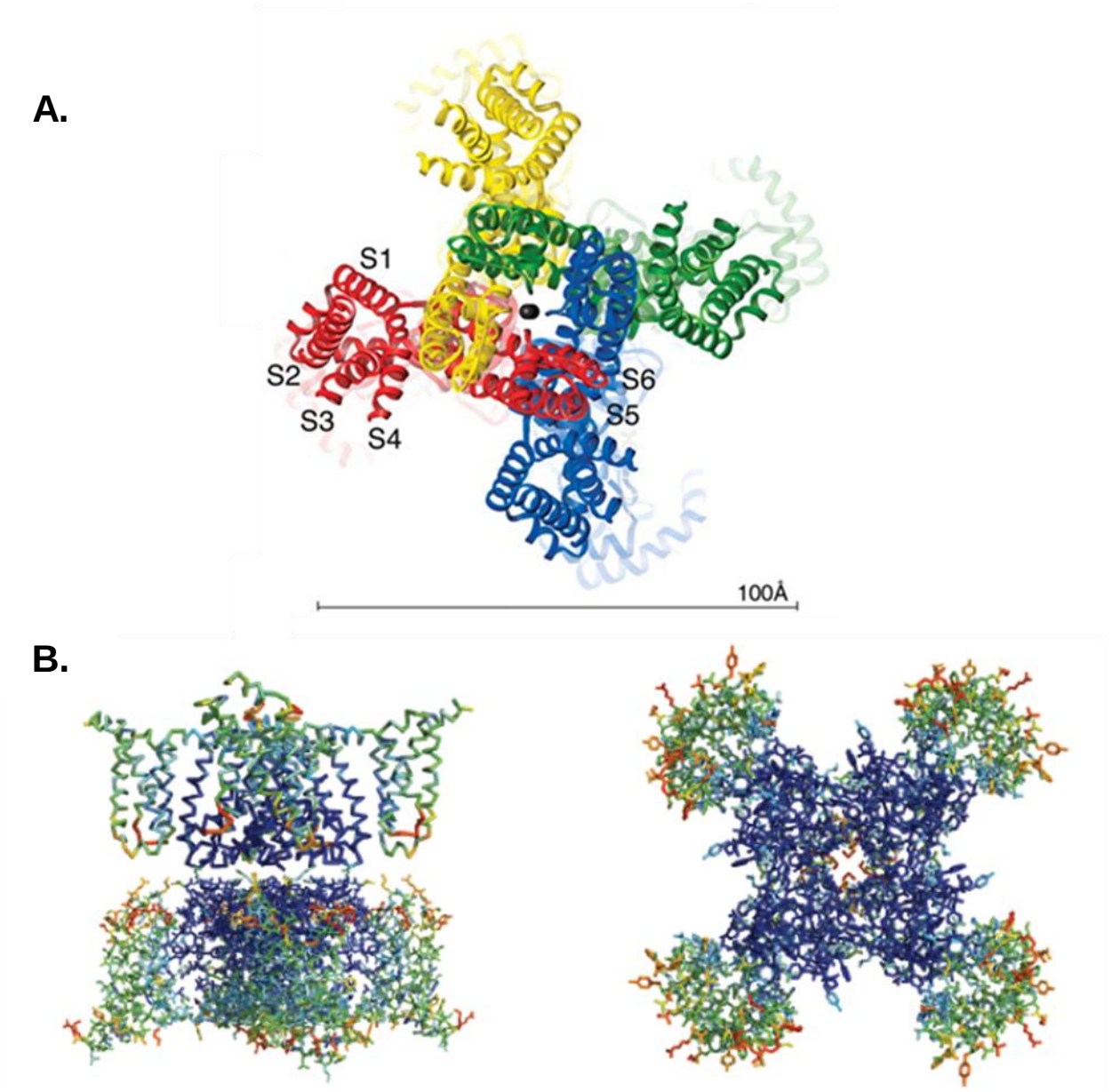

Figure 3: Crystal structures of a eukaryotic potassium channel chimera and a prokaryotic sodium channel (A) The crystal structure of the Kv1.2/2.1 chimera adapted from Long et al. (Long, Campbell et al. 2005). The S1-S6 helices are marked and each domain is shown as a different color. **(B)** The crystal structure of the NavAb channel adapted from Payendeh et al. (Payandeh, Scheuer et al. 2011). On the left, a side view of two stacked channels is shown. On the right is the top down view.

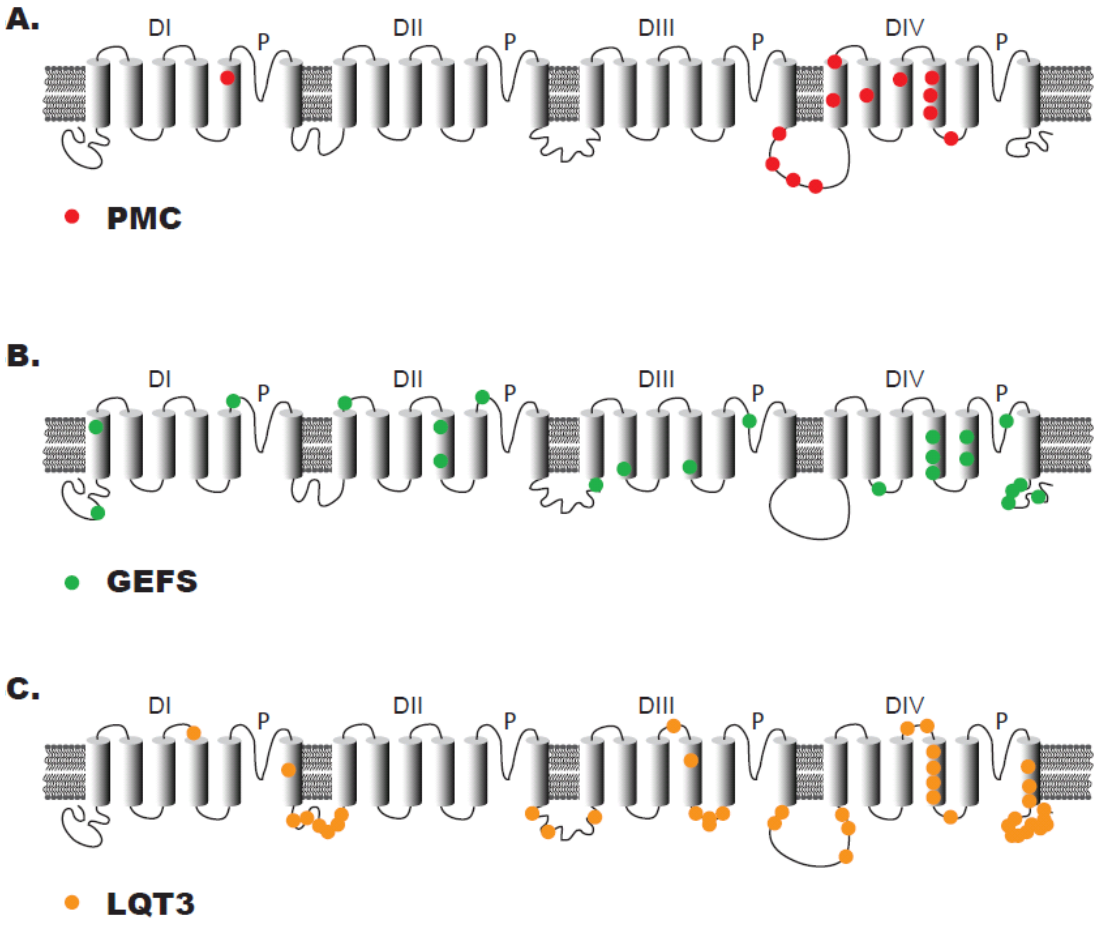

Figure 4: Sodium channel mutations are spread throughout the channel.

(A) The location of some of the mutations causing paramyotonia congenital (PMC). The figure was based on the review by Jurkat-Rott et al. (Jurkat-Rott, Holzherr et al. 2010) **(B)** Mutations resulting in generalized epilepsy with febrile seizures (GEFS). The figure was adapted based on the review by Catterall et al. (Catterall, Dib-Hajj et al. 2008). **(C)** The location of characterized mutations causing long QT syndrome 3 (LQT3). The figure was based on the review by Zimmer and Surber (Zimmer and Surber 2008).

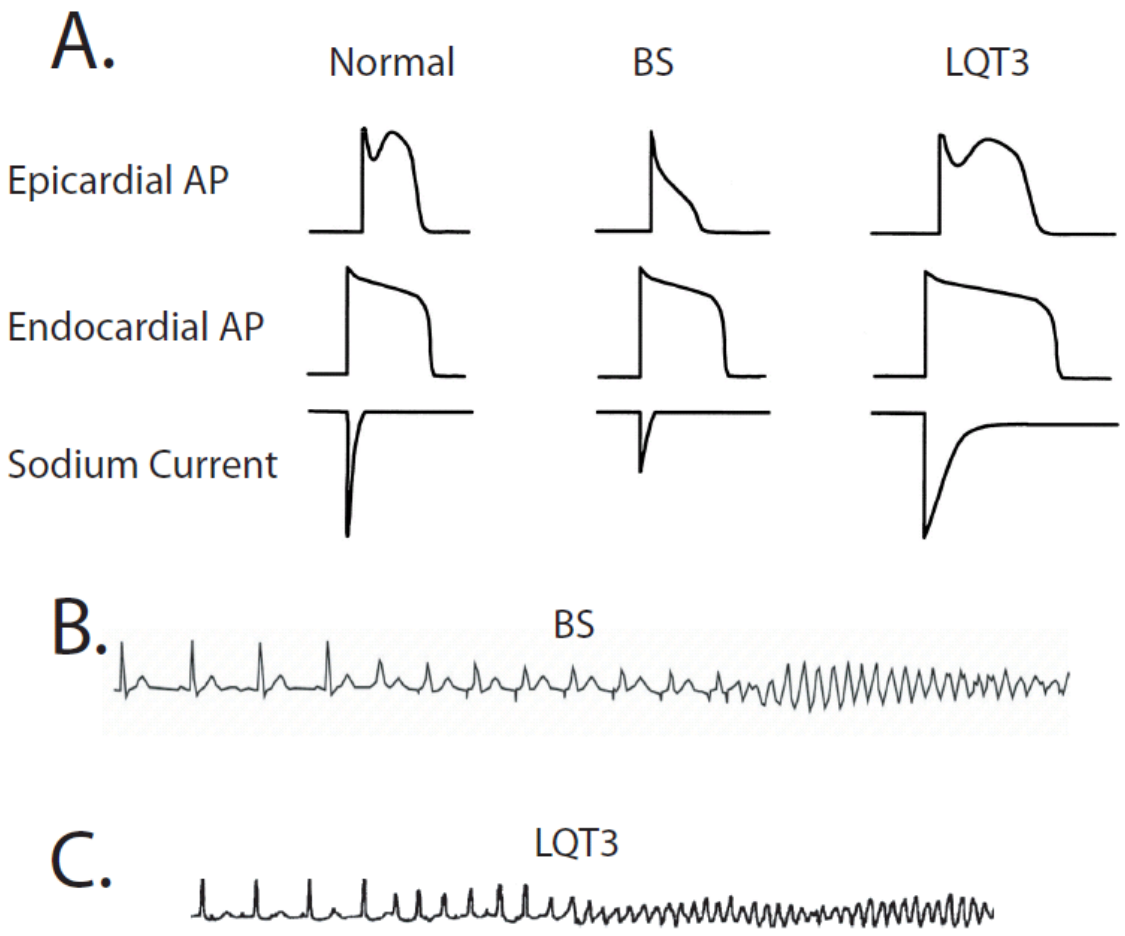

Figure 5: The effects of sodium channel mutations on cardiac action potentials and the electrocardiogram. (A) Examples of cardiac action potentials in normal cases, brugada syndrome (BS), and long QT syndrome 3 (LQT3). Underneath, the sodium currents (and the changes in sodium current caused by these two conditions) are shown for reference. This was taken from Bezzina et al. (Bezzina, Rook et al. 2001). **(B)** Depicted here is an electrocardiogram (EKG) for BS which degenerates into arrhythmia and ventricular fibrillation. This figure was taken from Bell and Siriwardena (Bell and Siriwardena 2000) . **(C)** An EKG for LQT3 which also degenerates into ventricular fibrillation. This figure panel was taken from Chinushi et al. (Chinushi, Kasai et al. 2002).

CHAPTER II

Experimental Procedures

2.1 Materials

Tetrodotoxin was purchased from Sigma-Aldrich (St. Louis, MO). Mu-conotoxin GIIIA (μ-CTX) was provided by the lab of Robert J. French (Calgary, Canada) or purchased from Bachem Americas (Torrance, CA). Methanesulfonic acid (MES) was purchased from Acros organics (Geel, Belgium). N- methyl-D-glucamine (NMG) was purchased from Sigma-Aldrich. Collagenase A was purchased from Roche (Madison, WI). The 1 kb DNA ladder was purchased from New England Biolabs (Ipswich, MA) and the low mass ladder from Invitrogen (Life Technologies, Madison, WI). All restriction enzymes were purchased from New England Biolabs. Fast AP dephosphatase was purchased from Fermentas (Glen Burnie, MD). Primers were synthesized by integrated technologies (East Providence, RI). The PFU-Ultra DNA polymerase from Agilent technologies (Santa Clara, CA) was used for PCR reactions. All other chemicals were obtained either from Fisher Scientific (Fitchburg, WI) or from Sigma-Aldrich.

2.2 Oocyte excision and preparation

Adult female *Xenopus laevis* from either Xenopus Express (Brooksville, FL) or Nasco (Fort Atkinson, WI) were prepared for oocyte excision by anesthetizing them in MS-222 (Sigma) until they lost their righting reflex and became unresponsive to toe pinch. A small, sterile incision was made just off of midline in the abdomen and lobes of oocytes were removed and placed in standard oocyte solution (SOS) without calcium (100 mM NaCl, 2 mM KCL, 1 mM $MgCl_2$ x 6 H_2O, and 5 mM HEPES at pH 7.2.). The animal was

then sutured using sterile Vicryl sutures (Ethicon 360, San Angelo, TX) and humanely euthanized via returning them to the anesthetic for an hour and transferring them to a designated -20 ^{o}C freezer.

In the case of a frog survival procedure, the surgery was carried out as stated above. Next, the frog was placed in clean water and allowed to recover for two hours before returning the animal to the holding area. For a period of at least two days, the animal was placed into an isolated tank and carefully observed for any complications. A single frog was used a maximum of five times. All animal care and procedures were carried out with the guidance and approval of the institutional care and use of animals committee at the University of Wisconsin - Madison.

Following their removal, the oocytes were mechanically dissociated using sterile forceps. Following two rinses in SOS without calcium, the oocytes were placed in 1 mg/ml Collagenase A dissolved in SOS without calcium and were placed on a turntable (VWR, Radnor, PA) for 20 minutes. After three rinses with SOS without calcium, the oocytes were again manually separated with sterile forceps and then they were returned to the collagenase for another 15 minutes. Following three rinses in SOS without calcium, the oocytes were observed under a dissection microscope (Ningbo Yong Jing Science And Education Equipments Co., Ningbo, China). If the oocytes were still in their follicular layers, they were returned to the collagenase for another 5 - 10 minutes. This process was repeated until 20 percent or more of the oocytes were defolliculated. Next, the oocytes were stored in SOS with 1.8 mM $CaCl_2$ x 2 H_2O, 100 μg/ml Gentamicin, and 1 mg/ml bovine serum albumin (Sigma- Aldrich). Oocytes were stored in an 18 ^{o}C

incubator (VWR). All oocyte solutions were measured for the correct osmolarity (200 - 210 mmol/kg) using a Wescor Vapro 5520 Osmometer (Logan, UT).

2.3 Mutagenesis and DNA preparation

Mutations were made using the QuikChange kit (Qiagen, Valencia, CA). Sequences were validated utilizing the reagents and sequencer of the Biotechnology Center at the University of Wisconsin - Madison and the Qiagen MagDTR resin and kit. Mutations were cloned into the pBSTA-Mu1-Z3 vector which is optimized for oocyte expression and contains an ampicillin resistance cassette. Constructs were transformed into chemically competent XL1-Blue cells prepared in the lab. Plasmid purification was carried out using the Qiagen mini-prep or midi-prep kits and the final concentration was assessed using a Nanodrop 2000c spectrophotometer (Thermo Scientific, Wilmington, DE).

2.4 RNA preparation and injection

DNA was linearized using the NotI enzyme and then the linearized DNA was purified using PelletPaint (EMD Millipore, Billerica, MA). RNA was made using the T7 RNA polymerase mMessage mMachine kit (Life Technologies, Grand Island, NY) and then concentrated by lithium chloride precipitation. The sodium channel α subunit was diluted in RNAse free water to a stock concentration of 2 μg/μl and the β_1 subunit was diluted to a stock concentration of 0.4 μg/μl and the concentrations were verified using the Nanodrop 2000c. All RNA was stored in a -80 ^{o}C freezer until needed.

For injection, an equal volume of α and β_1 subunit at 2 μg/μl and 0.4 μg/μl respectively were mixed together. Oocytes were selected and placed in sterile SOS without calcium and a micropipette was pulled using the PP-83 puller (Narishige, East

Meadow, NY). The tip of the pipette was broken off and the pipette was back loaded with mineral oil. The pipette was loaded onto a Nanoliter 2000 microinjector (World Precision Instruments; Sarasota, FL). The RNA was loaded into the pipette and 50.6 nl was injected into each oocyte. Following injection, oocytes were moved to SOS with calcium, and 100 μM DTT (unless stated otherwise), 0.2 mM EDTA, and 100 μg/ml Gentamicin and stored for 2 to 7 days in an 18 ^{o}C incubator until optimum expression levels were obtained.

2.5 Electrophysiological Experiments

2.5.1 Ionic currents using the two electrode voltage clamp technique

After storage in the 18 ^{o}C incubator for 1-3 days post injection, oocytes were assessed for sodium channel expression utilizing the two electrode voltage clamp (TEV) technique. Micropipettes were pulled using a P-97 flaming brown microelectrode puller (Sutter Instrument Co., Novato, CA) to a resistance of 0.2 to 0.7 MΩ. Oocytes were placed in 105 mM sodium external solution (105 mM NaOH, 20 mM HEPES, 2 mM $Ca(OH)_2$ and MES to pH 7.4) and then two microelectrodes with a AgCl wire and filled with 3 M KCl were inserted into the oocyte. The oocyte was clamped at -80 mV using an OC-725C Oocyte Clamp (Warner Instruments) and allowed to equilibrate for 5 minutes prior to recording. Next oocytes were stepped to -120 mV for 50 ms and then a voltage pulse train from -120 mV to 65 mV was applied for 20 ms and the oocyte was returned to -120 mV. A p/4 subtraction with a subtraction holding potential of -130 mV was used to subtract membrane leak and to minimize the capacitive transient. Data on the TEV was collected using pClamp 8 software (Molecular Devices, Sunnyvale, CA) and the resulting

traces were analyzed in Clampfit (Molecular Devices, Sunnyvale, CA) followed by Excel (Microsoft, Redmond, WA).

2.5.2 Ionic current measurements using the voltage clamp on cut open oocyte technique.

After storage in the 18 ^{o}C incubator for 2-4 days post injection, oocytes were placed into the voltage clamp on cut open oocyte setup for measurement of ionic currents. The oocytes were placed in 105 mM sodium external solution as described above and seated in the central chamber positioned over a hole leading into the lower chamber. Next, the top chamber was placed on top of the oocyte so that the membrane of the oocyte protruded through the hole and into the top chamber. The top chamber was filled with 105 mM sodium external solution and the bridges were added. All data was collected using the pClamp 10 software (Molecular Devices, Sunnyvale, CA).

The voltage clamp on cut open oocyte (COVG) technique works as described in (Stefani E 1998), briefly, 3M KCl agar bridges with platinum wire are placed in wells containing an AgCl wire and 3M KCl and into each separate bath. The top bath receives three electrodes: the P1, P2, and CC electrode. These electrodes are used to clamp the membrane of the oocyte to the command potential and to minimize the capacitive transient. Two electrodes, GS1 and GS2 go into the central guard chamber. Their function is to prevent leak from the top chamber into the lower bath chamber by electrically isolating the chamber. Finally, the bottom chamber receives the I bridge which is the current injection electrode. The lower membrane of the oocyte which protrudes into the bottom bath chamber is permeabilized using a mild detergent and this allows the I current injection bridge access to the interior of the oocyte. A sharp recording

electrode, V1, filled with KCl and a AgCl wire is inserted through the top membrane of the oocyte and then the membrane may be clamped to the command potential (see Fig. 1 for a diagram of both TEV and COVG).

Essentially, the COVG technique improves on the TEV technique by decreasing the area of membrane that must be clamped and also by decreasing the resistance to the clamp via the permeabilization of the lower membrane. These two factors increase the speed of the clamp and allow the operator to measure processes with much more rapid kinetics than is usual with the TEV. Unless otherwise stated, all COVG experiments were conducted in 105 mM NMG internal solution (105 mM NMG, 20 mM HEPES, 2 mM EGTA, and MES to pH 7.4).

After the placing the bridges, the lower bath solution was exchanged with saponin in NMG internal solution (3 mg/ml saponin). After the lower membrane of the oocyte was permeabilized, the lower solution was exchanged several times with 105 mM NMG internal solution. Next, a sharp microelectrode containing an AgCl wire and 3M KCl at 0.2-0.7 MΩ resistance was inserted into the oocyte membrane. Using a CA-1B clamp; (Dagan Instruments, Minneapolis, MN), the membrane was clamped to -80mV. To minimize the capacitive transient, capacitance compensation was carried out at voltages stepping from -100 to -90 mV. We allowed the oocytes to equilibrate for 5 minutes at -80 mV and then ionic currents were collected.

Ionic currents were elicited utilizing a pulse protocol that applied a 50 ms prepulse to -120 mV followed by a 30 ms pulse train from -110 mV to 65 mV and then returning to -120 mV. This protocol reduced the capacitive transient using a P/-4

subtraction protocol with a subtraction holding potential of -120 mV. Traces were analyzed in Clampfit and then in Excel.

2.5.3 Gating pore current studies

Gating pore currents were collected in 105 mM sodium external solution (for DI-CN, DIV-CN, DIV-CN-Y401S, and D400C-E755C-DIV-CN) or 105 mM potassium external (composed similarly to sodium external) solution (DII-CN and DIII-CN). Following equilibration at -80 mV for 5 minutes, gating pore currents were collected using a protocol that applied test pulses from −160 to −70 mV for 60 ms following a 50-ms prepulse to −120 mV. In the case of the TTX and μ-CTX experiments, the channels were then blocked with either 0.6 - 1.1 μM TTX or 6 - 25.7 μM μ-CTX. Central pore currents were elicited by test pulses ranging from -80 to 70 mV for 60 ms in order to confirm block. After the channels were completely blocked (such that no central pore ionic current could flux), the gating pore currents protocol was re-run and the traces collected after toxin application were normalized with respect to the maximum gating pore current measured before toxin was applied (at -160 mV).

In the case of the disulfide crossbridge experiments with the D400C-E755C-DI, DII, DIII, or DIV-CN constructs, following injection the oocytes were stored in SOS with calcium storage solution and 100 μg/ml Gentamicin. No EDTA or DTT was added to the solution for these experiments. The absence of DTT allows for disulfide formation. After equilibration of the oocytes for 5 minutes at -80 mV, gating pore currents were elicited with the protocol described above and then the oocytes were treated with 2 mM H_2O_2 in order to maximize disulfide formation. Following the application of H_2O_2, the oocytes were held at -80 mV for 5 minutes before gating pore currents were collected again.

Following this protocol, the solutions in both the top and middle chambers were exchanged for 105 mM sodium external solution containing 1 mM of freshly made DTT. The oocytes were held at 5 minutes at -80 mV so as to allow the DTT to break the disulfide bonds and then the gating pore currents protocol described above was repeated. All steps of this protocol were further performed on the DI, DII, DIII, and DIV-CN mutants so as to verify that H_2O_2 and DTT do not have an effect on the gating pore currents of the mutants without the cysteines present.

We further investigated the effects of slow inactivation on the DIV-CN gating pore currents. These experiments were carried out by first pulsing the channels from -120 mV to -10 mV for 20 ms to measure the ionic current and then a pulse train from -160 to 60 mV was applied for 60 ms before returning to -120 mV for 20 ms. We next used a cumulative slow inactivation protocol (modified from protocols used by Cummins and Sigworth and Townsend and Horn)(Cummins and Sigworth 1996; Townsend and Horn 1997). For the 30 s cumulative slow inactivation protocol, the oocytes were held at -10 mV for 30 s before beginning the protocol described above. Additionally, the oocytes were also held at -10 mV for 30 s in between every voltage step.

For all gating pore current experiments, no p/n subtraction protocol was utilized meaning that the initial kinetics are likely to be contaminated by capacitive transient. Offline leak subtraction was utilized to subtract any significant linear leak. The offline leak subtraction protocol was performed by observing the linear leak at three subsequent potentials where there was no central pore or gating pore current. A line was fit to those data points and the equation of the line was used to calculate the leak at each potential.

2.5.4 OFF gating current experiments

In order to observe the effects of a particular toxin on the movement of the gating charges in the WT channel, it was necessary to obtain recordings both before and after toxin application. To study gating currents, it is necessary to block the central pore current of the channel using a toxin. Typically, the toxin used for these experiments is TTX. However, we needed information on the characteristics of gating charge movement *before* toxin was applied. In order to do this, we decided to inactivate the channels and then measure the OFF gating currents (ie. the currents resulting from the return of the voltage-sensors to their resting conformations). In the case of these experiments, the solutions used were 105 mM NMG internal and external solution in order to limit the presence of permeable ions. The rationale behind performing these experiments was that inactivating the channels and replacing much of the permeable ions with NMG would limit the amount of current fluxing through the central pore of the channel. Additionally, the OFF gating currents are in an inward direction and any current fluxing through the central pore of the channel would have to be in an outward direction because the only source of permeable ions comes from the potassium inside the oocyte itself.

For these experiments, following capacitive compensation and equilibration at -80 mV for 5 minutes, the OFF gating currents were collected in the absence of any toxin. The protocol used to elicit these currents consisted of a 50 ms pulse to -130 mV followed by a 30 ms pulse to 50 mV. Next, a 20 ms voltage step train was applied from -130 to 50 mV, followed by a return to -130 mV. It was also necessary to subtract the leak and minimize the capacitive transient via a p/4 subtraction with a subtraction holding potential of -130 mV. Following the measurement of these currents in the absence of

toxin, either 0.6 - 1.1 μM TTX or 6 - 25.7 μM μ-CTX was used to block the channels. Following a 5 minute equilibration at -80 mV the protocol described above was repeated.

In Clampfit, the raw traces were first baselined near the end of the test pulse waveform. Next, all OFF gating currents were analyzed by integrating the OFF gating current to get charge movement over time and then they were fit to a single Boltzmann equation of the form:

$$Q/Q_{max}(V) = 1/(1 + \exp(-ze(V - V_{1/2})/KT))$$

where $V_{1/2}$ is the half maximal voltage, z is the apparent valence, e is the electronic charge, K is the Boltzmann constant, and T is the temperature (the Boltzmann fits were obtained by using the Excel solver function to minimize the sum of squared errors). In order to effectively compare the OFF gating currents collected before toxin to those collected after toxin, the currents were collected in the same oocyte and those OFF gating currents collected after toxin application were normalized to those collected before toxin was added.

2.5.5 Steady state inactivation experiments

All steady state inactivation experiments were carried out in 105 mM sodium external solution and 105 mM NMG internal solution. For all experiments that follow, the DII-CN mutant that was used was the triple neutralization mutant and not the double mutant used in prior experiments. The voltage-dependence of fast inactivation was assessed using a protocol that first applied a 20 ms prepulse to -120 mV followed by a 20 ms voltage step train from -170 to 50 mV. Next, a 1 ms hyperpolarization to -120 mV to close non-inactivated channels was followed by a 30 ms test pulse to -30 mV to assess

the fraction of channels inactivated. All steady state inactivation data was fit to a single boltzmann equation.

2.5.6 Entry into fast inactivation experiments

As with the steady state inactivation experiments, all entry into fast inactivation experiments were carried out in 105 mM sodium external and 105 mM NMG internal solutions. To measure the kinetics of entry into fast inactivation, a protocol was used that applied a 20 ms prepulse to -120 mV followed by a variable duration (from 0.1 to 50 ms) inactivation pulse at the specified inactivation voltage (from -120 to 0 mV). The inactivation pulse was followed by a brief 1 ms hyperpolarization to -100 mV. At each time duration, the fraction of channels that had not inactivated was measured at a 0 mV test pulse for 30 ms immediately following the 1 ms hyperpolarization (see Fig. 2 A).

2.5.7 Recovery from fast inactivation experiments

Again, these experiments were carried out in 105 mM sodium external and 105 mM NMG internal solutions. The kinetics of recovery from inactivation were assessed via a protocol that applied a 20 ms prepulse to -120 mV followed by a 30 ms inactivating pulse to -20 mV, a variable length recovery pulse (from 0.1 to 40 ms) at the indicated voltage, and then a 30 ms test pulse to -20 mV to measure the fraction of channels that recovered from inactivation during the recovery interval (see Fig. 2 B).

2.5.8 ON gating current experiments

These experiments were carried out in 105 mM NMG external and internal solutions. Channels were blocked using 6 to 25.7 μM μ-CTX and then allowed to equilibrate at -80 mV for 5 minutes. Next, the channels were pulsed to -130 mV for 52 ms and then a voltage pulse train from -170 to 45 mV was applied for 20 ms before

returning the membranes to -130 mV. To eliminate leak and subtract the capacitive transient, p/4 subtraction was carried out from a subtraction holding potential of 50 mV. Following data collection, the ON gating currents were integrated in clampfit to give us the charge movement in time. This data was then plotted versus voltage in order to give us the ON gating current charge-voltage (Q-V) relationship. The Q-V curves were either fit to a single or a double Boltzmann equation in Excel.

2.6 Data Analysis

2.6.1 Fits of entry into and recovery from fast inactivation

Both the entry into and the recovery from fast inactivation data exhibit a typical lag before either entry or recovery begins. This lag time changes based on the entry or recovery voltage and it is a critical indicator of the inactivation behavior of the construct in question. In order to obtain numerical values for both the time constants and the lag phase, entry and recovery data for each construct were fit to a bi-exponential equation with a variable lag (t_0) or in the case of the DIV-CN recovery from inactivation data to a mono-exponential equation with a variable lag. The bi-exponential equation was of the form:

$$F(x) = A_1(1+e^{((t-t0)/\tau1)}) + A_2(1-e^{((t-t0)/\tau2)}) \times H(t_0)$$

where A_1 is the amplitude of the fast component and A_2 is the amplitude of the slow component , t is the time, t_0 is the lag time, τ_1 is the time constant of the fast component and τ_2 is the time constant of the slow component, and the step function $H(t_0) = 0$ for $t < t_0$ and 1 for $t \geq t_0$.The mono-exponential equation followed the form:

$$F(x) = A(1+e^{(t-t0)/\tau)}) \times H(t_0)$$

where A is the amplitude, t is the time, t_0 is the lag time, τ is the time constant, and the step function $H(t_0) = 0$ for $t < t_0$ and 1 for $t \geq t_0$. These fits were performed using Matlab (Mathworks, Natick, MA).

2.6.2 Plotting graphs, testing significance, and figure building

Either Excel, Origin (OriginLab Northampton, MA), or Prism (GraphPad Software, La Jolla, CA) were used to plot all graphs. The error bars represented in each graph represent the standard error of the mean and for each experiment, there was a minimum of three separate tests. In all cases, figures were constructed using the Adobe Illustrator 10 program (San Jose, CA). Significance was determined using the Excel Analysis software and more specifically the student's t test with either paired or unpaired variables as appropriate.

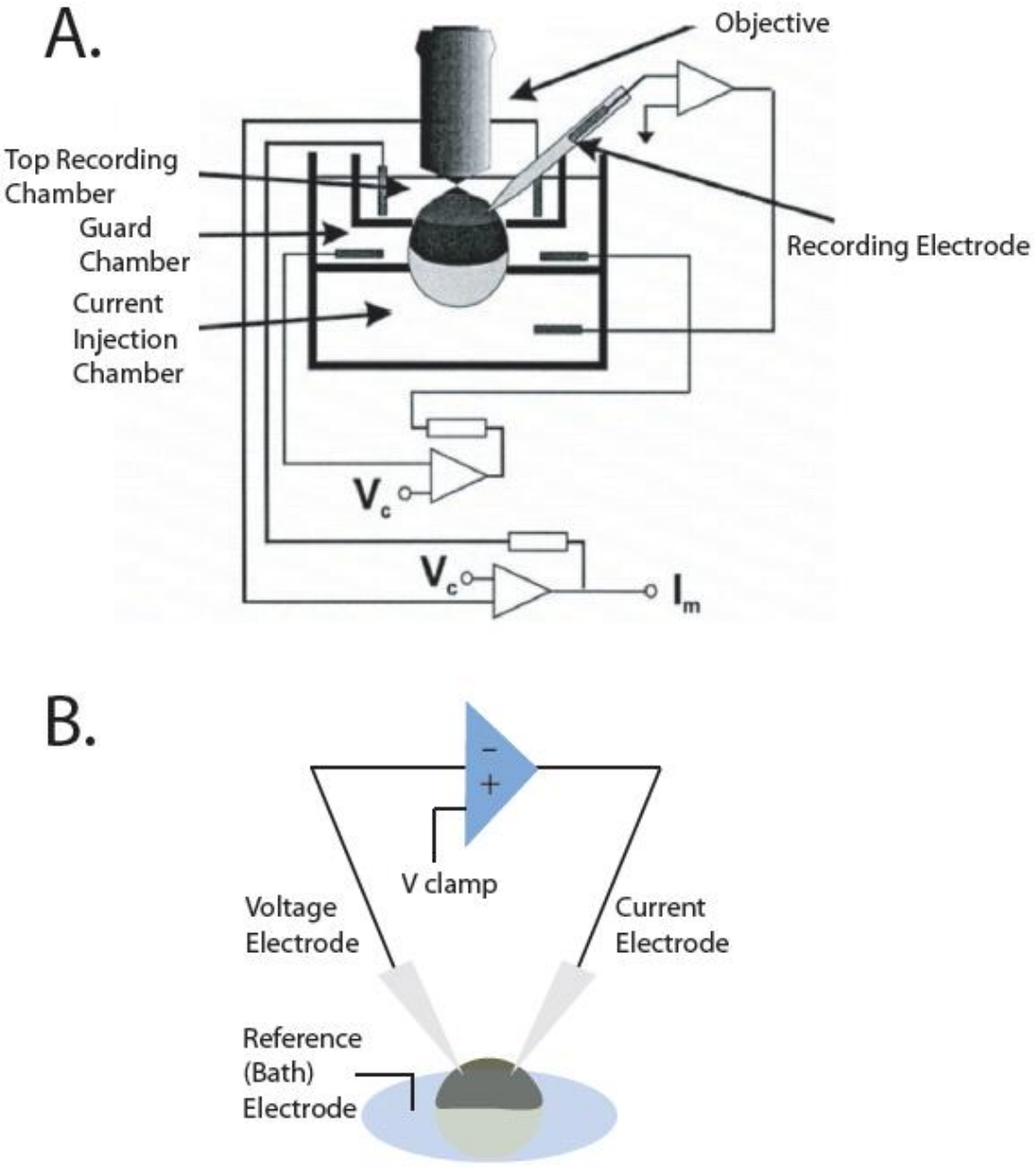

Figure 1: Diagrams depicting the voltage-clamp on cut open oocyte and the two electrode voltage clamp setups. (A) A schematic showing the basic setup for voltage clamp on cut open oocyte. **(B)** A diagram showing the two electrode voltage clamp setup.

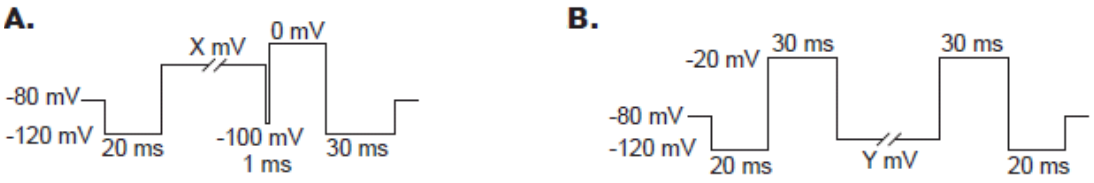

Figure 2: Entry and recovery from fast inactivation protocols.

(A) Pulse protocol for entry into inactivation where 'X' is varied by both time and voltage as specified. **(B)** Recovery from inactivation protocol where the recovery interval 'Y' is varied by both time and voltage as specified.

CHAPTER III

Determining the Connectivity Between the Selectivity Filter and the Voltage-Sensors

3.1 INTRODUCTION

The linkage between the voltage-sensors and the inner pore gate has been well-characterized. This canonical mode of coupling grants voltage-sensitivity to the channel opening process. However, there are important gating processes that involve other structures and regions of the channel. For example, the process of fast inactivation involves the inactivation loop, connecting domains III and IV, plugging the main pore of the channel from the inside (Armstrong, Bezanilla et al. 1973; Stühmer W 1989; West, Patton et al. 1992; Kirsch, Alam et al. 1994). Another gating process called slow inactivation is thought to resemble C-type in activation in potassium channels in which the selectivity filter region of the channel collapses and constricts the outer pore region of the channel (Lopez-Barneo, Hoshi et al. 1993; Liu, Jurman et al. 1996; Cordero-Morales, Cuello et al. 2006; Cordero-Morales, Cuello et al. 2006; Cuello, Jogini et al. 2010). Slow inactivation functions to set the waveform pattern in the brain by diminishing the long term availability of sodium channels under conditions of frequent firing (Fleidervish, Friedman et al. 1996). Additionally, slow inactivation is a natural brake to terminate aberrant excitation such as that which you would find during epilepsy, arrhythmias, and states during which the membrane is partially depolarized (as in ischemia).

Like activation and fast inactivation, slow inactivation is a voltage-dependent process (Schauf, Pencek et al. 1976). However, it is controversial whether the voltage-dependence of slow inactivation derives from its coupling to activation or through direct

coupling to one or more voltage-sensors. Previous work has shown that there is a voltage-sensor mode shift in which the charge-voltage (Q-V) curve of the channel is shifted to more hyperpolarized potentials after the membrane has been held at depolarized potentials for extended periods (Bezanilla, Taylor et al. 1982). A correlation was drawn between this voltage-sensor mode shift and the process of slow inactivation in potassium channels, suggesting that the change in voltage-sensor conformation triggered the slow inactivation process (Olcese, Latorre et al. 1997). While this is an attractive hypothesis, later studies from the same group revealed that the voltage-sensor mode shift was in fact an intrinsic property of the voltage-sensor. When an isolated voltage-sensor (Ci-VSP) was expressed, the authors determined that holding the membrane at a positive potential for an extended time caused a similar leftward shift in the Q-V curve of Ci-VSP (Villalba-Galea, Sandtner et al. 2008). It is still unclear whether or not the voltage-sensors are involved in triggering slow inactivation. In order to shed some light on this controversy, we elected to monitor the movement of individual voltage-sensors as we altered the conformation of the outer pore region.

The standard methods of observing voltage-sensor movement would be inappropriate in this study. The most common method for observing voltage-sensor movement is through the measurement of gating currents. Gating currents are the capacitive current generated by the movement of the charges of *all* the voltage-sensors across the membrane electric field. However, gating currents are typically recorded in the presence of an outer pore blocking toxin which in and of itself could alter the structure of the outer pore. The other obvious method for tracking the individual voltage-sensors is via the measurement of voltage-dependent changes in fluorescence from a probe attached

to a cysteine engineered into specific voltage-sensors. While voltage-clamp fluorimetery is a useful tool in understanding the role of the voltage-sensors, it has a crucial limitation. Perhaps the most critical problem in analyzing voltage-clamp fluorimetry data arises from the size of the fluorophore itself. Because environment sensitive probes such as Tetramethylrhodamine maleimide (TMRM) are large molecules, they have a tendency to monitor the conformational changes not only in the voltage-sensor, but also in neighboring regions of the protein as well. TMRM is large enough that it would possibly measure conformational changes both in the voltage-sensor and the pore. In order to detect any coupling between the voltage-sensor and the pore, we must be able to monitor the conformational changes of specific voltage-sensors separately from conformational changes in the pore. Due to these limitations, we utilized another method of tracking voltage-sensor movement called gating pore currents.

The voltage-sensors are hypothesized to move through aqueous or proteinaceous cavities referred to as gating pores (Islas and Sigworth 2001; Sokolov, Scheuer et al. 2005; Sokolov, Scheuer et al. 2007; Sokolov, Scheuer et al. 2010). At the narrowest point of the gating pore is the gating pore septum and at this region, the positive charges of the voltage-sensor act as a cork in the bottle that blocks the gating pore to permeation by any ions. Gating pore currents, also called omega currents, result from mutating one or more of the positively charged residues in the voltage-sensor and thus allowing ions to flux through the gating pore. These omega currents only flux when the mutated voltage-sensor is in a permissive position and as soon as the voltage-sensor moves out of position, the gating pore currents shut down. Thus, gating pore currents are a reliable conformational

indicator for the mutated voltage-sensor and any change in the voltage-dependence of voltage-sensor movement will result in altered gating pore currents.

We constructed mutants in which either the first two or three charges in one voltage-sensor at a time were neutralized to glutamine. These charge neutralization (CN) mutants exhibit ionic currents which are not blocked by the central pore blocker tetrodotoxin (TTX) and they are only active at hyperpolarized potentials at which the voltage-sensor is in its resting position. We used these currents to accurately report a specific mutant voltage-sensor's movement as we perturbed the conformation of the outer pore of the sodium channel with outer pore blockers and disulfide bonds. We hypothesized that altering the conformation of the selectivity filter region should result in changes in the gating pore currents of a voltage-sensor only if that voltage-sensor was coupled to the outer pore of the channel.

3.2 RESULTS

3.2.1 *Design and characterization of the charge neutralization mutants*

Design of the CN mutants in Nav1.4 was partially motivated by the recent discovery that mutations of specific residues in the S4 segments allow state-dependent ion flux through the voltage-sensors. In particular, it was observed that the neutralization of two paired charges in the DII voltage-sensor resulted in gating pore currents (Sokolov, Scheuer et al. 2005). For each domain mutant (ex. DI-CN), we neutralized the first three charges (the first two in DII) by mutating them to glutamine. All four CN mutants (the S4 sequences are shown in Fig. 1A) were functional (Fig. 1B) and we observed inward gating pore currents at hyperpolarized potentials that were not blocked by TTX (Fig. 2 and Fig. 3). Central pore currents were collected in 105 mM sodium external solution

(DI-CN, DIV-CN, and DIV-CN Y401S), in 52.5 mM sodium external solution (DII-CN), or 105 mM potassium external (DIII-CN) and 105 mM N-methyl D-glucamine (NMG) internal solution (for full composition, see Chapter II, 2.5.1). Central pore currents were elicited by test pulses ranging from -80 to 70 mV for 60 ms. Gating pore currents were collected either in 105 mM sodium external solution and 105 mM NMG internal solution (DI and DIV) or 105 mM potassium external solution and 105 mM NMG internal solution (DII and DIII) (see Chapter II, 2.5, for complete composition). The gating pore currents were elicited by test pulses from -160 mV to -80 mV for a duration of 60 ms (see Chapter II, 2.5.3).

3.2.2 *Effects of TTX and μ-CTX on the gating pore currents of DI, DII, DIII, and DIV*

To investigate the coupling between the voltage-sensors and selectivity filter region, we first attempted to perturb the conformation of the outer pore with TTX. TTX is an outer pore blocker known to bind close to the selectivity filter of the channel (Backx, Yue et al. 1992; Satin, Kyle et al. 1992; Leffler, Herzog et al. 2005; Zhang, McArthur et al. 2009; Zhang, Gruszczynski et al. 2010) and it is the toxin most commonly used in the recording of gating currents. We compared the gating pore currents of each domain both before and after concentrations of TTX (up to 1.1μM) at which the central pore was completely blocked (see Fig. 4). As expected, TTX did not block the gating pore currents through the CN mutants (see Fig. 3). Though TTX has little effect on the gating pore currents of DI, DII, or DIII, it causes a significant reduction in the gating pore currents through DIV-CN. The amplitude of the current was reduced by as much as 74% at -110 mV ($p<0.05$). Increasing the concentration of TTX

up to ten fold caused no further inhibition of the DIV-CN gating pore currents (see Fig. 5). This suggests that the TTX effect on DIV-CN is maximal.

TTX alters the DIV gating pore currents under conditions where the central pore currents are completely blocked (see Fig. 4), however, there are two alternative explanations as to how TTX is affecting the DIV voltage-sensor. One explanation is that TTX alters the DIV voltage-sensor's behavior after binding to its site in the main pore of the channel. The alternate explanation is that TTX binds to the DIV-CN voltage-sensor and directly blocks the gating pore currents. In an attempt to disprove this second explanation, we constructed the DIV-CN mutant in the background of a mutation that renders the channel nearly insensitive to TTX block (Y401S). The Y401S mutation is next to the selectivity determining DEKA locus (Heinemann, Terlau et al. 1992; Chiamvimonvat, Perez-Garcia et al. 1996; Favre, Moczydlowski et al. 1996; Perez-Garcia, Chiamvimonvat et al. 1997; Huang, Favre et al. 2000) and this residue is known to be critical for TTX binding (Backx, Yue et al. 1992; Satin, Kyle et al. 1992). We hypothesized that if TTX exerted its effect on the DIV voltage-sensor from its binding site in the selectivity filter, then TTX would have no effect on the Y401S DIV-CN mutant. TTX had no effect on the gating pore currents through the DIV voltage-sensor in the Y401S DIV-CN mutant and therefore must be bound to its site in the central pore in order to alter the behavior of the DIV voltage-sensor (see Fig. 6).

TTX is a positively charged toxin with a net charge of +1 at physiological pH. Therefore, we tested whether TTX was affecting the DIV voltage-sensor via a direct electrostatic interaction or by an allosteric mechanism. In an attempt to discriminate between these two possible mechanisms, we selected a much more highly charged outer

pore blocker, μ-conotoxin (μ-CTX). At physiological pH, μ-CTX has a net nominal charge of +6 and therefore, we would hypothesize that if the effect of TTX on the DIV voltage-sensor is mediated via electrostatics then μ-CTX should have an even greater impact on the DIV-CN gating pore currents.

We applied μ-CTX to each of the CN mutants at concentrations sufficient to completely block the central pore (up to 25.7 μM) (see Fig. 7) and observed that μ-CTX did not affect the gating pore currents of DI, DII, and DIII. Additionally, μ-CTX application resulted in a much smaller reduction (16% at most) in the DIV-CN gating pore currents (see Fig. 8).

We further analyzed the gating pore current data by plotting residual gating pore currents after toxin versus voltage and found that the μ-CTX inhibition of the DIV gating pore currents is voltage independent, but this is not the case for the TTX inhibition of DIV gating pore currents (see Fig. 9). The TTX inhibition of the DIV-CN gating pore currents is more marked at depolarized potentials and because these experiments are done at concentrations of TTX where the central pore is completely blocked, the voltage-dependence exhibited here can't be due to the voltage-dependence of TTX binding to the pore.

3.2.3 *The effect of TTX and μ-CTX on the OFF gating currents of wildtype sodium channel*

The previous experiments were all conducted in a mutant background, leaving open the possibility that the coupling observed between the outer pore and the DIV voltage-sensor exists only in the mutant DIV-CN background. To eliminate this as a

possibility, we measured the effect of TTX on a wildtype (WT) sodium channel background.

To measure gating currents, the central pore of the channels is blocked using a toxin such as TTX or μ-CTX. The block of the central ion conductance allows for the gating currents to be isolated. However, we needed to measure the gating currents both before and after toxin block in order to detect any changes in voltage-sensor behavior induced by the toxin. Therefore, we elected to inactivate the channels with a 30 ms step to 50 mV. Next, we applied a voltage pulse train from -130 to 50 mV to measure the OFF gating currents (the capacitive transient generated by the voltage-sensors moving back to their resting position). The experiments were conducted in 105 mM NMG external and internal (for full protocol and solution composition see Chapter II, 2.5). We recorded well defined non-linear charge movements without pore blockers and when we integrated these OFF gating currents to get a Q-V curve, it was saturated on both ends (see Fig. 10) meaning that there was minimal ionic contamination.

We compared the WT OFF gating currents before and after the application of saturating concentrations of TTX and we found that the total OFF gating charge was reduced by 24% (Fig. 11). Unlike TTX, μ-CTX caused no reduction in the total OFF gating charge. This is consistent with the minimal effect of μ-CTX on the gating pore currents of DIV-CN. When recording these OFF gating currents, it was necessary to apply a p/-4 subtraction at a holding potential of -130 mV in order to separate the OFF gating currents from the capacitive transient. Since the leak subtraction was implemented at -130 mV, if there was a shift in the Q-V curve to more hyperpolarized potentials, this could result in a fraction of the OFF gating current being subtracted erroneously.

Therefore, due to subtraction, a decrease in the total charge of the OFF gating currents could in fact represent a leftward shift in the Q-V curve.

3.2.4 *The effect of a disulfide bond in the selectivity filter on gating pore currents*

Though the above results supported the existence of coupling between the outer pore region and the voltage-sensor of DIV, all of these experiments were done in the presence of TTX. Therefore, it was essential that we determine whether the coupling between the selectivity filter region and the DIV voltage-sensor was present under normal physiological conditions or was an artifact induced by the binding of TTX. For this reason, we began searching for a way to perturb the conformation of the outer pore without using a pore blocking toxin.

Balser et al. discovered that mutating both D400 and E755 to cysteine resulted in a mutant channel with the ability to form a spontaneous disulfide that blocked off all ionic currents through the central pore. When the D400C/E755C disulfide bond was broken using a reducing agent, the central pore ionic currents were recovered (Benitah, Ranjan et al. 1997; Tsushima, Li et al. 1997; Ong, Tomaselli et al. 2000; Xiong, Li et al. 2003; Xiong, Farukhi et al. 2006). This disulfide bond is in the DEKA selectivity filter and is also near the TTX binding site and therefore was ideal for altering the conformation of the outer pore. We hypothesized that a disulfide bond in the selectivity filter might prevent structural rearrangements and unmask intrinsic conformational coupling between the selectivity filter and the voltage-sensors.

We constructed D400C/E755C in the background of the DI, DII, DIII, and DIV-CN mutants and measured gating pore currents in the presence and absence of the disulfide bond. In our hands, the D400C/E755C mutants frequently exhibited small

residual ionic currents through the central pore and therefore we added 2-4 mM H_2O_2 to maximize disulfide formation (see example currents for DIV-CN in Fig. 12). In reducing conditions (1 mM dithiothreitol, DTT), we observed robust sodium currents upon depolarization for all of our mutants. We compared the gating pore currents of DI, DII, DIII, and DIV-CN both in oxidizing and reducing conditions (for the full solution compositions, check Chapter II, 2.5) and found that a disulfide bond in the selectivity filter had no effect on the omega currents of the D400C/E755C DI, DII, or DIII as compared to control. However, the gating pore currents of D400C/E755C DIV-CN increased substantially when the disulfide bond was reduced in DTT (70% at -140 mV) (Fig. 13). The gating pore currents of the DI, DII, DIII, and DIV-CN controls without the cysteine mutations were minimally affected by either H_2O_2 or DTT showing that the observed effects are due to the disulfide bond.

3.2.5 *The effects of slow inactivation on the DIV-CN gating pore currents*

Though we could say confidently that the selectivity filter region was conformationally coupled to the DIV voltage-sensor, we had no solid information to link this conformational transition to the process of slow inactivation. In an attempt to draw a parallel between slow inactivation and the DIV voltage-sensor, we chose to measure the DIV-CN gating pore currents both before and after slow inactivation.

We first recorded the gating pore currents of DIV-CN using a holding potential of -80 mV and the channels were pulsed from -120 to -10 mV for 20 ms in order to measure ionic currents. Directly after this pulse, a 60 ms voltage step train from -160 to 60 mV was applied in order to measure the gating pore currents and then the membrane was returned to -120 for 20 ms. Due to the long length of the slow inactivation protocol, we

chose to use a cumulative slow inactivation procedure modified from protocols developed by others (Cummins and Sigworth 1996; Townsend and Horn 1997). To slow inactivate the channels, we held the oocytes at -10 mV for 30s and re-applied the protocol above. In between every voltage pulse, the oocytes were returned to the -10 mV holding potential for 30 s. We found that the gating pore currents of DIV-CN reduce after slow inactivation (Fig. 14). To see whether this decrease in DIV-CN gating pore currents was reversible, we allowed the channels to recover at -80 mV for 10 minutes and we found that during this time, the gating pore currents begin to recover (though it should be noted that the recovery from slow inactivation is incomplete) (Fig. 14; Recovery).

Taken together, our results suggest a possible role for the DIV voltage-sensor in the process of slow inactivation. However, this experiment can't narrow out the possibility that the reduction in the DIV gating pore currents could be due to an intrinsic voltage-sensor mode shift at depolarized potentials. In order to properly characterize the role of the DIV voltage-sensor in the process of slow inactivation, it would be necessary to characterize the Q-V curves of the isolated DIV voltage-sensor before and after holding at depolarized potentials, but these experiments are beyond the scope of this work.

3.3 DISCUSSION

It is very well established that the voltage-sensors are connected to the activation gate. When the local membrane potential depolarizes, the voltage-sensors move into their activated positions and cause the activation gate of the channel to open. The activation gate of voltage-gated ion channels is thought to be on the intracellular side of the channel. State dependent MTS accessibility studies on the potassium channel have pinpointed the

location of the activation gate to the intracellular face of the pore (Liu, Holmgren et al. 1997). Additionally, crystal structures both for potassium channels and for a bacterial voltage-gated sodium channel suggest an intracellular location for the activation gate (Long, Campbell et al. 2005; Payandeh, Scheuer et al. 2011). Therefore, the coupling between the intracellular pore and the voltage-sensors has become a mainstream idea. Though the coupling between the voltage-sensors and the inner pore of the channel has long been accepted in the field, there is little concrete evidence to suggest that there are voltage-sensors coupled to the selectivity filter region of the channel.

To approach this question, we used mutations that resulted in domain specific gating pore currents through the voltage-sensors as conformational indicators. While monitoring the behavior of one voltage-sensor at a time, we perturbed the structure of the selectivity filter region of the channel. We reasoned that should a voltage-sensor be coupled to the outer pore of the channel, we should be able to observe changes in the behavior of that voltage-sensor on modification of the structure of the selectivity filter region.

We found that TTX, resulted in a large decrease in the gating pore currents through the fourth voltage-sensor. In order to exert its effect, TTX must bind to its site in the central pore of the channel. Additionally, TTX inhibited the gating pore currents of DIV more effectively at depolarized potentials. Because gating pore currents shut off when the voltage-sensor in question activates, this would suggest that TTX biases the voltage-sensor of DIV to its activated state. Unlike TTX, μ-CTX caused only a small reduction in the DIV gating pore currents (16% versus the 65% induced by TTX). The effect of μ-CTX was voltage-insensitive with a static inhibition at all voltages. We further

found that TTX, but not μ-CTX, reduced the total gating charge of the WT OFF gating currents.

It might seem surprising that two outer pore blockers should exhibit such widely different effects on the voltage-sensors. However, there are differences between the two toxins in terms of size and binding sites. TTX binds more deeply into the pore of the channel with a critical interaction residue (Backx, Yue et al. 1992; Satin, Kyle et al. 1992) being right above the selectivity-determining DEKA locus (Heinemann, Terlau et al. 1992; Favre, Moczydlowski et al. 1996; Perez-Garcia, Chiamvimonvat et al. 1997; Huang, Favre et al. 2000). On the other hand, μ-CTX is a large peptide toxin and is unable to bind as deeply in the pore as TTX (Zhang, McArthur et al. 2009; French, Yoshikami et al. 2010; Zhang, Gruszczynski et al. 2010). We suggest that the closer proximity of TTX to the selectivity filter is at least partially responsible for its greater effects on the DIV voltage-sensor.

In relation to the toxins, it should also be noted that these experiments suggest that the measurement of gating currents through the use of TTX as a pore blocker is not appropriate. Our data suggest that TTX modifies the very phenomenon it has been used so thoroughly to study. Though μ-CTX also causes an alteration of the DIV voltage-sensor behavior, this is by comparison, a relatively small effect.

We also observed that slow inactivation caused a reduction in the gating pore currents of DIV. These results and those previous potentially put forth the DIV voltage-sensor as a source for the voltage-dependence of the slow inactivation process. However, our results do not rule out the explanation that the reduction in DIV gating currents caused by long depolarizations might be due to a separate voltage-sensor mode shift

process. That said, these data suggest that the DIV voltage-sensor may represent an attractive target for drugs developed to alter the slow inactivation process.

In the course of these experiments we also determined that disulfide crosslinking two of the DEKA residues resulted in a specific reduction of the DIV-CN gating pore currents. This effect could be reversed by applying DTT to reduce the disulfide bond. This last piece of data is critical in that it proves that the effects we have been measuring on the DIV voltage-sensor are not solely a property of TTX itself. Therefore, we conclude that the DIV voltage-sensor is coupled to the selectivity filter region of the sodium channel in its native state.

Regardless of the potential for the DIV voltage-sensor to play a role in slow inactivation these data are an important finding. To our knowledge, these data are the first solid evidence for the existence of non-canonical voltage-sensor to pore coupling. In addition to the traditional voltage-sensor to inner pore gates coupling, sodium channels exhibit coupling of a voltage-sensor to the outer pore. Such findings add another layer of complexity to the functioning of the heterologous sodium channel and indeed, perhaps differential coupling in the unique domains may underlie the functional specialization of each domain and allow for far more intricate gating behavior than was originally deemed possible.

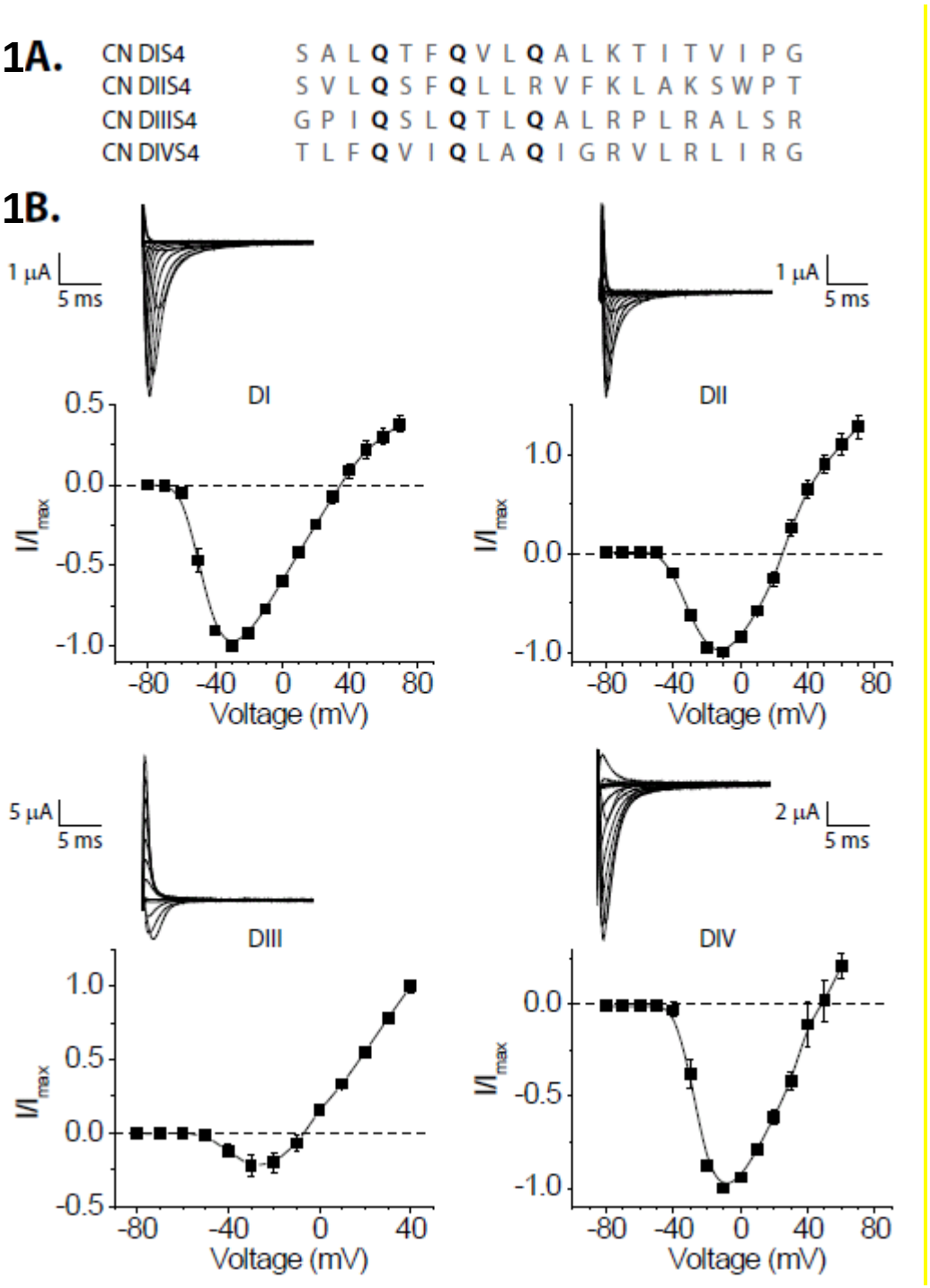

Figure 1: Functionality of the charge neutralized sodium channel mutants. (A) The sequence of the altered S4 segments of all four mutants. The sites which were mutated to glutamines are shown in red. **(B)** Current-voltage relationships for each of the mutants with a representative family of traces are shown. Each graph represents the mean ± SE of

at least three independent experiments. Also note that the ionic currents at more depolarized potentials are, in some cases, contaminated by gating currents.

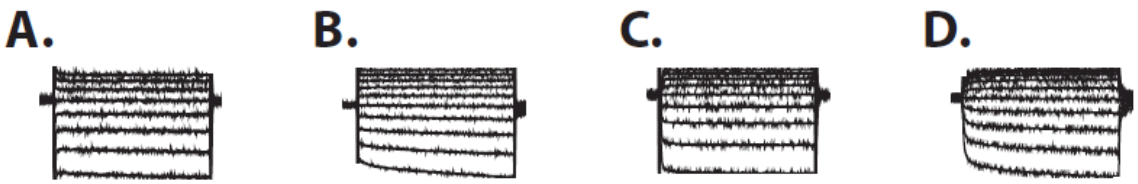

Figure 2: Charge neutralizations in the voltage-sensors generate gating pore currents. (A) Example gating pore currents through the altered DI-CN voltage-sensor. **(B)** Gating pore currents generated via neutralizations in the DII-CN voltage-sensor. **(C)** DIII-CN gating pore currents shown as above. **(D)** Gating pore currents through the mutated DIV voltage-sensor in DIV-CN.

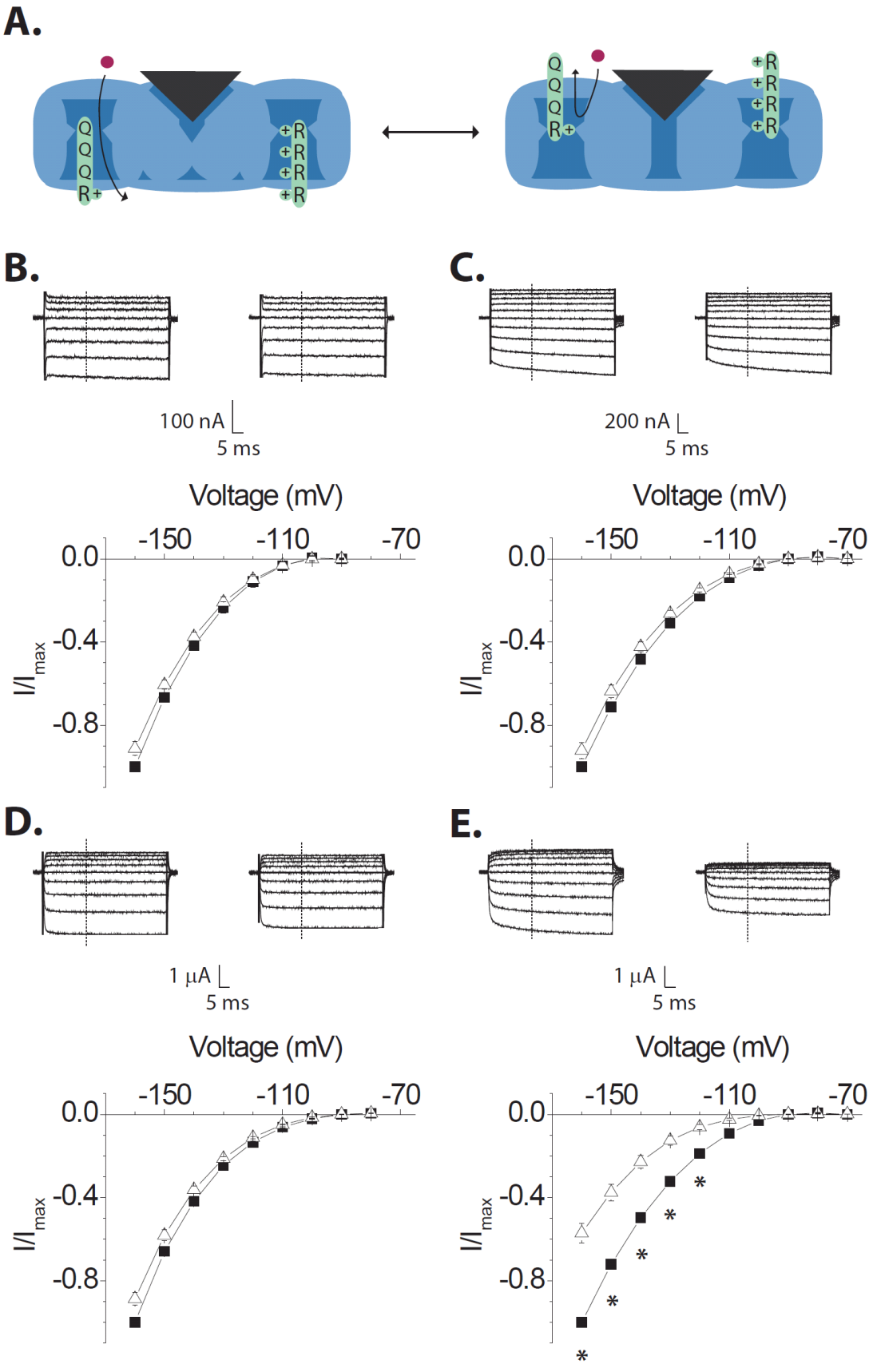
A.
Q
Q
Q
R+
+R
+R
+R
+R
B.
100 nA
5 ms
C.
200 nA
5 ms
Voltage (mV)
-150
-110
-70
0.0
-0.4
-0.8
I/I max
D.
1 µA
5 ms
E.
1 µA
5 ms
*

Figure 3: Effect of TTX on gating pore currents through the individual voltage-sensors. (A) A schematic diagram depicting the conformational processes that produce voltage-dependent gating pore currents. The left panel shows the channel where the main pore is closed and the voltage-sensors are in a resting conformation. In this condition, the mutant voltage-sensor is in a permissive position for gating pore currents. Currents through the central pore are blocked by a pore toxin. The right panel depicts the channel with the voltage-sensors in an activated conformation and the remaining charges in the mutant voltage-sensor move into a position that blocks the flux of gating pore current. A family of gating pore currents before (left; filled square) and after (right; unfilled triangle) addition of TTX from the DI-CN **(B)**, DII-CN **(C)**, DIII-CN **(D)** and DIV-CN **(E)** mutants **(Top)**. Normalized current-voltage plots of the same **(Bottom)**. The currents at each voltage were measured at the end of 20 ms, marked as a dashed line in the figure. Each plot represents the mean ± SE of at least three independent experiments. Asterisks denote statistical significance with a p-value of less than 0.05.

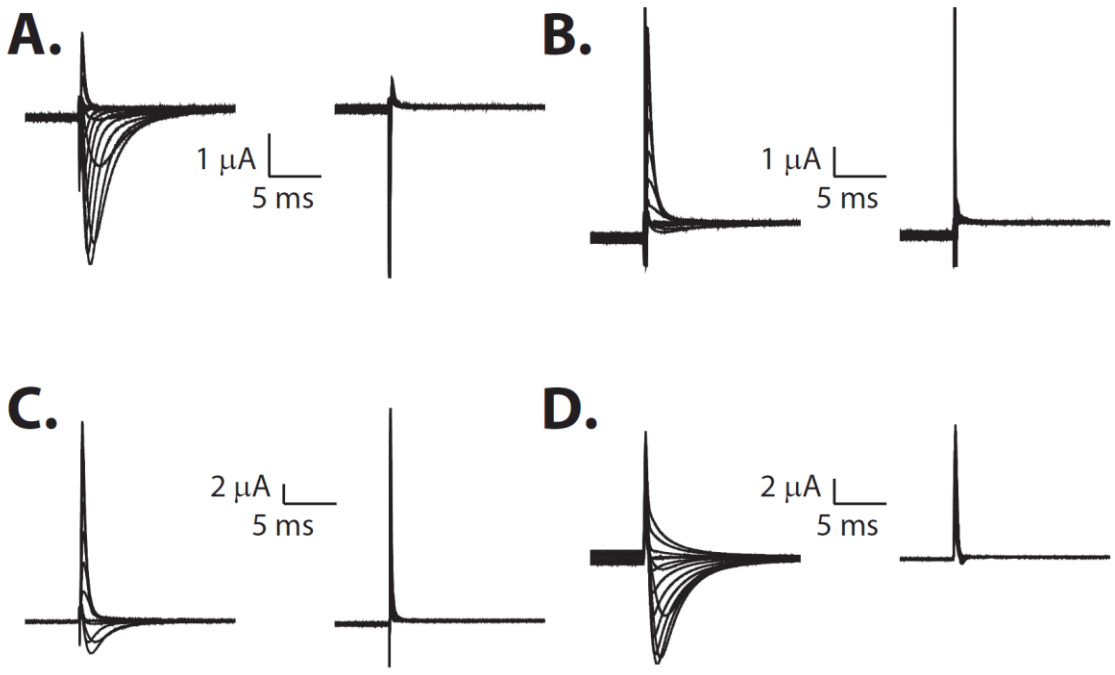

Figure 4: Tetrodotoxin completely blocks the central pore currents through the CN mutants. A family of ionic currents elicited by depolarization before (left) and after (right) addition of TTX for DI-CN **(A)**, DII-CN **(B)**, DIII-CN **(C)** and DIV-CN **(D)**. DI-CN and DIV-CN were recorded in the presence of 105 mM Na^+-Mes external solution whereas DII-CN and DIII-CN were obtained in presence of K^+-Mes external solution. The pulse protocol used was same as reported in Chapter II (2.5.3).

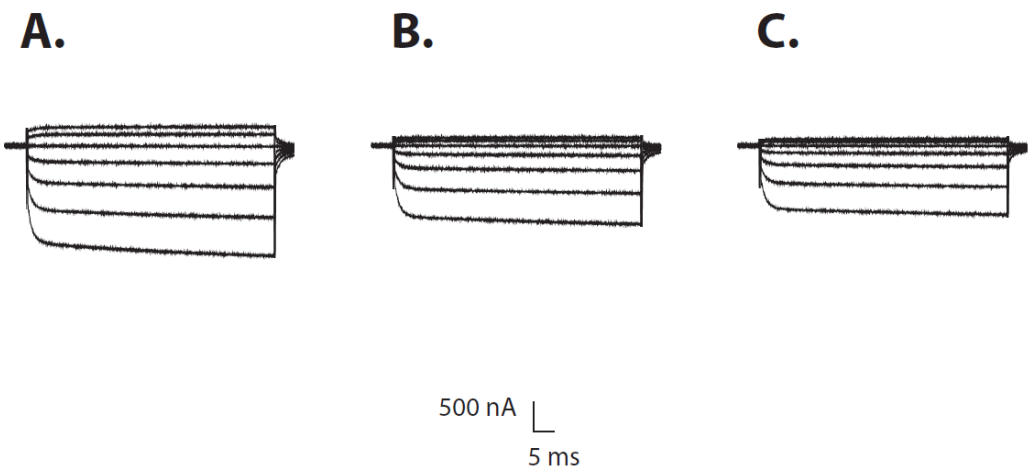

Figure 5: Effect of increasing concentrations of TTX on DIV-CN gating pore currents. A family of DIV-CN gating pore currents before TTX addition **(A)**, in 1 μM TTX **(B)**, and in 10 μM TTX **(C)**. Gating pore currents were recorded in the presence of 105 mM Na^+-Mes external solution. The pulse protocol used was same as reported in the methods.

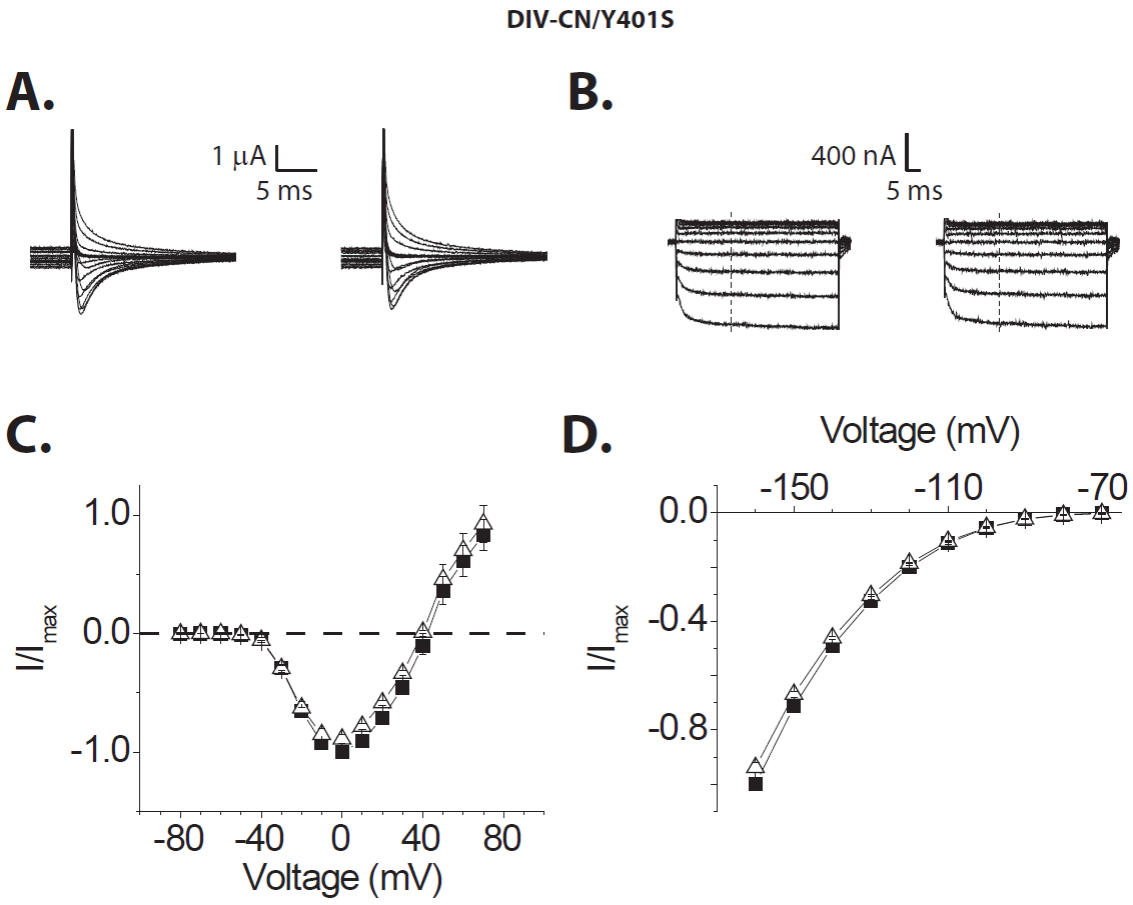

Figure 6: TTX does not inhibit gating pore currents of the DIV-CN/Y401S mutant. **(A)** A family of DIV-CN/Y401S traces shown before (left) and after (right) TTX application (Top). **(B)** A family of gating pore currents before (left) and after (right) addition of TTX from the DIV-CN/Y401S mutant (above). **(C)** Current-voltage (I-V) relationship of the DIV-CN/Y401S mutant in absence (unfilled triangle) and presence (filled square) of TTX. The voltage protocol is the same as in the methods. Data was collected in the presence of 105 mM Na^+-Mes external solution. **(D)** Normalized current-voltage plots of the gating pore currents from the DIV-CN/Y401S mutant before (filled square) and after (unfilled triangle) addition of TTX. The currents were recorded in the presence of 105 mM Na^+-Mes external solution using voltage protocols described in the

Chapter II (2.5.3). The currents were normalized to the maximum current measured before toxin, typically at -160 mV. The currents at each voltage were measured at the end of 20 ms, marked as a dashed line (B). Each current-voltage plot represents the mean ± SE of four experiments.

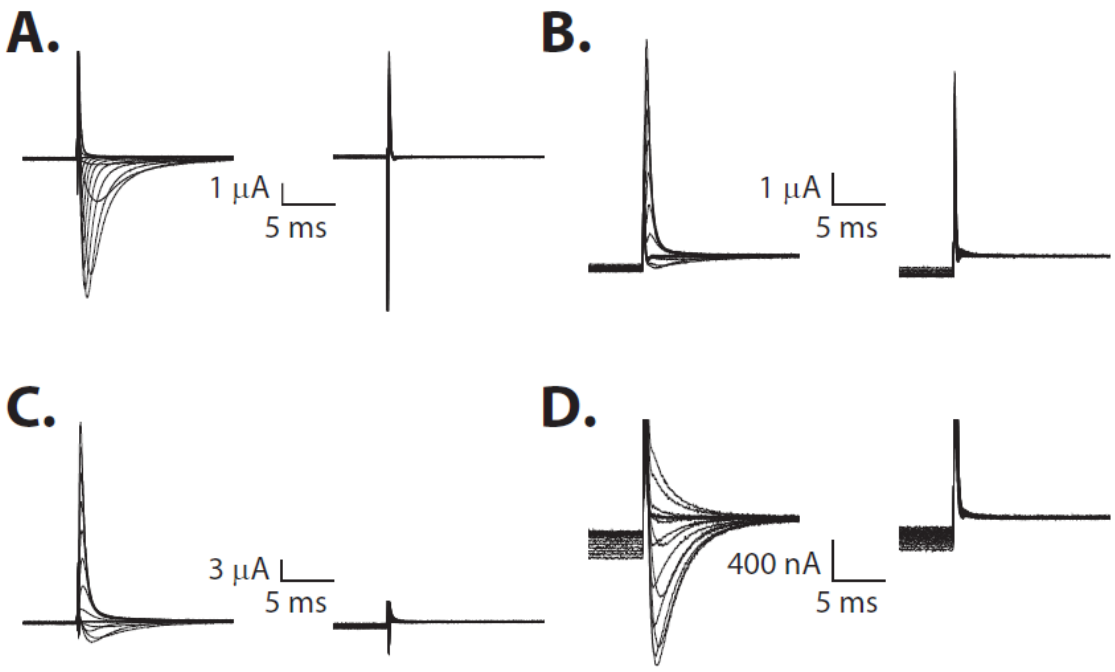

Figure 7: µ-conotoxin completely blocks the central pore currents of the CN mutants. Example ionic current traces elicited by depolarization before (left) and after (right) addition of µ-CTX for DI-CN **(A)**, DII-CN **(B)**, DIII-CN **(C)** and DIV-CN **(D)**. As before, the ionic currents of DI-CN and DIV-CN were recorded in the presence of 105 mM Na^+-Mes external solution whereas those for DII-CN and DIII-CN were obtained in presence of K^+-Mes external solution. The pulse protocol used was same as reported in Chapter II (2.5.3).

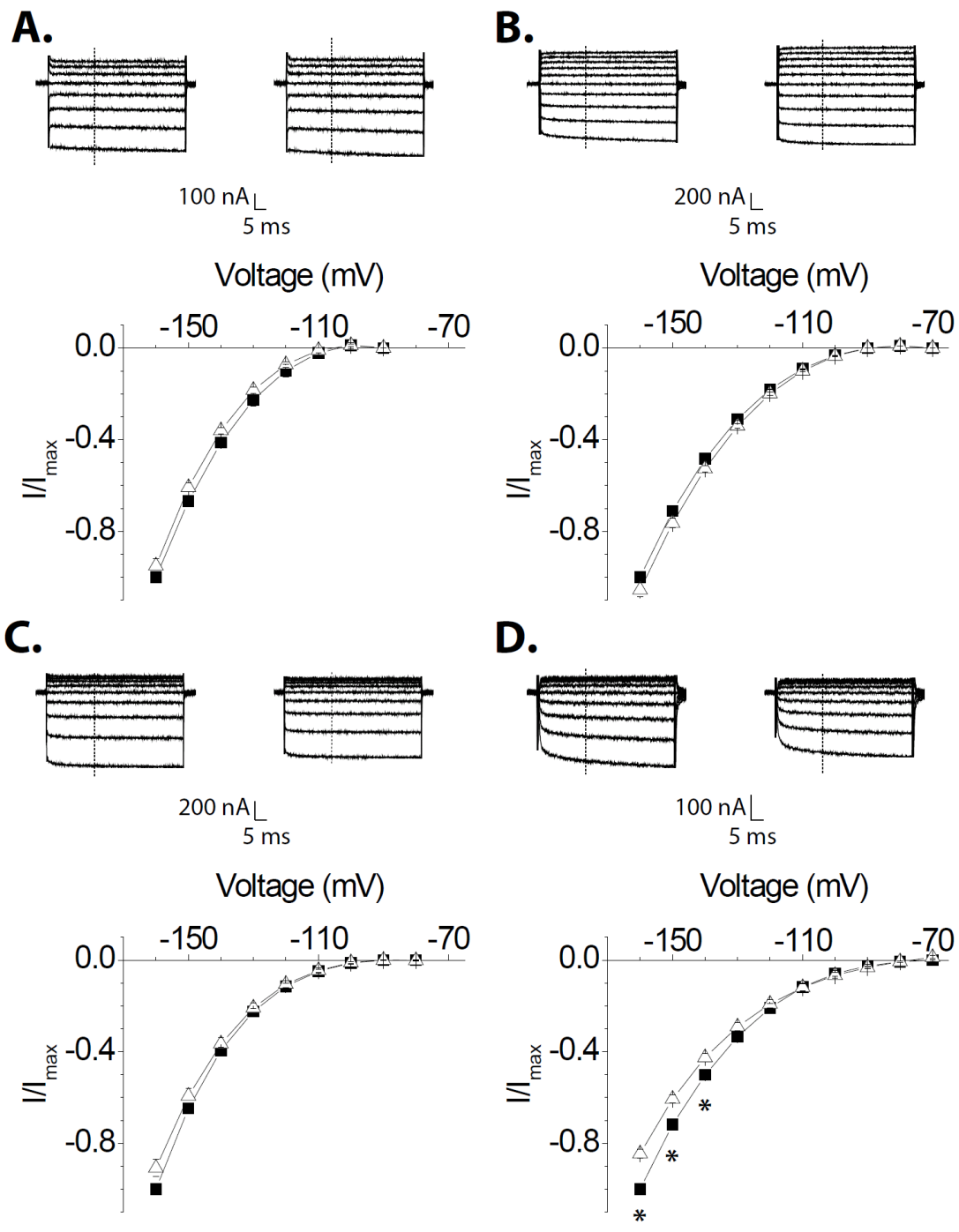

Figure 8: Effect of μ-CTX on gating pore currents through the individual voltage-sensors. A family of hyperpolarization activated currents before (left; filled square) and after (right; unfilled triangle) addition of μ-CTX from the DI-CN **(A)**, DII-CN **(B)**, DIII-CN **(C)** and DIV-CN **(D)** mutants **(Top)**. Normalized current-voltage plots of the same

(Bottom). The currents were recorded and normalized following the protocol described in the methods. The currents at each voltage were measured at the end of 20 ms, marked as a dashed line in the figure. Each plot represents the mean ± SE of at least three independent experiments. Asterisks denote statistical significance with a p-value of less than 0.05.

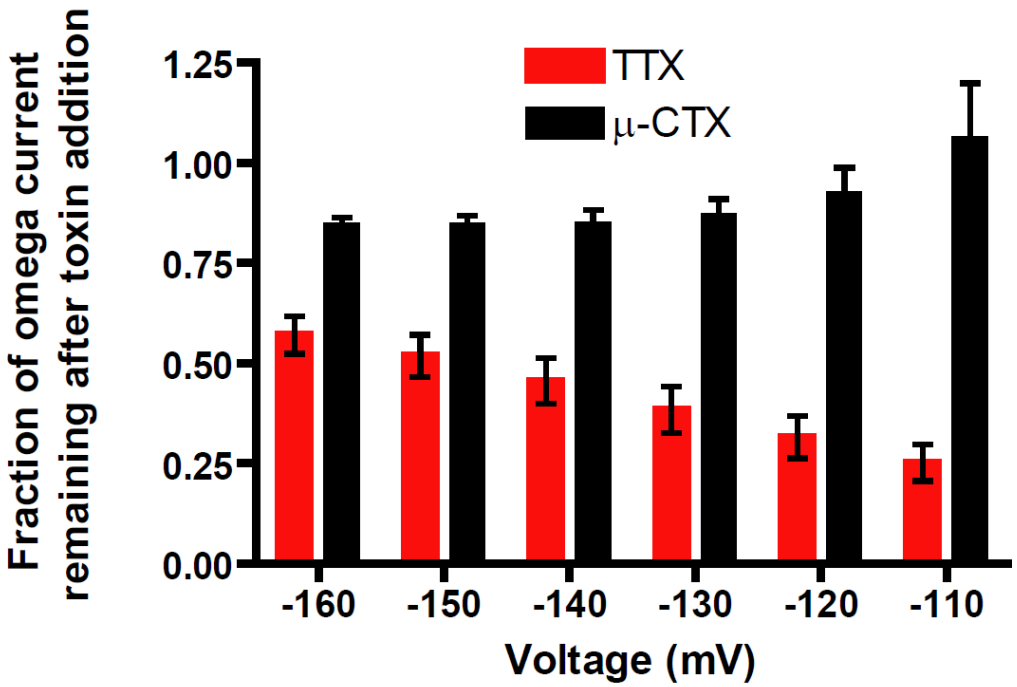

Figure 9: Voltage-dependence of TTX and μ-CTX inhibition of DIV gating pore currents. A plot of the fraction of DIV hyperpolarization activated current remaining after toxin addition versus voltage. Each graph represents the mean ± SE of five independent experiments. The fraction of gating pore current remaining after toxin addition was calculated by dividing the currents obtained after toxin addition by the currents obtained before toxin was added (following normalization).

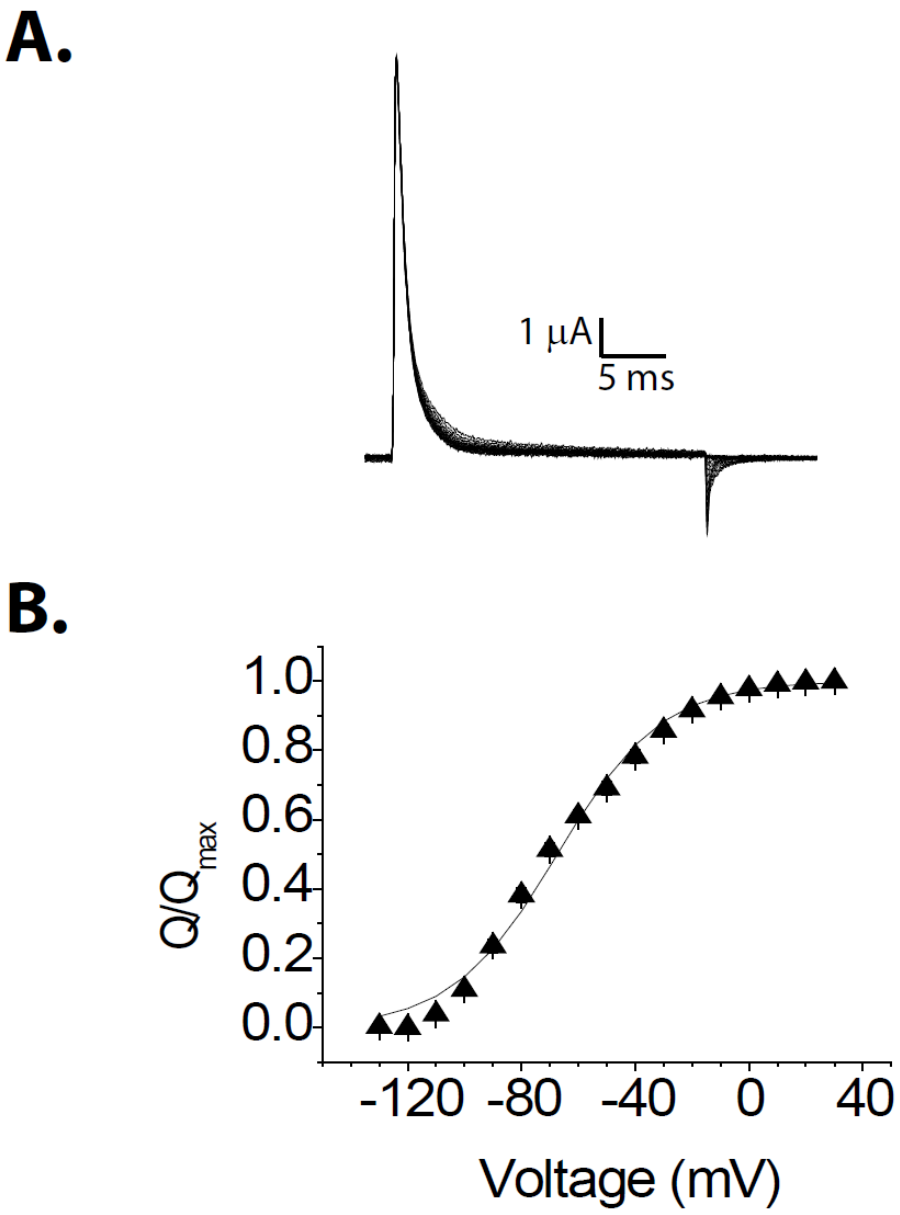

Figure 10: Wildtype OFF gating currents obtained in the absence of pore blocker. **(A)** Wildtype OFF gating currents in the absence of pore blocker. The voltage protocol used is the same as in the methods. **(B)** Wildtype charge-voltage plots shown in the absence of pore blocker. Each plot represents the mean ± SE of eleven independent experiments.

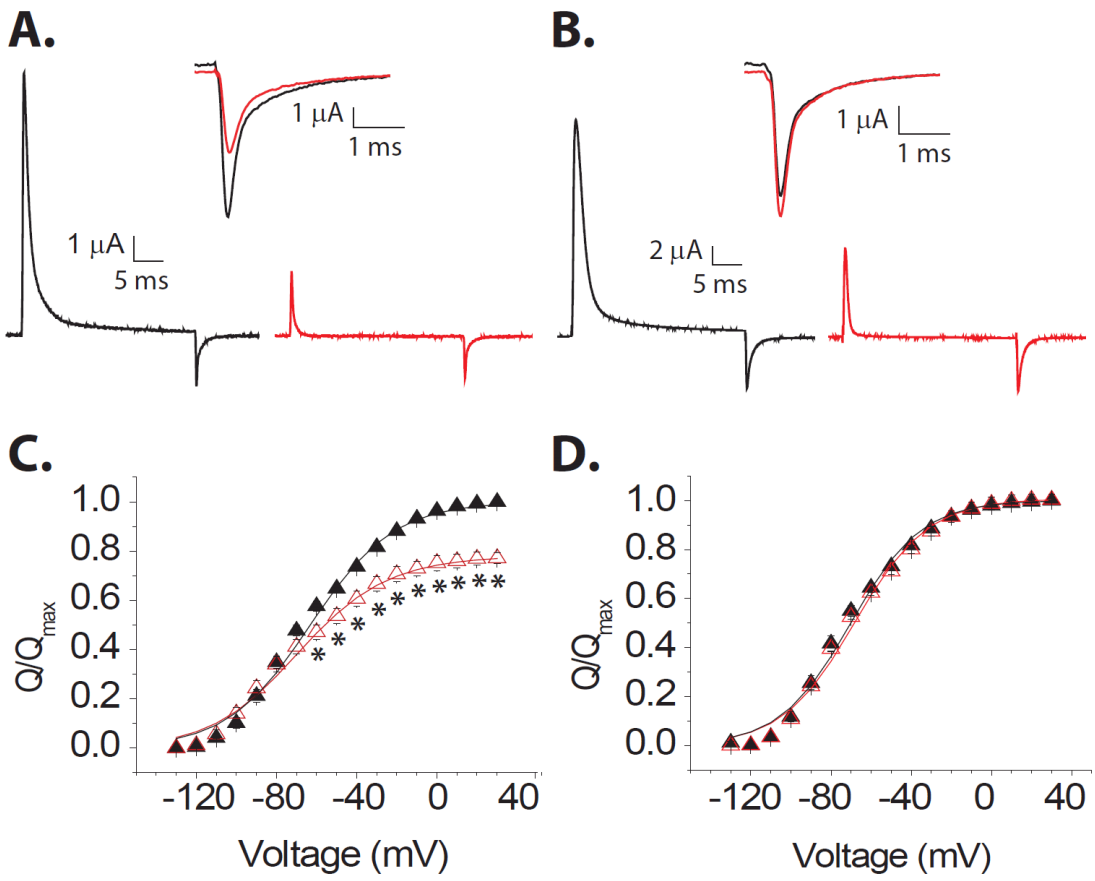

Figure 11: OFF gating currents from the wildtype sodium channel in absence and presence of outer pore blockers. (A) Wildtype OFF gating currents before (black trace) and after (red trace) TTX. The OFF gating current traces on an enlarged scale are shown as an inset. **(B)** Wildtype OFF gating currents before (black trace) and after (red trace) µ-CTX. The OFF gating current traces are shown enlarged as an inset. **(C)** Charge-voltage curves of the wildtype channel in the presence (filled triangle) and absence (empty triangle) of TTX. Each plot represents the mean ± SE of at least four independent experiments. See the methods for a description of the protocol. Statistical significance is denoted by an asterisk ($p < 0.01$). **(D)** Charge-voltage curves of the wildtype channel before (filled triangle) and after (empty triangle) block of sodium currents by µ-CTX shown as in (C).

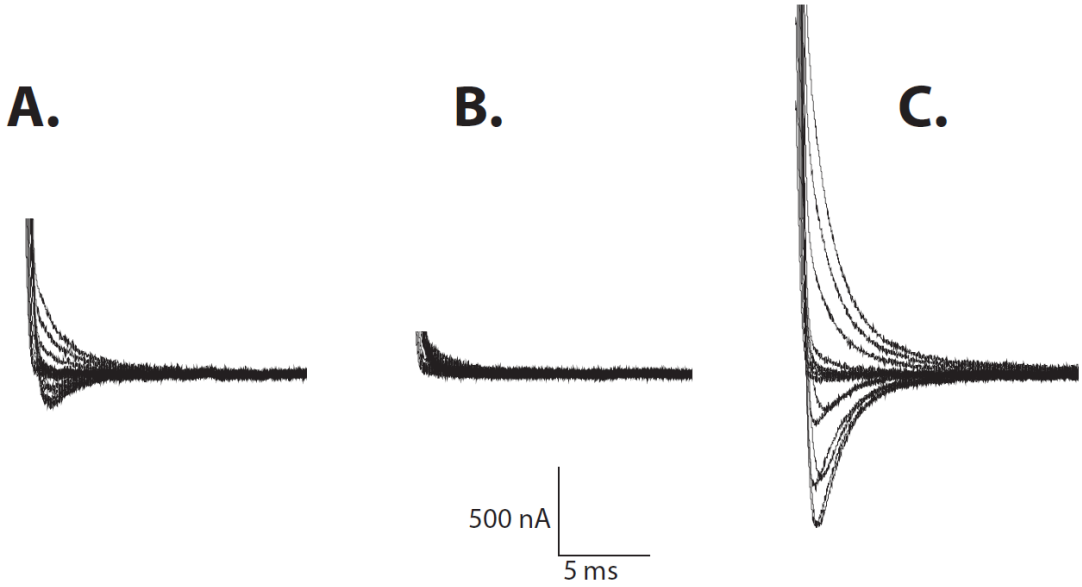

Figure 12: Representative sodium current traces under varying redox conditions in D400C/E755C DIV-CN. A family of ionic currents from oocytes expressing the D400C/E755C DIV-CN mutant **(A)**, in presence of 2 mM H_2O_2 **(B)**, and upon addition of 1 mM DTT after washout of H_2O_2 **(C).** All traces were collected from the same oocyte in presence of 105 mM Na^+-Mes external solution using a voltage protocol listed in methods.

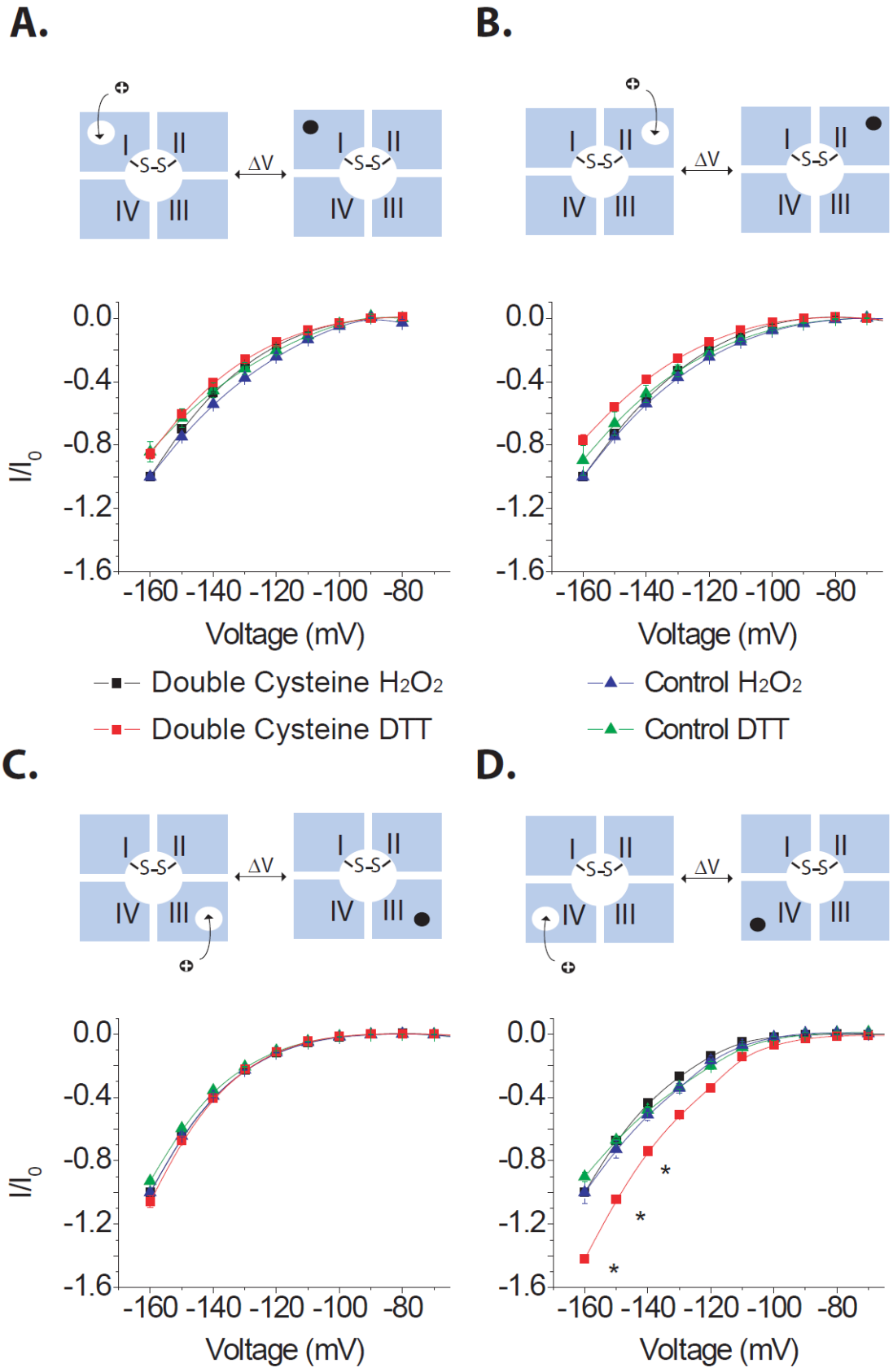
A.
B.
C.
D.
I
II
III
IV
S-S
ΔV
0.0
-0.4
-0.8
-1.2
-1.6
I/I0
-160 -140 -120 -100 -80
Voltage (mV)
Double Cysteine H2O2
Double Cysteine DTT
Control H2O2
Control DTT
*

Figure 13: Effect of disulphide crossbridge formation in the outer pore of the sodium channel on gating pore currents through the DI, DII, DIII, and DIV voltage-sensors. Above each of the panels, a schematic diagram depicting gating pore currents through individual voltage-sensors is shown. Upon depolarization the gating pores in individual domain close which allows us to monitor the conformational movements of individual domains. In all cases, the pore is trapped in an inactivated conformation by disulphide crosslinking. **(A)** Normalized current-voltage plots of D400C/E755C DI-CN gating pore currents in H_2O_2 (black squares) and DTT (red squares) compared to the DI-CN control in H_2O_2 (blue triangles) and DTT (green triangles). **(B)** Normalized current-voltage plots of D400C/E755C DII-CN gating pore currents compared to those of DII-CN. The symbols are used as in (A). **(C)** Normalized current-voltage curves of D400C/E755C DIII-CN gating pore currents compared to the DIII-CN control. The symbols are the same as in (A). **(D)** Normalized current-voltage curves of D400C/E755C DIV-CN gating pore currents as compared to those of the DIV-CN control. Each plot represents the mean ± SE of at least three independent experiments. I_o refers to the H_2O_2 traces collected at -160 mV. The data were normalized to I_o for the controls and for the double cysteine mutants. Asterisks denote statistical significance with a p-value of less than 0.03.

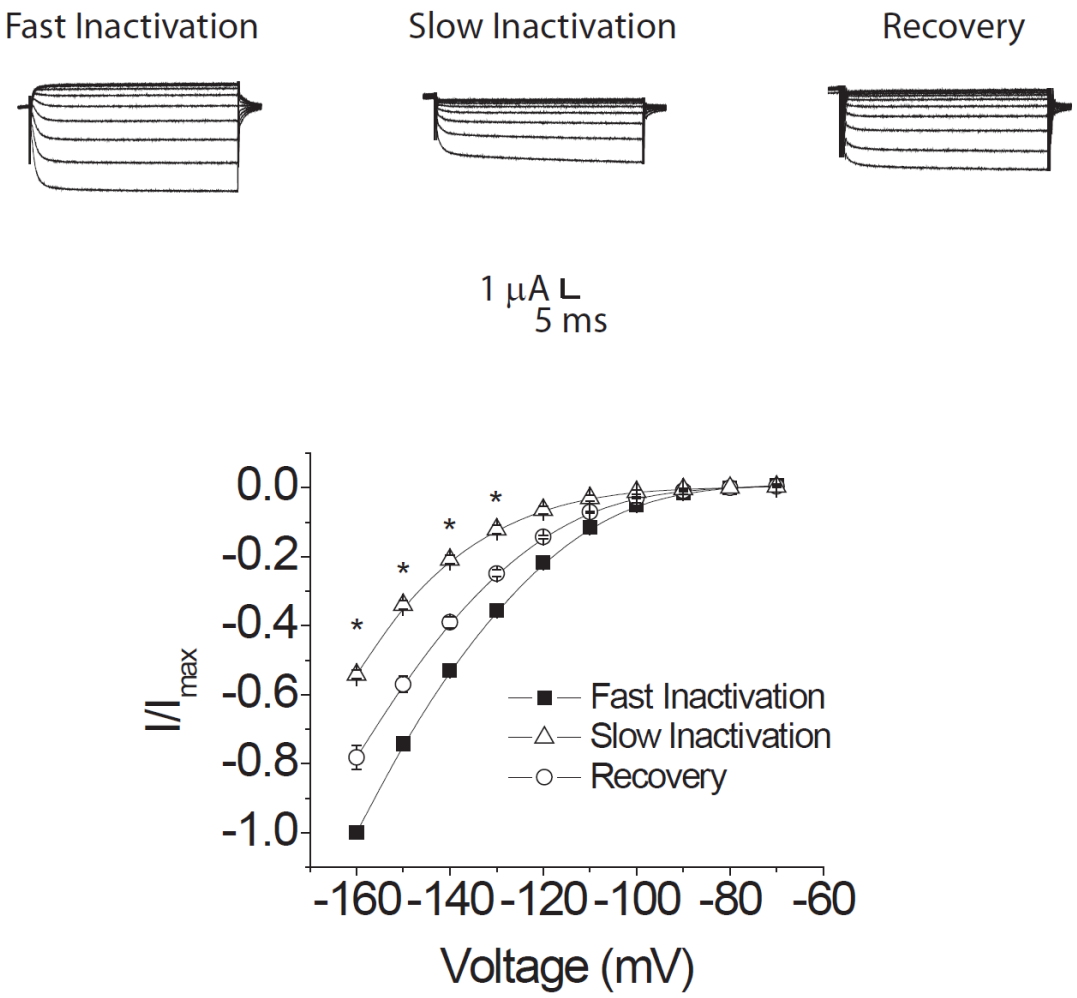

Figure 14: The effect of cumulative slow inactivation on the DIV-CN gating pore currents. A family of gating pore currents (above) is shown after fast inactivation, after a 30 s cumulative slow inactivation protocol, and after a 10 min recovery at -80 mV. Normalized current-voltage plots of the DIV-CN gating pore currents (below) before slow inactivation (filled squares), after a 30 s cumulative slow inactivation protocol (unfilled triangles), and after a 10 min recovery at -80 mV (unfilled circles). The channels were pulsed from -120 mV to -10 mV for 20 ms to measure the ionic current and then a pulse train from -160 to 60 mV for 60 ms was collected before returning to -120 mV for

20 ms. Our cumulative inactivation protocol was modified from protocols used by Cummins and Sigworth and Townsend and Horn (Cummins and Sigworth 1996; Townsend and Horn 1997). For the 30 s cumulative slow inactivation protocol, the oocytes were held at -10 mV for 30 s before beginning the protocol described above and were also held at -10 mV for 30 s in between every voltage-step. Each plot represents the mean ± SE of six independent experiments. Asterisks denote statistical significance from the gating pore currents collected after fast inactivation ($p<0.02$).

CHAPTER IV

The role of the DIV voltage-sensor in fast inactivation of the sodium channel

4.1 INTRODUCTION

In the sodium channel, the voltage-sensors of the non-identical domains that form the α-subunit are thought to have different roles in the process of channel gating. This hypothesis has come about through various suggestive lines of evidence. Generally speaking, if all of the voltage-sensors were involved both in the activation and inactivation processes, a disruptive mutation in one voltage-sensor could be expected to affect both processes. However, this is not necessarily the case. For example, locking the DII voltage-sensor into one conformation with a photo-activatable crosslinker had the effect of reducing ionic currents at all potentials but had no effect on the inactivation process. Conversely, when the same experiments are carried out on the DIV voltage-sensor, it was found that locking the DIV S4 caused a large inhibition of inactivation and an *increase* in currents at all potentials (likely due to defective inactivation) (Horn, Ding et al. 2000).

Furthermore, the kinetics of voltage-sensor movement in each of the domains appears to be different as well. Placing an environmentally sensitive fluorophore on the top of one voltage-sensor allows the experimenter to measure voltage-dependent changes in fluorescence and, by extension, the kinetics of voltage-sensor movement. As might be expected for a process preceding activation, the movement of the first three voltage-sensors occurs before the development of ionic currents. However, this is not the case for the DIV voltage-sensor whose movement is slower and appears to correlate with the development of current decay (Chanda and Bezanilla 2002).

Another set of two paired papers in which charges were replaced in the voltage-sensors of different domain led to a different claim. They found that while most of the mutations in the DI and DII voltage-sensors resulted in leftward shifts in fast inactivation, most of the mutations in DIV resulted in no significant effects on inactivation. Furthermore, the authors were able to provoke shifts in different directions in the voltage of half maximal activation through various mutations in each domain. These results led them to conclude that the voltage-sensors of all four domains were involved in both activation and inactivation (Kontis, Rounaghi et al. 1997; Kontis 1997).

Much of the above data led to the current view in the field that different voltage-sensors are involved differently in the processes of activation and inactivation. Despite numerous suggestions that the DIV voltage-sensor is involved in the process of inactivation, it remains unclear whether the movement of the DIV voltage-sensor is the sole trigger of the inactivation process or there is some other contributing factor. Complicating the issue, there is evidence for the DIII voltage-sensor to be involved in inactivation as well. Inactivation of the sodium channel results in the immobilization of the DIII and DIV voltage-sensors, but not DI or DII (Cha 1999). Furthermore, a mutation to a charged residue in the DIII S4-S5 linker is known to disrupt inactivation and a compensatory mutation (of an opposite charge) in the inactivation loop may partially rescue this effect (Smith and Goldin 1997). It has been suggested that the DIII and DIV S4-S5 linkers may actually form part of the inactivation loop docking site (Miyamoto, Nakagawa et al. 2001).

Disease mutations affecting inactivation may be found scattered about the channel but are especially dense in DIII and DIV. These diseases can have a devastating impact

causing a variety of cardiac arrhythmias (long QT syndrome and Brugada syndrome), epileptic seizures (generalized epilepsy with febrile seizures), muscle weakness (hyperkalemic periodic paralysis, paramyotonia congenita, and myasthenic syndrome), and even extreme pain (paroxysmal extreme pain disorder and erythromelalgia). Due to the clearly important role of inactivation in channel functioning in both normal and disease states, it is important to pinpoint the structures and processes that are involved. A better understanding of sodium channel fast inactivation is necessary in order to develop more effective treatments for the battery of sodium channel diseases.

Though the voltage-sensors contain multiple positive charges in their sequences, not all of these may pass through the whole length of the electric field. In the potassium channel, it was found that it was only the first four charges that contributed to the gating charge of the channel (Aggarwal and MacKinnon 1996; Seoh, Sigg et al. 1996). However, in the sodium channel, the fourth charge appears to make no contribution to the total charge of the channel and it is the first three charges which are the gating charges (Sheets and Hanck 2002). In the potassium channel, the neutralization of the first three charges of the voltage-sensors led to the development of a channel with voltage-independent gating. The authors suggested that this was because they had locked the voltage-sensors of the channel into an activated position (Bao, Hakeem et al. 1999).

Based on the results above, we reasoned that if we neutralized the first three gating charges of one voltage-sensor, we could use those mutants to study the activation and inactivation behavior of a channel where one voltage-sensor is defunct. By studying inactivation in the functional absence of one voltage-sensor at a time, we hoped to determine the role of each individual voltage-sensor in the process of fast inactivation.

4.2 RESULTS

4.2.1 Characterization of the voltage-sensor mutants

In order to study channel gating behavior where one voltage-sensor is defunct, we chose to neutralize the first three most critical gating charges in one voltage-sensor at a time by mutating them to glutamine. We then expressed the resulting constructs in *Xenopus* oocytes and found that all four mutants formed functional channels. We collected ionic currents either using the two electrode voltage clamp technique (in 105 mM sodium external solution) or the voltage-clamp on cut open oocyte technique (in 105 mM sodium external solution and 105 mM N-methyl D-glucamine (NMG) internal solution). For full solution compositions, see Chapter II, 2.5. Ionic currents were elicited by holding at -120 mV for 50 ms and then applying a voltage pulse train from -110 to 65 mV (at 5 mV increments) for 30 ms and returning to -120 mV. A p/-4 subtraction protocol was used with a subtraction holding voltage of -120 was used to minimize the capacitive transient and subtract the leak. We plotted the conductance-voltage (G-V) relationships for each of the mutants and the WT and fit the data to a single Boltzmann equation of the form:

$G/G_{max}(V) = 1/(1+\exp(-ze)(V-V_{1/2})/KT))$

where $V_{1/2}$ is the half maximal voltage, z is the apparent valence, e is the electronic charge, K is the Boltzmann constant, and T is the temperature.

Neutralizing the first three charges in all domains (D) resulted in a leftward shift of the G-V curve with the V_{max} values being approximately -20.5 mV for the WT, -36.5 mV for DI-CN, -25.1 mV for DII-CN, -26.4 mV for DIII-CN, and -23.1 mV for DIV-CN (see Fig. 1). Therefore, we can conclude that the neutralization of the first three gating

charges in one voltage-sensor allows the channel to open at voltages that are more hyperpolarized than the WT. If one considers that in order for the channel to open, the voltage-sensors must activate, this result tallies with the hypothesis that neutralizing the gating charges in a voltage-sensor locks that voltage-sensor in its activated position, thereby making the channel easier to open. However, all four mutants exhibit gating pore current through the altered voltage-sensor. In order for gating pore current to flux, the voltage-sensor must be in a permissive position. Because the gating pore current of all four mutants rectifies (see Chapter 3 Figs. 2, 3, and 4), we can conclude that the voltage-sensors are still mobile. Should a voltage-sensor be locked in one position, we would expect to see a constitutive linear leak at all voltages. Therefore, we hypothesize that the neutralization mutations are instead biasing the voltage-sensors toward their activated positions such that they become easier to activate.

4.2.2 Effects of neutralization mutations on the steady state inactivation behavior of the channel

To investigate the role of each voltage-sensor in the steady state fast inactivation of the sodium channel, we used our neutralizations to observe steady state inactivation in the functional absence of one voltage-sensor at a time. Steady state inactivation data (and all other data unless explicitly stated) was collected utilizing the voltage clamp on cut open oocyte technique and all data was acquired in 105 mM sodium external solution and 105 mM NMG internal solution (for full composition see Chapter II, 2.5). Our protocol operated by applying a 20 ms pulse to -120 mV followed by a 100 ms voltage step train from -170 mV to 50 mV to allow the channels to fast inactivate. Next, a 1 ms

hyperpolarization to -120 mV was applied followed by a 30 ms test pulse to -30 mV and a return to -120 mV.

Analyzing the currents elicited at the test pulse allows the experimenter to determine the fraction of channels that did not fast inactivate at each potential and thus assess the voltage-dependence of fast inactivation. We found that neutralizations in the DI, DII, or DIII voltage-sensors caused small hyperpolarizing shifts in the steady state inactivation curves relative to the WT. However, the DIV-CN mutant exhibited a steady state inactivation curve which was drastically shifted to the left. The midpoint values for each construct were approximately -62.1 mV for the WT, -69.3 mV for DI-CN, -66.1 mV for DII-CN, -68.7 mV for DIII-CN, and -137.3 mV for DIV-CN. These midpoint values were obtained by fits of the data to a single Boltzmann equation. However, as can be seen from the figure (see Fig. 2), the steady state inactivation curve of DIV-CN never saturates and therefore, the midpoint value of the DIV-CN mutant may be much further left shifted than can be determined by our equipment.

These data show that when the gating charges of the DIV voltage-sensor are neutralized to glutamine, the altered channels are able to fast inactivate at voltages much more hyperpolarized than the WT. This suggests a unique role for the DIV voltage-sensor in setting the voltage-dependence of the fast inactivation process.

4.2.3 Effects of charge neutralizations in each voltage-sensor on entry into fast inactivation

How quickly a channel enters into inactivation is a major determining feature of that channel's overall gating behavior. A rapid entry and exit from inactivation leads to a channel that has a shorter effective refractory period and is able to quickly reset and

respond to new stimuli. Prior to channel entry into inactivation, there is a typical lag phase where the channels remain open and do not inactivate. This lag gives the channels time to conduct ionic current before inactivation sets in (see Fig. 3). Another property of fast inactivation is that channels are able to inactivate faster at more depolarized potentials. Due to the importance of the voltage-dependent entry into fast inactivation in determining a channel's unique biophysical properties, we determined to look at the effects of gating charge neutralizations in specific voltage-sensors on the characteristics of entry.

We assayed entry into fast inactivation via a protocol which started by applying a voltage jump to -120 mV for 20 ms. Next, the channels were jumped to a specified inactivating voltage for a variable time (from 0.1 to 50 ms) before being hyperpolarized to -100 mV for 1 ms. Finally, the fraction of channels inactivated during that duration of inactivation pulse were assayed utilizing a 30 ms test pulse to 0 mV (see Chapter II, 2.5.6 and Chapter II Fig. 1). When we tested the entry into fast inactivation for the WT and the CN mutants, we found that DI, DII, and DIII, like WT, maintained a lag before entry into fast inactivation (see Fig. 3 A-E). This lag appeared to be slightly shorter for the DIII-CN construct. However, DIV-CN exhibited no lag before inactivation at any voltage where inactivation occurred (see Fig. 3 F).

To provide a better quantitative measure of the kinetics of entry into fast inactivation, we fit our data to a bi-exponential function with a variable lag (t_0) of the form: $F(x) = A_1(1 - \exp(-(t-t_0)/\tau_1) + A_2(1 - \exp(-(t-t_0)/\tau_2 \times H(t_0)$ (for a full description, see chapter II 2.6.1). While a clear voltage-dependence is reflected for the fast tau of the WT as well as DI, DII, and DIII-CN, much of the voltage-dependence in the fast tau for the

DIV-CN mutant is eliminated (see Fig. 3 G). Additionally, while the lag time in WT, DI, DII, and DIII-CN is observed to decrease at more depolarized inactivation pulses, there appears to be little change in the lag time of DIV-CN with essentially no lag observed at any voltage (see Fig. 3 H). Together, these results suggest that much of the voltage-dependence of entry into fast inactivation arises from the activity of the DIV voltage-sensor.

4.2.4 Effects of charge neutralizations on closed state fast inactivation

Most of the fast inactivation that occurs in the WT sodium channel is open state fast inactivation: the channels open and *then* they inactivate. One would expect a channel that exhibits mainly open state inactivation to have kinetics of inactivation that are closely matched to the macroscopic channel opening. However, it is also possible for channels to enter into the inactivated state from the closed state. This closed state inactivation has a higher probability to occur at more depolarized voltages and one would visualize this as a deviation of the kinetics of entry into inactivation from those of macroscopic channel opening (ie. the inactivation will begin to precede channel opening). As closed state inactivation can be a major determinant of channel availability, we determined to test for alterations of closed state inactivation caused by our gating charge neutralizations.

We averaged ionic current traces collected near the midpoint of each construct's conductance-voltage relationship. We chose to use traces collected at -20 mV for the WT and DIV-CN, and -30 mV for DI, DII and DIII-CN. In all cases, the averaged currents display error bars representing standard error of the mean. These traces were then inverted and overlaid with the relevant entry into inactivation plot at those voltages and

scaled in time so that they matched. Next, the G-V curve for each construct was utilized to calculate the maximum fraction of channels activated at that potential and the currents were scaled such that the peak current matched that relative P_o on the plot.

For the WT, the kinetics of entry into fast inactivation are closely matched to those of macroscopic channel opening. This suggests that there is a low probability for closed state inactivation in the WT channel when at a voltage near the Vm. For both DI and DII-CN, the entry into inactivation kinetics significantly lag the macroscopic channel opening when at voltages near their Vm. The DIII-CN entry into inactivation plot, when matched with the macroscopic opening kinetics reveals that there may be a slightly higher propensity for the channels to closed state inactivate than in the WT when at voltages close to the Vm. This effect is even more pronounced for DIV-CN, with the DIV-CN mutant clearly entering into inactivation faster than the channels open (see Fig. 4). Mutation of the DI or DII voltage-sensor gating charges increases the gap between channel opening and channel inactivation. On the other hand, neutralizing the gating charges of the DIV voltage-sensor and, to a smaller degree, the DIII voltage-sensor allows for the channels to quickly enter inactivation from the closed state.

4.2.5 Effects of gating charge neutralizations on recovery from fast inactivation

Another parameter we chose to investigate was recovery from fast inactivation. How quickly channels recover from inactivate regulate how long they remain in the inactivated state and thus dictate how quickly they become available to respond to another stimulus. We assayed recovery from inactivation by applying a voltage pulse protocol that started at -120 mV for 20 ms followed by a 30 ms inactivating pulse to -20 mV. Next, a hyperpolarized pulse was given at a specified recovery voltage for a variable

time (from 0.1 to 40 ms). This recovery interval was followed by a test pulse to -20 mV for 30 ms.

As with entry, there is a typical lag before recovery from inactivation begins. In the WT channel, this lag before entry begins is very short and the channel recovery begins almost immediately after the recovery pulse begins. All of the charge neutralization mutants exhibit a slowed recovery from inactivation with a longer lag period than in the WT. Relative to the others, the effects of the mutations on the DIII-CN construct is smaller. Once again, DIV-CN exhibits the greatest effects with the mutations in the fourth voltage-sensor result in the longest lag before recovery (see Fig. 5). In DIV-CN, the time to half maximal recovery is greater than every other construct at -110 mV and more than double that of WT or the other mutants at -180 mV.

To quantify our results, we fit our data to an exponential function with a variable lag (t_0). In the case of the WT, DI, DII, and DIII-CN the equation that best fit the data was bi-exponential (as reported above), however, the DIV-CN data was best represented by a mono-exponential equation of the form: $F(x) = A(1-\exp(-(t-t_0)/\tau) \times H(t_0)$ (for a full description see chapter II 2.6.1). At almost every recovery voltage, the DIV-CN construct has the largest tau value (see Fig. 5 G) and also the longest lag before recovery begins (see Fig. 5 H). As each of the mutants exhibit slowed recovery from fast inactivation, it is possible that each voltage-sensor may in fact play a role in recovery, with the DIV voltage-sensor making the most critical contribution to channel recovery from inactivation.

4.2.6 Slow component or not? The effects of neutralization on the DIV voltage-sensor

Gating currents are an electrophysiological way to track the behavior of voltage-sensors. In observing the typical gating currents of the WT channel, two kinetic components may be distinguished, one fast, and one slow. A previous study dealing with the kinetics of voltage-sensor activation observed that the first three voltage-sensors moved before the channel opened. This result would be expected for a process that must precede channel opening. However, the movement of the fourth voltage-sensor is much slower and in fact trails the opening of the channel. This study linked the movement of the fourth voltage-sensor to the inactivation of the channel (Chanda and Bezanilla 2002). It is thought that the fast component of gating current relates to channel opening and the slow component relates both to the movement of the DIV S4 and to inactivation.

Due to these observations and to our prior results, we elected to characterize the kinetics of the DIV-CN gating currents and compare them with those of the WT channel. Keeping in mind that tetrodotoxin alters gating currents, we chose to make gating current measurements in the toxin μ-conotoxin instead. We hypothesized that a set of mutations altering the voltage-dependent behavior of fast inactivation should affect the slow component observed in gating currents as well.

At first glance, it is clear that the DIV-CN gating currents have a characteristically sharper appearance than those of the WT channel (see Fig. 6 A). Additionally, the neutralizations in the DIV voltage-sensor result in a large leftward shift in the charge-voltage (Q-V) relationship (see Fig. 6 B). Such a leftward shift in the Q-V curve would make sense if a voltage-sensor moving at more depolarized voltages is suddenly able to move at voltages more hyperpolarized than previously.

To aid in the comparison of the WT gating currents with those of DIV-CN, we chose to overlap the two currents at -10, 0, 10 and 30 mV with WT in black and DIV-CN in gray (see Fig. 7 A). Closer examination reveals that much of the slow component of the DIV-CN gating currents is absent. The slow component of gating currents has previously been suggested to be associated with the process of fast inactivation and therefore, based on our data, we reasoned that the slow component might be reduced or absent and that it might track be due to the movement of the DIV voltage-sensor.

We elected to fit the gating currents of both WT and DIV-CN to a double exponential at several voltages. These fits should numerically reveal whether the slow component of gating is absent or reduced. We fit each individual gating current trace to a bi-exponential function:

$F(t) = A_1(\exp^{(-t/\tau 1)}) + A_2(\exp^{(-t/\tau 2)}) + C$

We averaged either the fast tau values or the slow tau values together and plotted them versus voltage (see Fig. 7 B). As can be seen from these plots, the fast and slow tau values for the DIV-CN mutant do not vary widely with voltage. The fast tau becomes slightly faster in as the voltages become more depolarizing while the slow tau becomes slightly slower. The changes in the DIV-CN tau values are almost linear. On the other hand, the WT fast and slow taus change noticeably with voltage with the slow tau becoming the fastest at around -30 mV and then slowing again and the fast tau becoming the slowest at around -30 mV and then speeding up.

We also investigated the percent amplitude of the fast and slow components for both WT and DIV-CN. The percent fast amplitude was defined as:

$\%A_{fast} = (A_{fast}) \div (A_{fast} + A_{slow})$

In the case of the WT, the slow component reaches its highest contribution (about 43%) at -20 mV and then begins to drop again. On the other hand, the contribution of the slow component of DIV-CN is small and almost linear, reaching a maximum of approximately 18% at -40 mV (see Fig. 7 C). These data suggest that neutralization of the first three charges of the DIV voltage-sensor removes a large portion of the slow component of gating currents. This suggests that, at least in part, the DIV voltage-sensor is responsible for the slow component present in gating currents. Furthermore, as the slow component of gating has been correlated to the fast inactivation of the channel, these results provide additional support for the importance of the DIV voltage-sensor in fast inactivation.

4.3 DISCUSSION

Due to the importance of fast inactivation in voltage-gated sodium channel function, we sought to track down the voltage-sensitive elements that give the process it's voltage-dependence. We chose to determine which of the voltage-sensors were critical in this process by neutralizing the top three and most crucial gating charges in one voltage-sensor at a time. We found that the neutralization of the first three gating charges in the DIV voltage-sensor dramatically shifted the steady state inactivation curve to more hyperpolarized potentials. In addition, the mutations in the DIV voltage-sensor resulted in the loss of much of the voltage-dependence of entry into inactivation and eliminated the lag before fast inactivation can occur.

These data make sense if you make the assumption that the mutations lock the voltage-sensor in question into its activated state, however, as stated above, this is not the case. In order for us to see rectifying gating pore currents through the mutated voltage-sensors, they must be mobile. Therefore, we cannot assume a stationary voltage-sensor as

the cause for these behavioral changes. How then can we best explain the effects of the mutations in the DIV voltage-sensor on entry into inactivation and steady state inactivation? On observing the charge-voltage curves of the DIV-CN mutant next to that of the WT, it becomes plain that the gating charges of the DIV-CN construct are moving at voltages that are more hyperpolarized than the WT. Additionally, if one plots the current-voltage relationship of the gating pore currents through the DIV voltage-sensor, you will find that the majority of the gating pore current has switched off by -120 mV. This suggests that the mutant DIV voltage-sensor has mostly moved out of the permissive position by -120 mV. Therefore, though the CN mutations do not lock the voltage-sensors into an activated conformation, it seems likely that they bias them toward their activated positions.

Our data makes attractive the model where the DIV voltage-sensor must activate in order for the channels to enter into fast inactivation. As entry into inactivation was only characterized back to -120 mV, a voltage by which the mutated fourth voltage-sensor of DIV-CN is mostly activated, the lack of lag in the DIV-CN entry into inactivation begins to make sense. Furthermore, the movement of the fourth voltage-sensor in DIV-CN at more hyperpolarized potentials than the WT DIV S4 would allow for channels to begin inactivating at more hyperpolarized voltages than is usual.

Further, our data show that mutating gating charges in the DIV S4 allow the channel to enter into fast inactivation from the closed state. Taking these data together, it seems probable that the DIV voltage-sensor must move in order for fast inactivation to occur. When in its resting position, the DIV voltage-sensor or the S4-S5 linker may occlude the docking site of the inactivation loop or otherwise restrict its access. As the

DIV S4 begins to activate, it allows the inactivation loop to interact with its docking site and its binding inactivates the channel. In the case of the DIV-CN construct, because the voltage-sensor has already mostly moved into its activated position by the voltages tested, the inactivation loop is free to access its binding site even at hyperpolarized voltages. Thus, the kinetics of entry into fast inactivation for the DIV-CN mutant may actually be reflective of the time required for the inactivation loop to bind to its docking site in the pore.

Each of the CN mutants further exhibit a slowing of recovery from fast inactivation. The largest effect is again observed for the DIV-CN construct. In order for the channel to recover from inactivation, it is thought that two things must occur: one or more of the voltage-sensors must return to their resting configurations and the inactivation particle must pop out of its docking site. Keeping in mind that the voltage-sensors are biased toward their activated states, if we assume that only the fourth voltage-sensor must return to its resting position in order for the channel to recover from inactivation, then we can explain why the DIV-CN mutant exhibits the longest lag before recovery from inactivation. However, neutralizations in the other three voltage-sensors also slow recovery from inactivation, albeit to a lesser extent, and this suggests that the other voltage-sensors play a role in recovery from inactivation as well..

Consider also a scenario where the principle voltage-dependence of recovery from inactivation is derived from the DIV voltage-sensor. If one were to mutate the gating charges responsible for recovery from inactivation, one would naively expect to remove the voltage-dependence of recovery from inactivation, however, this clearly does not occur. We propose a model in which the DIV voltage-sensor must return to its resting

position in order for the channel to recover. In the WT condition, the voltage-dependence for the movement of the DIV S4 comes largely from the DIV voltage-sensor itself but is also derived partially through coupling to the other voltage-sensors. However, on removal of the primary gating charges of the DIV voltage-sensor, the voltage-dependence of returning the fourth voltage-sensor to resting comes primarily from the other three voltage-sensors. This scenario would serve to explain the slowing of recovery from inactivation induced not only by neutralizations in the DIV S4, but also that induced by mutations in the voltage-sensors of DI, DII, and DIII.

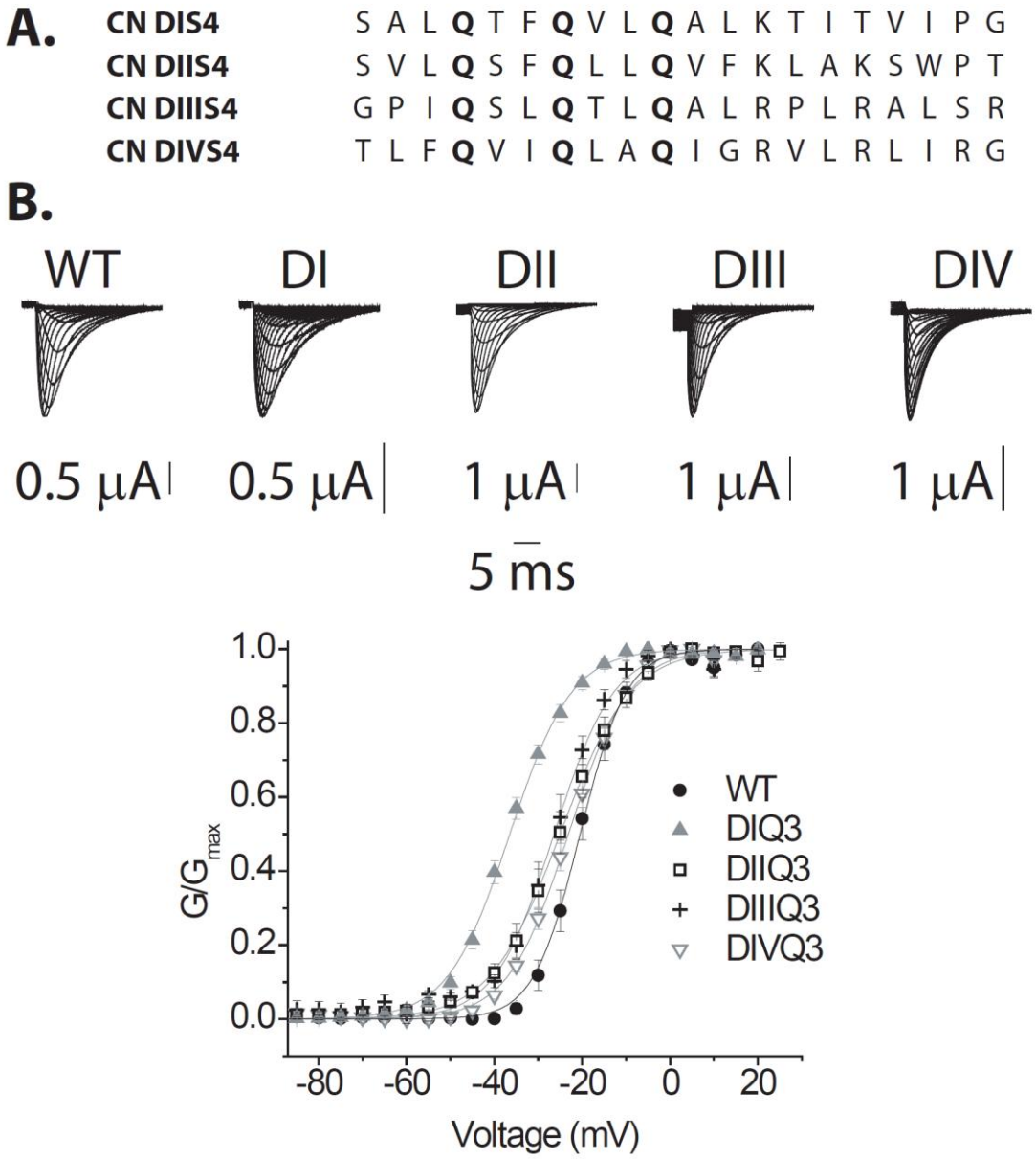

Figure 1: Characterization of the charge-neutralization mutants. (A) Sequence alignments of the altered voltage-sensors. Mutations are marked in bold. **(B)** A representative family of ionic current traces for the WT and the mutants (above). The normalized conductance-voltage relationships of the WT and CN mutants (below). The voltage pulse protocols used are reported in the methods. The lines represent fits of each data set to a single Boltzmann equation.

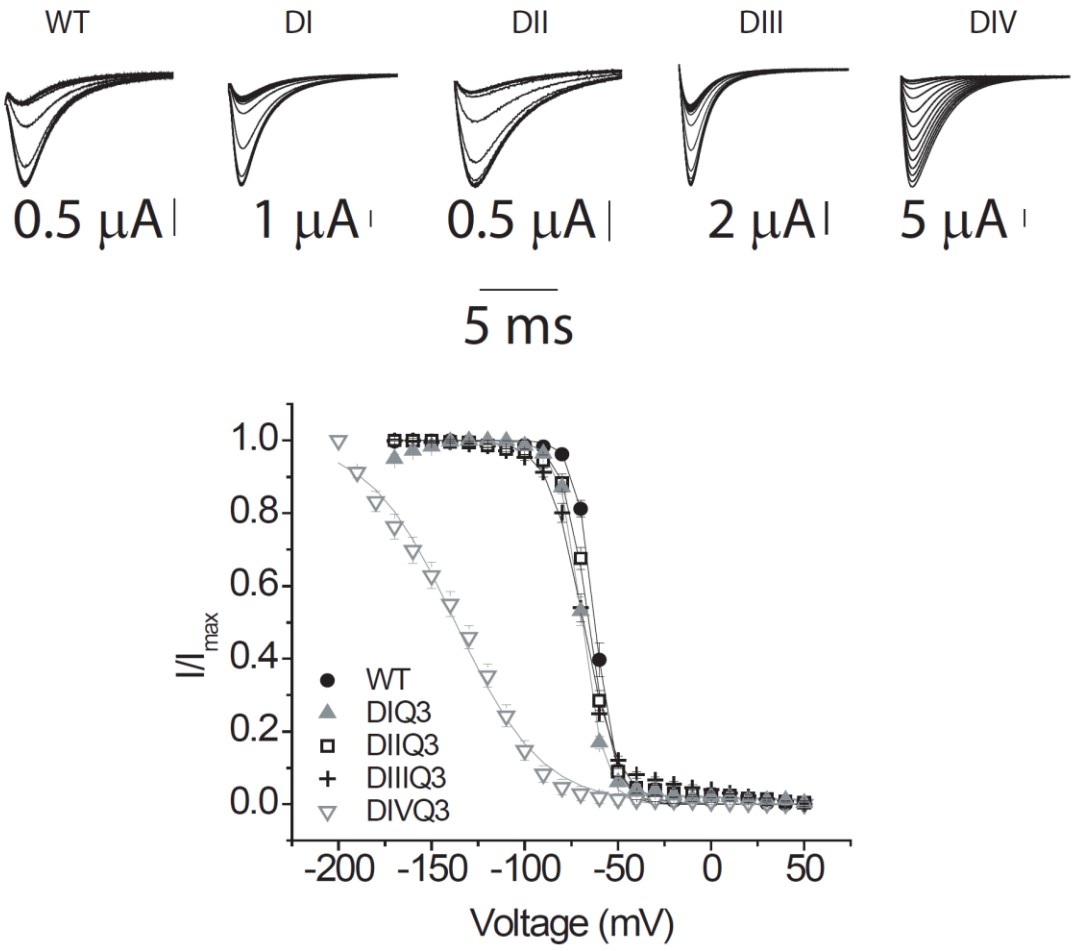

Figure 2: The characteristics of steady state fast inactivation in the WT and CN mutants. A representative family of currents after steady state fast inactivation has been achieved (above). Normalized steady state inactivation curves from the WT and CN mutants. The voltage protocols used are reported in the methods. Lines reflect a fit of each data set to a single Boltzmann function.

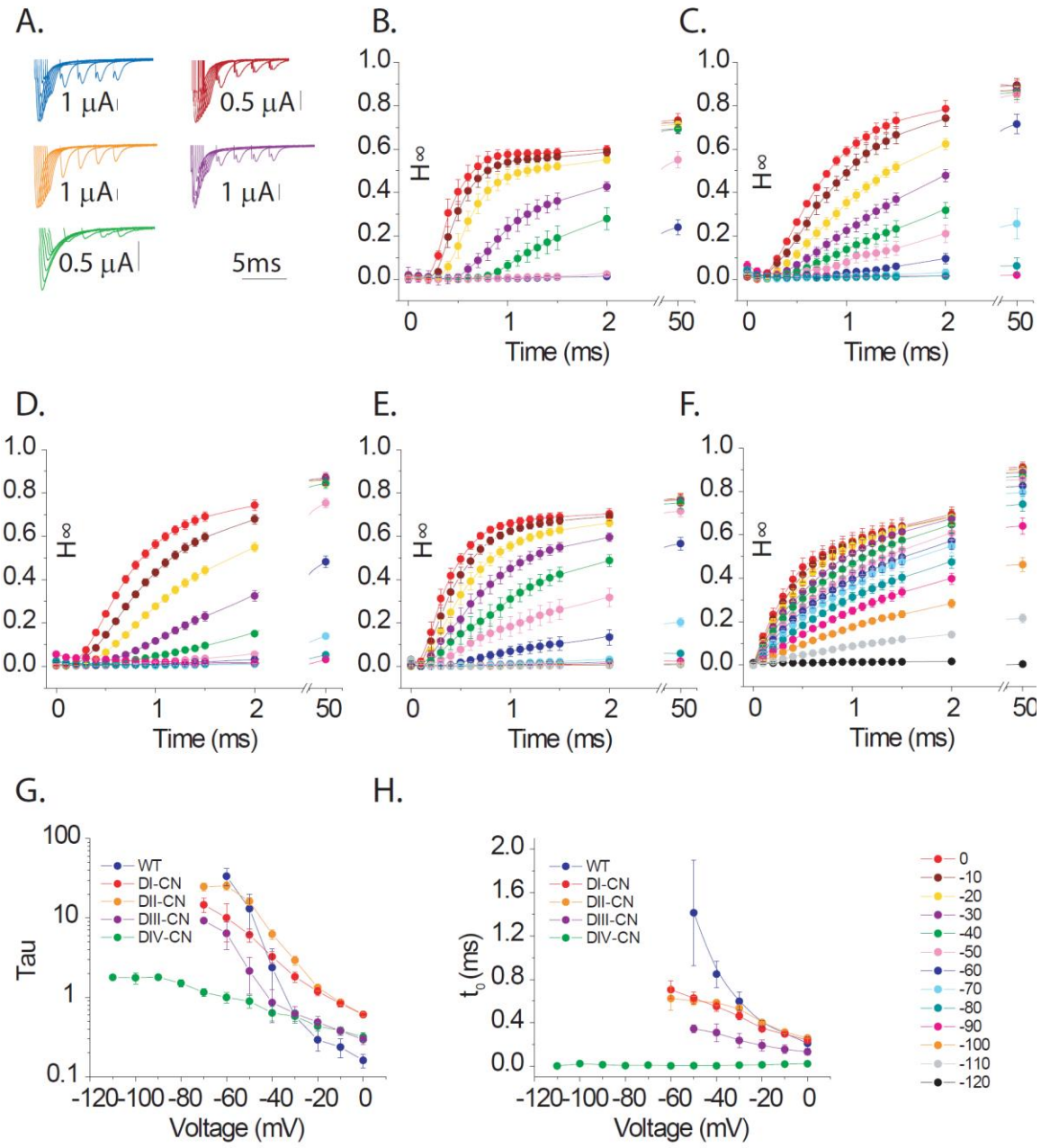

Figure 3: The effects of charge neutralizations in a specific voltage-sensor on entry into fast inactivation. (A) Representative families of traces showing WT (blue), DI (red, DII (orange), DIII (purple), and DIV-CN (green) entry into fast inactivation at -30 mV. **(B)** Plots of WT entry into fast inactivation at each voltage. **(C)** The same for DI-CN. **(D)** DII-CN as in B. **(E)** DIII-CN shown as in B. **(F)** DIV-CN as above. **(G)** The tau values of

entry into fast inactivation for the WT and CN mutants. **(H)** The delay (t_0) before entry into fast inactivation begins for WT and the CN mutants. Tau values were generated through fitting to a double exponential equation of the form: $F(x) = A_1(1- e^{(-(t-t0)/\tau1)}) + A_2(1- e^{(-(t-t0)/\tau2)}) \times H(t_0)$.

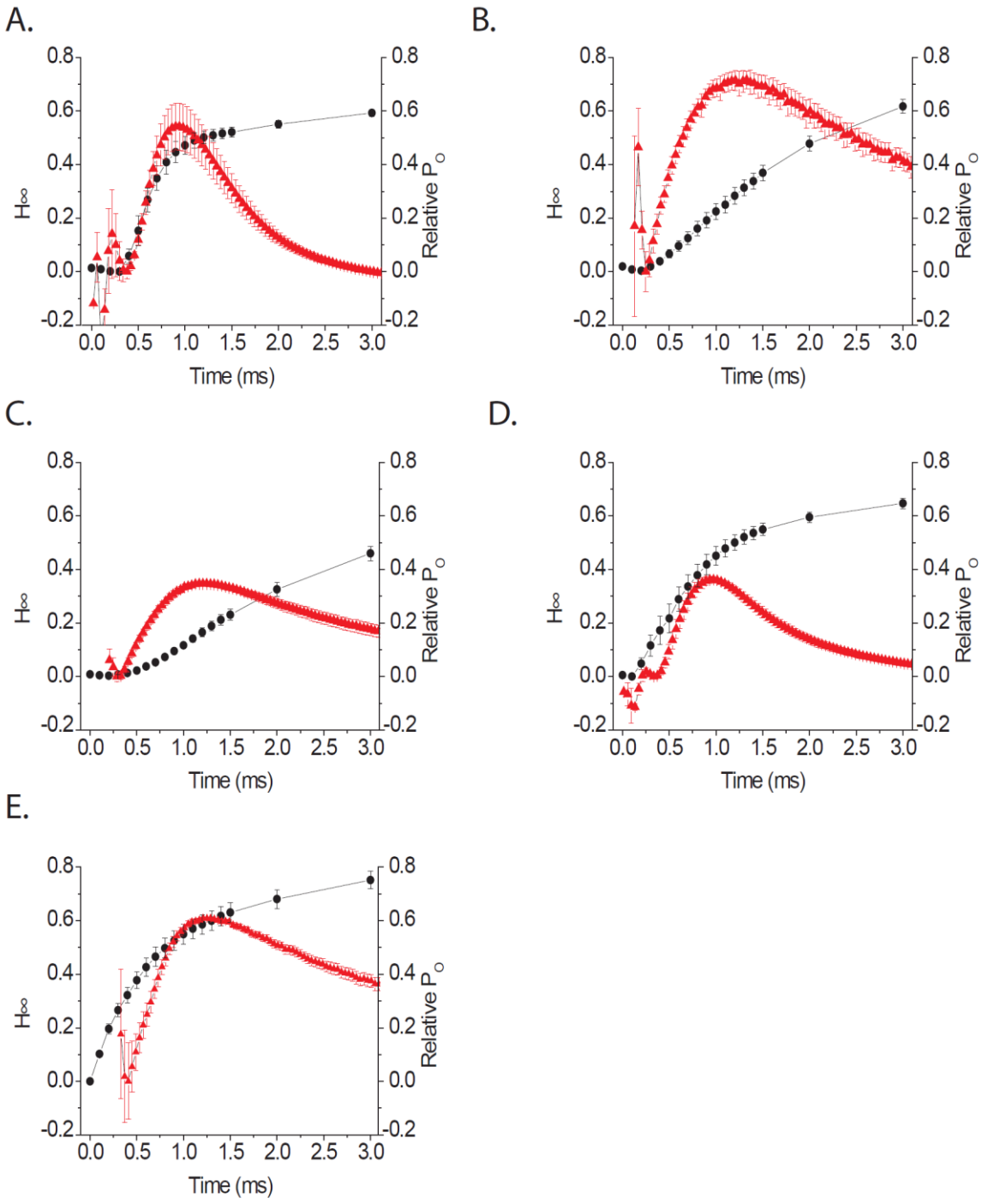

Figure 4: The effects of charge neutralizations in specific voltage-sensors on closed state inactivation. (A) An average WT ionic current trace collected at -20 mV scaled in time to match the plot of WT entry into fast inactivation at -30 mV. **(B)** DI-CN represented as above at -30 mV. **(C)** DII-CN as in A at -30 mV. **(D)** DIII-CN represented

as in A at -30 mV. **(E)** DIV-CN shown as above at -20 mV. The voltages used were chosen to be at or near the respective V_m values of their conductance-voltage curves. The peak of current was scaled to the relative open probability indicated by their conductance-voltage curves at the voltages used. The error bars represent the standard error of the mean.

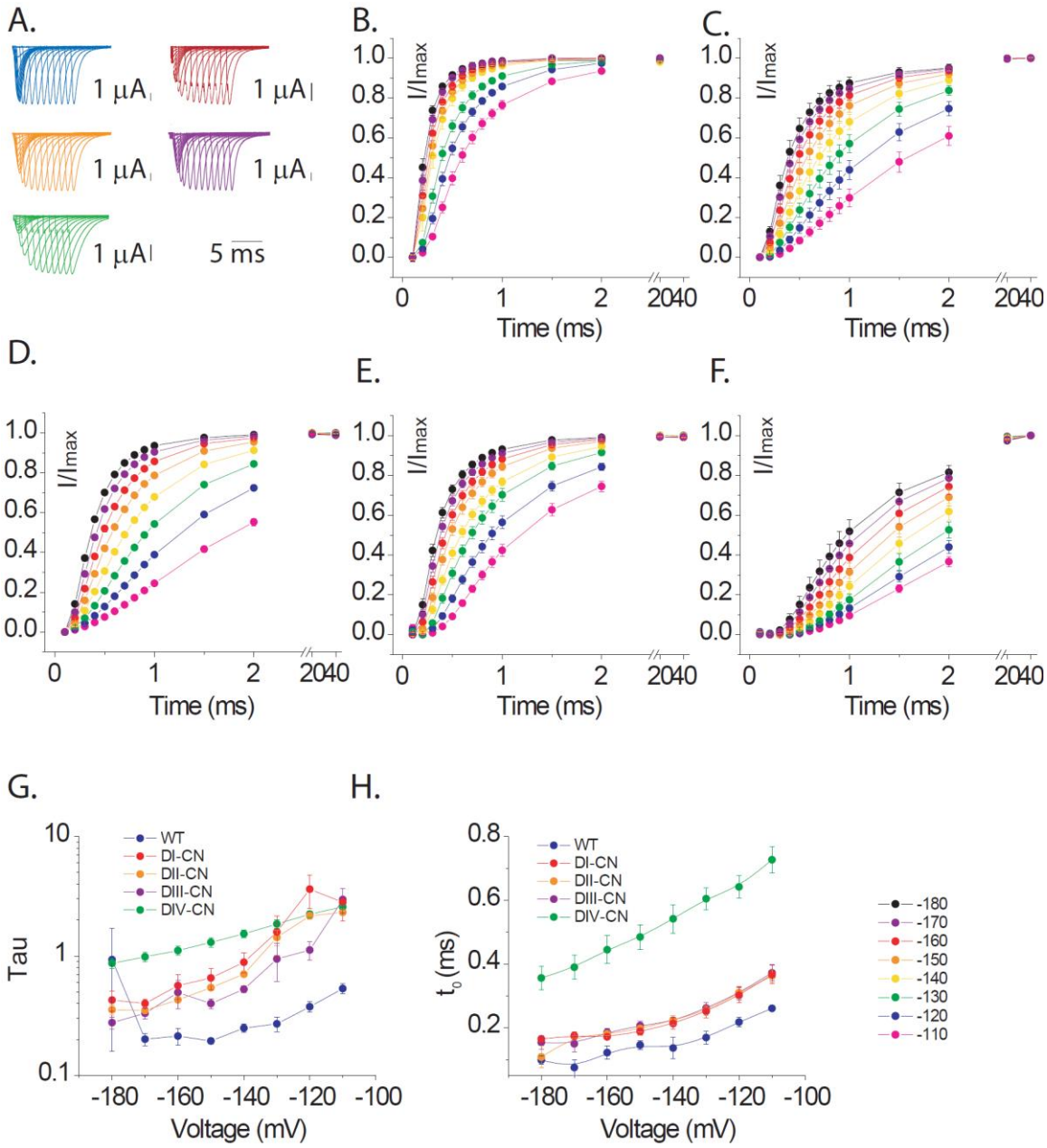

Figure 5: The effects of charge neutralizations in specific voltage-sensors on recovery from fast inactivation. (A) Example traces showing recovery from fast inactivation at -140 mV for WT (blue), DI (red), DII (orange), DIII (purple), and DIV-CN (green). **(B)** Graphs of WT recovery from fast inactivation at each voltage. **(C)** The same for DI-CN. **(D)** DII-CN as in B. **(E)** DIII-CN shown as in B. **(F)** DIV-CN shown as

above. **(G)** Tau values for recovery from fast inactivation of WT and the CN mutants. **(H)** The delay (t_0) before recovery from fast inactivation occurs at each voltage for WT and the CN mutants. Tau values were generated through fitting to a single exponential equation of the form: $F(x) = A(1- e^{(-(t-t0)/\tau)}) \times H(t_0)$ or a double exponential equation as indicated in the figure 3 legend.

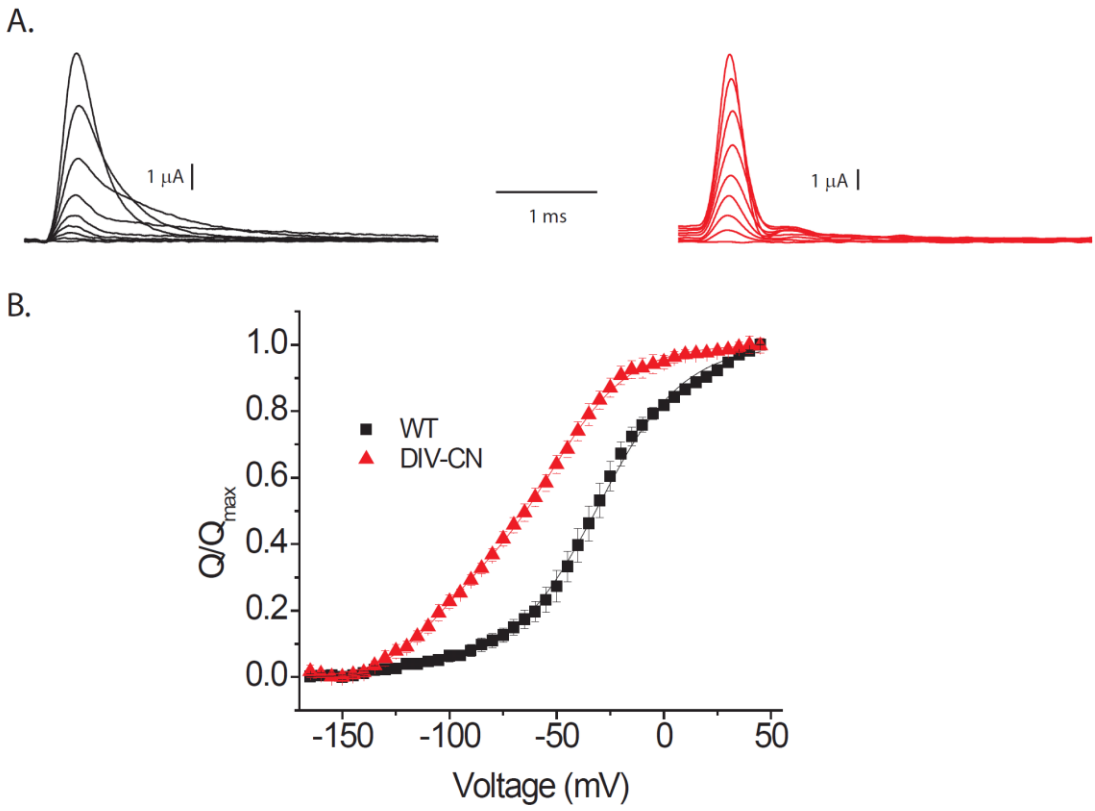

Figure 6: The effects of voltage-sensor charge neutralizations on the gating current characteristics of the WT and DIV-CN. (A) Example traces collected in µ-conotoxin are shown for WT (black) and DIV-CN (gray). **(B)** Graphs of the charge voltage (Q-V) relationships of WT (black squares) and the DIV-CN mutant (gray triangles). Error bars represent standard error of the mean ($n \geq 4$).

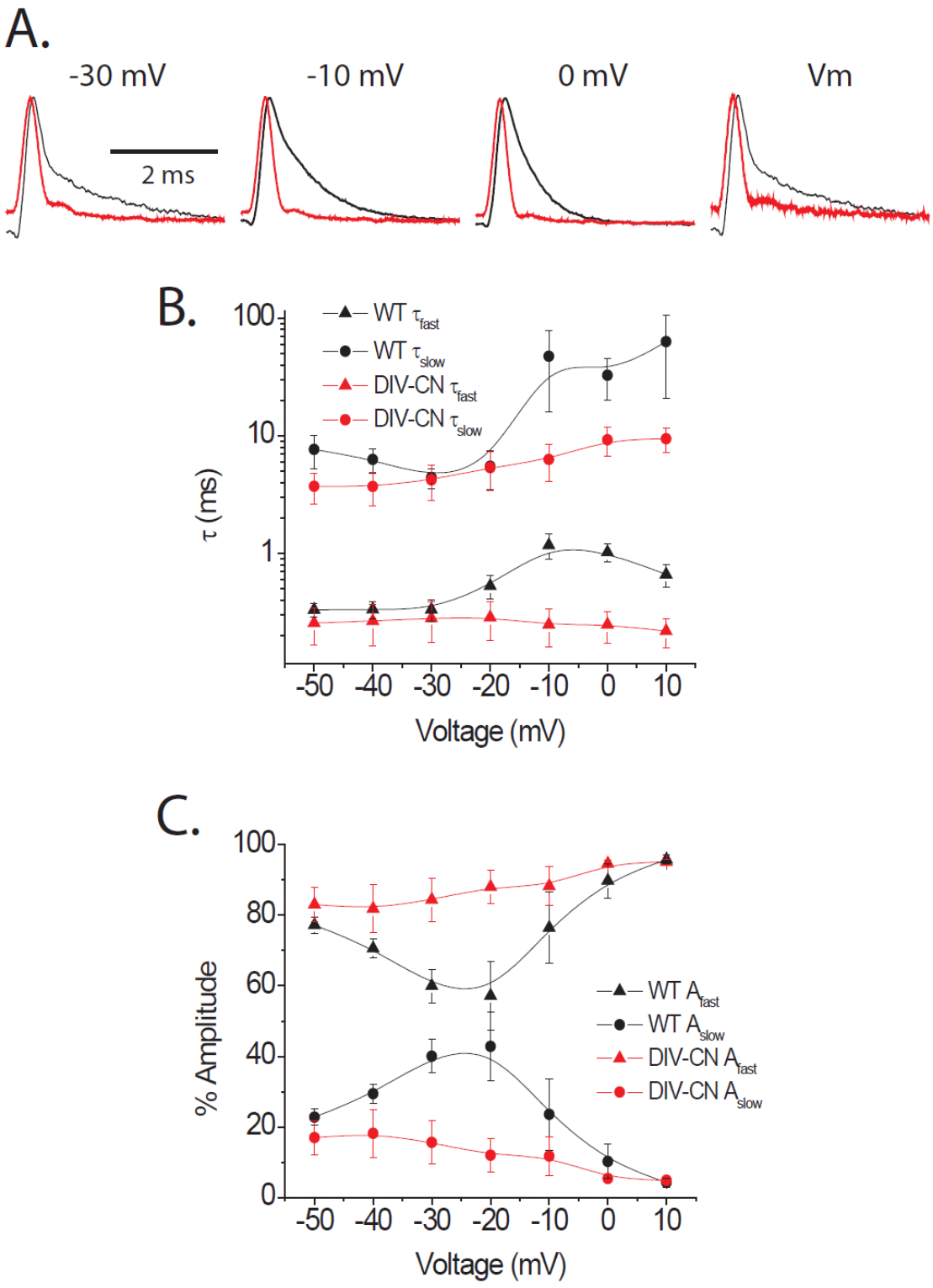
A.
-30 mV
-10 mV
0 mV
Vm
2 ms
B.
WT τfast
WT τslow
DIV-CN τfast
DIV-CN τslow
τ (ms)
100
10
1
-50 -40 -30 -20 -10 0 10
Voltage (mV)
C.
% Amplitude
100
80
60
40
20
0
WT Afast
WT Aslow
DIV-CN Afast
DIV-CN Aslow
-50 -40 -30 -20 -10 0 10
Voltage (mV)

Figure 7: The DIV-CN neutralizations reduce the slow component of the gating currents. (A) Example traces are shown overlapping for WT (black) and DIV-CN (red) at -30 mV, -10 mV, 0 mV, and near their respective midpoint values (Vm) on the Q-V curve shown above. **(B)** The WT and DIV-CN gating currents were each fit to a double exponential to obtain the fast and slow tau values at each voltage which were then plotted in (B). Fast taus are represented as triangles with WT in black and DIV-CN in red. Slow taus are represented as circles with WT in black and DIV-CN in red. **(C)** The fast (triangles) and slow (circles) amplitudes obtained from the bi-exponential fits are plotted against each other for WT (black) and DIV-CN (red). Error bars represent the standard error of the mean for at least 4 experiments.

Chapter V

Conclusions and Future Directions

Multiple past studies have determined that the voltage-sensors of different domains may have different roles (Chen 1996; Kontis 1997; Kontis and Goldin 1997; Horn, Ding et al. 2000; Chanda and Bezanilla 2002; Bosmans, Martin-Eauclaire et al. 2008). However, there existed some controversy as to whether only the DIV voltage-sensor was involved in fast inactivation (Kontis 1997; Kontis and Goldin 1997; Cha 1999). Additionally, the prevalent thought in the field was that slow inactivation derived its voltage-dependence solely through coupling to the activation process. Most of the prior evidence connecting the process of slow inactivation to voltage-sensor behavior hinged on the correlation of the voltage-sensor mode shift to slow inactivation. However, this mode shift was observed in non-inactivating channels as well as an isolated voltage-sensor (Piper, Varghese et al. 2003; Mannikko, Pandey et al. 2005; Villalba-Galea, Sandtner et al. 2008). Additionally, the mode shift behavior does not correlate with c-type inactivation in the potassium channel (Haddad and Blunck 2011). This study provides concrete evidence that the DIV voltage-sensor is the principle voltage-sensor involved in fast inactivation. Furthermore, we found that the DIV voltage-sensor is specifically coupled to the selectivity filter region of the channel, making the DIV S4 a good candidate for providing the voltage-dependence in slow inactivation as well.

5.1 The DIV voltage-sensor is coupled to the selectivity filter of the sodium channel

In order for the Nav channel to produce normal, well-coordinated action potentials, the channels must be able to inactivate. Under normal conditions, the sodium channel opens, conducts briefly, and quickly fast inactivates. During periods of sustained

activity or when the membrane is depolarized for long durations, sodium channels enter into the long term slow inactivated state. Slow inactivation in the sodium channel is thought to resemble C-type inactivation in the Kv channel with a selectivity filter collapse blocking conduction (Lopez-Barneo, Hoshi et al. 1993; Balser, Nuss et al. 1996; Liu, Jurman et al. 1996; Townsend and Horn 1997; Vilin, Fujimoto et al. 2001). This being the case, should a voltage-sensor provide the voltage-dependence of slow inactivation, it would follow that this voltage-sensor should be coupled to the selectivity filter region of the channel.

In our studies, by making either triple (DI, DIII, and DIV-CN) or double (DII-CN) neutralizations in a specific voltage-sensor, we were able to create gating pore currents (see Chapter III, Fig. 2) that were sensitive to the conformation of the individual voltage-sensor (Sokolov, Scheuer et al. 2005). As these currents did not pass through the central pore, a central pore blocking toxin such as TTX should only have an effect on the gating pore currents of a specific voltage-sensor if TTX alters the behavior of that voltage-sensor. We found that TTX had little effect on the DI, DII, or DIII-CN voltage-sensors. However, TTX caused a large reduction (by as much as 74%) in the DIV-CN gating pore currents (see Chapter III, Fig. 3). This pointed to the specific alteration of the DIV voltage-sensor by TTX. We further found that the effect of TTX on the DIV voltage-sensor was saturated and that TTX must be bound to its site in the outer pore in order to exert its effect (see Chapter III, Figs. 5 and 6). TTX, but not μ-CTX also causes a reduction in the total gating charge of the WT channel.

The above results suggested that the effects of TTX were likely based either in an electrostatic or an allosteric interaction. However the more highly charged outer pore

blocker μ-CTX had much less of an effect on the DIV voltage-sensor (see Chapter III Fig. 8), suggesting that the effects were likely caused via an allosteric interaction. TTX also inhibited the DIV-CN gating pore currents more efficiently at less hyperpolarized voltages, suggesting that TTX may favor the DIV voltage-sensor in an activated conformation.

The formation of a disulfide bond in the selectivity filter of the DIV-CN mutant channel also causes a reduction (around 70%) of the DIV-CN gating pore currents. Therefore, it is not likely to be TTX itself that is inducing the coupling between the DIV voltage-sensor and the selectivity filter. Together, the above results firmly suggest that the DIV voltage-sensor is coupled to the selectivity filter region of the channel. This unique type of coupling led us to form the hypothesis that the DIV voltage-sensor might provide voltage-dependence to the process of slow inactivation.

We next found that slow inactivation has the property of reducing the gating pore currents through the DIV-CN mutant. This particular reduction in gating pore currents after a long standing depolarization of the membrane most likely reflects a lower probability of the DIV voltage-sensor to be in a resting position. Since the voltage-sensor is not in its resting conformation where gating pore currents can flux, this explains the reduction that we observe in gating pore currents. The DIV voltage-sensor likely assumes a conformation that is either an activated position, or a 'relaxed' conformation as reported by the Bezanilla group (Villalba-Galea, Sandtner et al. 2008).

Previously, it was determined that the voltage-sensors exhibit a 'mode-shift' after long depolarizations. The membrane was held at depolarized potentials for an extended period (minutes) and then hyperpolarized again briefly before measuring the gating

currents. When the gating currents were recorded, the Q-V curve was greatly shifted to the left (charges moved at more hyperpolarized voltages). It was observed that this shift in the Q-V curve tied together well with the development of slow inactivation in sodium channels (Bezanilla, Taylor et al. 1982; Olcese, Latorre et al. 1997). However, it was later determined that an isolated voltage-sensor not connected to a pore (from the voltage-sensing phosphatase ci-VSP) exhibited a similar mode-shift behavior (Villalba-Galea, Sandtner et al. 2008). This finding complicates the interpretation of the results of our slow inactivation experiments. The decrease that we find in the gating pore currents of DIV-CN after long held depolarizations could be interpreted simply as an intrinsic mode-shift of the voltage-sensors and could be coincidental with the development of slow inactivation. This statement aside, it still remains an attractive hypothesis that the mode-shift behavior of the DIV voltage-sensor triggers the process of slow inactivation in the sodium channel.

5.2 The DIV voltage-sensor is the critical voltage-sensor in the process of fast inactivation

Previous studies in the potassium channel identified the first four charges of the Kv voltage-sensors as the most important charges. This study further hypothesized that the neutralization of these charges likely locked the affected voltage-sensor in its activated position (Bao, Hakeem et al. 1999). In the sodium channel, however, it was observed that the neutralization of the fourth charge caused little reduction in the total gating charge of the channel, leading to the hypothesis that the first three charges in the sodium channel were the most critical in gating behavior (Sheets and Hanck 2002). In order to parse out the role of each individual voltage-sensor in the process of fast

inactivation, we decided to create mutants in which the first three charges of one voltage-sensor at a time were neutralized to glutamine.

We determined that the voltage-sensors were in fact still mobile, as suggested by the voltage-dependent characteristics of the gating pore currents through each voltage-sensor. In the case of each of CN mutants, the neutralizations caused small to moderate leftward shifts in the G-V curves as compared to the WT channel (from an approximately 3 mV shift to a 16 mV shift). These data suggested that the channels were activating at slightly more hyperpolarized voltages than the WT channel and led us to suspect that while the mutations did not lock the voltage-sensors in their activated conformations, they might bias the affected voltage-sensor toward its activated conformation.

We next measured the voltage-dependence of fast inactivation for each of our CN mutants and found that for DI, DII, and DIII-CN, the triple neutralizations produced a slight leftward shift in their steady state inactivation curves as compared to the WT. On the other hand, the midpoint value of the DIV-CN steady state inactivation curve was drastically shifted to the left, with an estimated midpoint value of -137 mV (as compared to -62 mV in the WT). As the steady state inactivation curve of the DIV-CN mutant never reaches saturation at hyperpolarized voltages, the midpoint value of this construct is likely underestimated. Therefore, when three charges of the DIV voltage-sensor are neutralized, the affected channels are able to fast inactivate at much more hyperpolarized voltages than in the WT condition.

We further found that the lag before channels are able to enter fast inactivation was reduced for each of the neutralizations as compared to WT and abolished for the DIV-CN mutant. Fitting the data to a bi-exponential equation with a variable lag (see

Chapter II 2.6.1), we found that while the WT, DI, DII, and DIII-CN mutants exhibited clear voltage-dependence to fast tau, this was greatly reduced for the DIV-CN mutant. Additionally, while the lag for the WT, DI, DII, and DIII-CN reduced as more and more depolarized voltages were applied no similar trend was observed for the DIV-CN mutant. Therefore, the DIV-CN channels are able to enter into inactivation almost instantaneously.

Next, we attempted to match the kinetics of entry into fast inactivation to those of the ionic currents of each construct. We chose to use data collected at voltages that were near the midpoint value of the G-V curves for each mutant. Next, we normalized the ionic currents to their relative P_o on the graph (for example if the current was collected at the Vm of the G-V curve where half of the channels are open, the current would be normalized to 0.5). In cases where the channel is able to enter closed state inactivation, the entry into fast inactivation would occur ahead of the development of ionic current. We found that the kinetics of the ionic current in the WT matched closely with the development of fast inactivation. DI and DII-CN, on the other hand, revealed a delay after the development of ionic current before entry into fast inactivation occurred. The DIII-CN plot reveals that these neutralizations may slightly increase the propensity for these channels to close state inactivated. The entry into fast inactivation for DIV-CN occurs well before the development of ionic currents, suggesting that neutralization of charges in the DIV S4 makes it much more likely for the channels to enter closed state inactivation.

Next, we observed the recovery from inactivation behavior of each of the CN mutants. Similar to entry into fast inactivation, the recovery from inactivation exhibits a

typical lag phase before recovery can begin. All of the CN mutants exhibited a longer lag phase relative to the WT. As in earlier cases, the DIV-CN mutant presented with the largest change in the lag phase before recovery from inactivation with the time to half maximal recovery more than double the WT at -180 mV. These data suggest that while all of the voltage-sensors could potentially contribute to recovery from inactivation, it is likely the DIV S4 which is the most critical.

On observing WT gating currents, it is easy to see that there are two components, one fast and one slow. While the movement of the first three voltage-sensors precedes the activation of the channel, the fourth voltage-sensor appears to move more slowly (Chanda and Bezanilla 2002). The faster component of the gating current is thought to relate to channel opening and the slower component to inactivation.

As the fourth voltage-sensor moves more slowly and is important in fast inactivation, we elected to study the kinetics of the DIV-CN gating currents to determine whether the DIV voltage-sensor is the source of the slow component of gating. We found that the neutralization of the first three charges in the DIV voltage-sensor resulted in the removal of most of the slow component of gating. This result suggests that the DIV S4 is the major source of the slow component of gating. Furthermore, the DIV charge neutralizations resulted in a large leftward shift in the Q-V curve relative to the WT. This shift was much larger than the shift predicted solely by the reduction in the total charge of the channel. A leftward shift in the Q-V curve is consistent with the hypothesis that the altered DIV voltage-sensor is now able to move at more hyperpolarized voltages. Together, these data provide further support for the hypothesis that the DIV S4 is the critical voltage-sensor for fast inactivation.

5.3 A working model for Nav channel fast and slow inactivation

When the membrane potential reaches the threshold for sodium channel activation, the voltage-sensors begin to activate. The voltage-sensors of DI, DII, and DIII reach their activated positions faster than the DIV voltage-sensor. It has been previously suggested that the activation of the first three voltage-sensors may be enough to open the channel, however, this remains controversial (Sheets and Hanck 1995; Sheets, Kyle et al. 2000). While in its resting position, either the DIV S4-S5 linker or the DIV voltage-sensor itself blocks access of the inactivation loop to its docking site. As the DIV S4 activates, the inactivation loop is able to bind to its docking site and then blocks conduction.

In the case of the DIV-CN mutant, the DIV voltage-sensor has likely become biased heavily toward its activated position. This seems probable for two reasons: the gating pore currents have largely shut off by -120 mV (see Chapter III Figs. 3 and 8) and the Q-V curve of the DIV-CN mutant has shifted to more hyperpolarized voltages (see Chapter IV Fig. 6). For each of the voltages for which we measured the kinetics of entry into fast inactivation the altered DIV voltage-sensor has likely already activated. If you consider fast inactivation to be a simple two step process in which the DIV voltage-sensor must move and then the inactivation loop needs to bind its docking site, then we have effectively removed the first step of this process. I hypothesize that the rates of entry into fast inactivation may therefore reflect the intrinsic rates for the binding of the inactivation loop to its docking site.

Given our results, it is reasonable to state that the voltage-dependence of fast inactivation is derived from the voltage-dependent movement of the DIV voltage-sensor.

The altered DIV-CN voltage-sensor is moving at more hyperpolarized voltages. Therefore, it follows that if fast inactivation derives its voltage-dependence from the DIV voltage-sensor then the steady state inactivation curve should also shift to more hyperpolarized voltages.

Next, in order for the channel to reset itself for the next action potential, it must recover from inactivation. Based on our data for entry into fast inactivation, it would be reasonable to expect that in order for the channel to recover from fast inactivation, the DIV voltage-sensor must return to its resting conformation. In this case, we would predict an extended lag before recovery from fast inactivation as compared to the WT. Indeed, we do observe a larger lag for DIV-CN recovery from fast inactivation than for the WT or any of the other CN mutants. However, this data set becomes much more complicated to interpret when one observes that DI, DII, and DIII-CN also exhibit slower recovery from inactivation (albeit to a smaller degree). Therefore, I hypothesize that in the WT condition, much of the voltage-dependence of recovery from fast inactivation is derived from the DIV voltage-sensor. However, another source of the voltage-dependence of recovery from inactivation is obtained from the DI, DII, and DIII voltage-sensors via their coupling to the DIV S4. I also hypothesize that in order for a Nav channel to recover from fast inactivation, the DIV voltage-sensor must move into its resting position. Once the DIV voltage-sensor returns to its resting position, the inactivation loop can no longer occupy its binding site, and it pops off, allowing the channel to recover from inactivation (see Fig. 1).

In situations where the membrane remains depolarized for an extended stretch of time, the sodium channel undergoes slow inactivation. In the potassium channel, the

process of C-type inactivation greatly resembles sodium channel slow inactivation and it is thought that these two processes involve the collapse of the selectivity filter in the outer pore of the channel. This voltage-dependent process sculpts brainwave patterns and acts as a safeguard against erratic activity as well. Since we found that the DIV voltage-sensor is coupled to the selectivity filter region of the channel, I put forth the DIV S4 as a candidate for supplying the process of slow inactivation with it's voltage-dependence.

When the membrane is depolarized for long stretches of time, voltage-sensors undergo a mode-shift in which they tend to activate at much more hyperpolarized voltages than normally expected. This mode shift behavior can be found even in the isolated voltage-sensor, but I hypothesize that in the sodium channel, the mode-shift behavior of the fourth voltage-sensor may trigger the selectivity filter collapse of slow inactivation.

These findings indicate that the DIV voltage-sensor may be an important pharmacological target for modulation of slow inactivation. Drugs that modify slow inactivation such as Lacosamide may alter the behavior of the DIV voltage-sensor. Once a role of the DIV voltage-sensor in slow inactivation is confirmed, these data may help to explain the inverse relationship of fast inactivation and slow inactivation. When fast inactivation is eliminated, it has been found that slow inactivation is able to occur more quickly (Featherstone, Richmond et al. 1996; Wang, Bonner et al. 2003). If the DIV voltage-sensor does in fact play a role in both fast and slow inactivation, it would follow that a change in one process could affect the other. It may prove possible in the future to tip the balance of fast and slow inactivation using drugs that target the DIV voltage-

sensor. This would have potential utility in the treatment of sodium channel diseases ranging from arrhythmias to epilepsy.

5.4 Future directions

Our studies have shown that the DIV voltage-sensors is the principal voltage-sensor involved with fast inactivation and also brings to light the possibility that the DIV voltage-sensor may be a trigger for slow inactivation as well. To our knowledge, our data is the first to show an alternative mode of coupling other than the canonical inner pore gates to voltage-sensor coupling. This work suggests that differential coupling may underlie the functional specificity of different domains and further may allow for sodium channels and other heteromeric channels to participate in far more complex gating behaviors than previously thought possible. Our work also pinpoints the DIV voltage-sensor as an important potential target for treating illnesses that result in gain of function or loss of function in the sodium channels via modulation of the inactivation process.

However, there is still much work to be done. The DIV voltage-sensor is just one of the components involved in inactivation. Other sites, such as the inactivation loop docking site or the precise regions involved in slow inactivation, have yet to be clearly identified. Our fast inactivation data are explained well by a model in which the DIV voltage-sensor must move out of the way in order for the inactivation loop to bind, unfortunately, in the absence of a crystal structure of a mammalian Nav channel, these mechanisms remain purely speculative in nature. Moreover, we remain unable to definitively state that the conformational change in the selectivity filter that is coupled to the DIV voltage-sensor is slow inactivation and as of yet, we are unable to determine the

molecular pathway for this coupling. At this juncture we can only state that there is *a* conformational change in the selectivity filter that *may* be related to slow inactivation.

Moving forward, it would perhaps be advisable for future research to involve true locking of the voltage-sensors into either a closed or activated conformation. Though our experiments likely bias the voltage-sensors into their activated conformations, our approach still allows for some voltage-sensor movement and therefore may not be as clean. Moreover it would be ideal to study channels in which all gating charges are present if only to more effectively track down the degree of charge carried by each voltage-sensor. Furthermore, much work must still be done on the phenomenon of slow inactivation. It would perhaps prove beneficial to determine whether the voltage-dependence of slow inactivation is changed by either the DIV-CN mutations relative to DI, DII, DIII-CN, and the WT or by using a construct in which one voltage-sensor is locked in a resting or activated conformation. In conclusion, our experiments have identified some of the keystones necessary for the understanding the process of both fast and slow sodium channel inactivation.

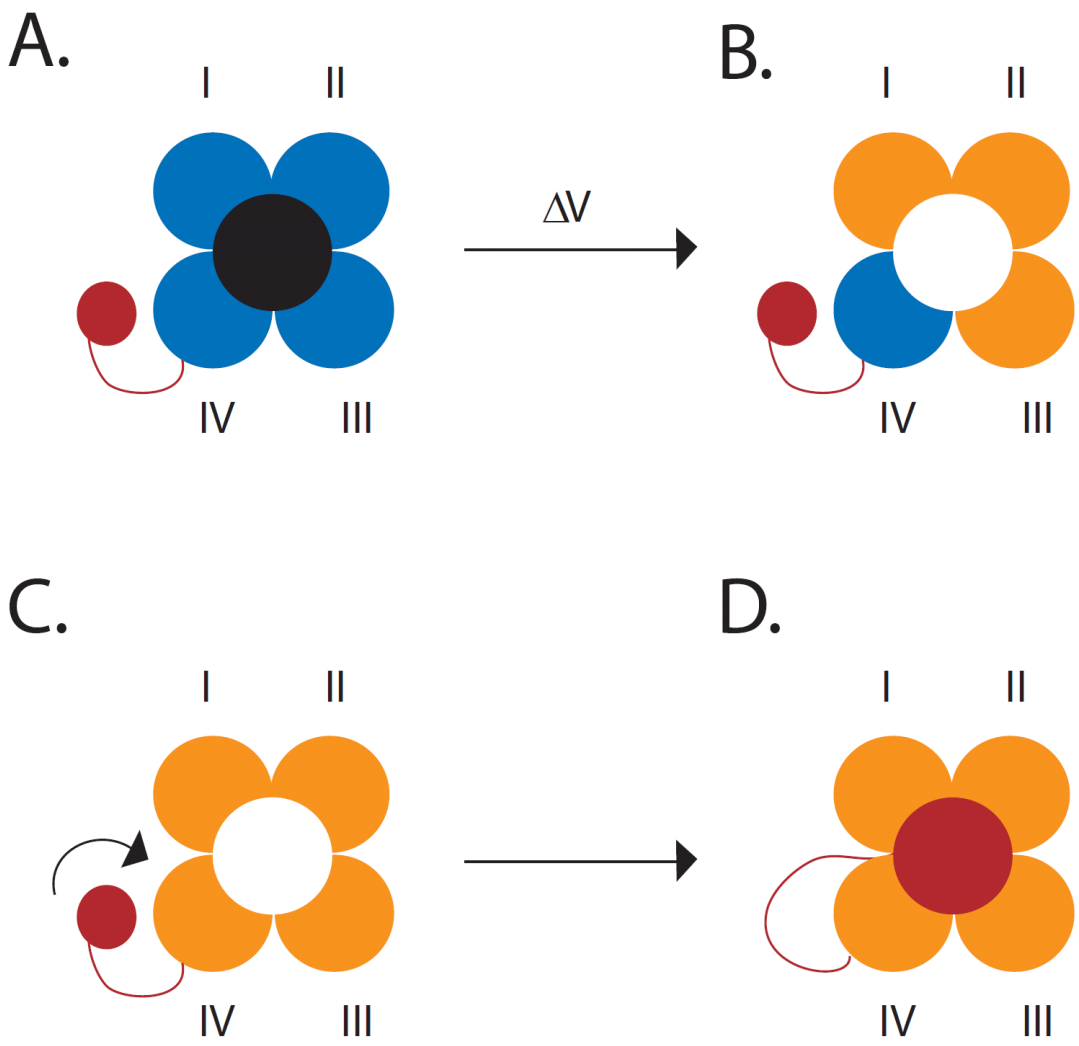

Figure 1: A model for the involvement of DIV S4 in fast inactivation. (A) A diagram depicting the closed pore (black circle) and resting voltage-sensors (blue circles) of the sodium channel. The inactivation particle (red) is tethered to the DIV S4. **(B)** After depolarization, the first three voltage-sensors activate (orange circles), and the pore opens (white circle). **(C)** The DIV S4 activates and this allows the inactivation particle to move towards its binding site. **(D)** The inactivation particle binds to its docking site and the channel fast inactivates.

REFERENCES

Aggarwal, S. K. and R. MacKinnon (1996). "Contribution of the S4 segment to gating charge in the Shaker K+ channel." Neuron **16**(6): 1169-1177.

Anklesaria, P., J. Teixido, et al. (1990). "Cell-cell adhesion mediated by binding of membrane-anchored transforming growth factor alpha to epidermal growth factor receptors promotes cell proliferation." Proc Natl Acad Sci U S A **87**(9): 3289-3293.

Antzelevitch, C., P. Brugada, et al. (2002). "Brugada syndrome: a decade of progress." Circ Res **91**(12): 1114-1118.

Armstrong, C. M. and F. Bezanilla (1973). "Currents related to movement of the gating particles of the sodium channels." Nature **242**(5398): 459-461.

Armstrong, C. M., F. Bezanilla, et al. (1973). "Destruction of sodium conductance inactivation in squid axons perfused with pronase." J Gen Physiol **62**(4): 375-391.

Backx, P. H., D. T. Yue, et al. (1992). "Molecular localization of an ion-binding site within the pore of mammalian sodium channels." Science **257**(5067): 248-251.

Balser, J. R., H. B. Nuss, et al. (1996). "External pore residue mediates slow inactivation in mu 1 rat skeletal muscle sodium channels." J Physiol **494 (Pt 2)**: 431-442.

Bao, H., A. Hakeem, et al. (1999). "Voltage-insensitive gating after charge-neutralizing mutations in the S4 segment of Shaker channels." J Gen Physiol **113**(1): 139-151.

Bell, D. and A. Siriwardena (2000). "Phrenic nerve injury following blunt trauma." J Accid Emerg Med **17**(6): 419-420.

Benitah, J. P., Z. Chen, et al. (1999). "Molecular dynamics of the sodium channel pore vary with gating: interactions between P-segment motions and inactivation." J Neurosci **19**(5): 1577-1585.

Benitah, J. P., R. Ranjan, et al. (1997). "Molecular motions within the pore of voltage-dependent sodium channels." Biophys J **73**(2): 603-613.

Benzinger, G. R., C. L. Drum, et al. (1997). "Differences in the binding sites of two site-3 sodium channel toxins." Pflugers Arch **434**(6): 742-749.

Bezanilla, F. (2000). "The voltage sensor in voltage-dependent ion channels." Physiol Rev **80**(2): 555-592.

Bezanilla, F. and C. M. Armstrong (1975). "Kinetic properties and inactivation of the gating currents of sodium channels in squid axon." Philos Trans R Soc Lond B Biol Sci **270**(908): 449-458.

Bezanilla, F., R. E. Taylor, et al. (1982). "Distribution and kinetics of membrane dielectric polarization. 1. Long-term inactivation of gating currents." J Gen Physiol **79**(1): 21-40.

Bezzina, C. R., M. B. Rook, et al. (2001). "Cardiac sodium channel and inherited arrhythmia syndromes." Cardiovasc Res **49**(2): 257-271.

Bosmans, F., M. F. Martin-Eauclaire, et al. (2008). "Deconstructing voltage sensor function and pharmacology in sodium channels." Nature **456**(7219): 202-208.

Catterall, W. A., S. Dib-Hajj, et al. (2008). "Inherited neuronal ion channelopathies: new windows on complex neurological diseases." J Neurosci **28**(46): 11768-11777.

Cha, A., P.C.Ruben, A.L.George, Jr., E.Fujimoto, and F.Bezanilla. (1999). "Voltage sensors in domains III and IV, but not I and II, are immobilized by Na+ channel fast inactivation." Neuron **22**: 14.

Chahine, M., A. L. George, Jr., et al. (1994). "Sodium channel mutations in paramyotonia congenita uncouple inactivation from activation." Neuron **12**(2): 281-294.

Chanda, B., O. K. Asamoah, et al. (2005). "Gating charge displacement in voltage-gated ion channels involves limited transmembrane movement." Nature **436**(7052): 852-856.

Chanda, B. and F. Bezanilla (2002). "Tracking voltage-dependent conformational changes in skeletal muscle sodium channel during activation." J Gen Physiol **120**(5): 629-645.

Chen, L. Q., V.Santarelli, R.Horn, and R.G.Kallen. (1996). "A unique role for the S4 segment of domain 4 in the inactivation of sodium channels." Journal of General Physiology **108**: 7.

Chiamvimonvat, N., M. T. Perez-Garcia, et al. (1996). "Depth asymmetries of the pore-lining segments of the Na+ channel revealed by cysteine mutagenesis." Neuron **16**(5): 1037-1047.

Chinushi, M., H. Kasai, et al. (2002). "Triggers of ventricular tachyarrhythmias and therapeutic effects of nicorandil in canine models of LQT2 and LQT3 syndromes." J Am Coll Cardiol **40**(3): 555-562.

Chopra, N. and B. C. Knollmann (2011). "Genetics of sudden cardiac death syndromes." Curr Opin Cardiol **26**(3): 196-203.

Cordero-Morales, J. F., L. G. Cuello, et al. (2006). "Voltage-dependent gating at the KcsA selectivity filter." Nat Struct Mol Biol **13**(4): 319-322.

Cordero-Morales, J. F., L. G. Cuello, et al. (2006). "Molecular determinants of gating at the potassium-channel selectivity filter." Nat Struct Mol Biol **13**(4): 311-318.

Cuello, L. G., V. Jogini, et al. (2010). "Structural mechanism of C-type inactivation in K(+) channels." Nature **466**(7303): 203-208.

Cummins, T. R. and F. J. Sigworth (1996). "Impaired slow inactivation in mutant sodium channels." Biophys J **71**(1): 227-236.

Davidenko, J. M., L. Cohen, et al. (1989). "Quinidine-induced action potential prolongation, early afterdepolarizations, and triggered activity in canine Purkinje fibers. Effects of stimulation rate, potassium, and magnesium." Circulation **79**(3): 674-686.

Favre, I., E. Moczydlowski, et al. (1996). "On the structural basis for ionic selectivity among Na+, K+, and Ca2+ in the voltage-gated sodium channel." Biophys J **71**(6): 3110-3125.

Featherstone, D. E., J. E. Richmond, et al. (1996). "Interaction between fast and slow inactivation in Skm1 sodium channels." Biophys J **71**(6): 3098-3109.

Fleidervish, I. A., A. Friedman, et al. (1996). "Slow inactivation of Na+ current and slow cumulative spike adaptation in mouse and guinea-pig neocortical neurones in slices." J Physiol **493 (Pt 1)**: 83-97.

French, R. J., D. Yoshikami, et al. (2010). "The tetrodotoxin receptor of voltage-gated sodium channels--perspectives from interactions with micro-conotoxins." Mar Drugs **8**(7): 2153-2161.

Goldin, A. L. (2003). "Mechanisms of sodium channel inactivation." Curr Opin Neurobiol **13**(3): 284-290.

Grant, A. O. (2005). "Electrophysiological basis and genetics of Brugada syndrome." J Cardiovasc Electrophysiol **16 Suppl 1**: S3-7.

Greffrath, W., S. T. Schwarz, et al. (2009). "Heat-induced action potential discharges in nociceptive primary sensory neurons of rats." J Neurophysiol **102**(1): 424-436.

Haddad, G. A. and R. Blunck (2011). "Mode shift of the voltage sensors in Shaker K+ channels is caused by energetic coupling to the pore domain." J Gen Physiol **137**(5): 455-472.

Hanck, D. A. and M. F. Sheets (1995). "Modification of inactivation in cardiac sodium channels: ionic current studies with Anthopleurin-A toxin." J Gen Physiol **106**(4): 601-616.

Heinemann, S. H., H. Terlau, et al. (1992). "Calcium channel characteristics conferred on the sodium channel by single mutations." Nature **356**(6368): 441-443.

Hilber, K., W. Sandtner, et al. (2001). "The selectivity filter of the voltage-gated sodium channel is involved in channel activation." J Biol Chem **276**(30): 27831-27839.

Hilden, S. and L. E. Hokin (1975). "Active potassium transport coupled to active sodium transport in vesicles reconstituted from purified sodium and potassium ion-activated adenosine triphosphatase from the rectal gland of Squalus acanthias." J Biol Chem **250**(16): 6296-6303.

Hille, B. (2001). Ion channels of excitable membranes. Sunderland, Mass., Sinauer.

Hodgkin, A. L. and A. F. Huxley (1952). "A quantitative description of membrane current and its application to conduction and excitation in nerve." J Physiol **117**(4): 500-544.

Hodgkin, A. L. and R. D. Keynes (1955). "Active transport of cations in giant axons from Sepia and Loligo." J Physiol **128**(1): 28-60.

Horn, R., S. Ding, et al. (2000). "Immobilizing the moving parts of voltage-gated ion channels." J Gen Physiol **116**(3): 461-476.

Huang, C. J., I. Favre, et al. (2000). "Permeation of large tetra-alkylammonium cations through mutant and wild-type voltage-gated sodium channels as revealed by relief of block at high voltage." J Gen Physiol **115**(4): 435-454.

Islas, L. D. and F. J. Sigworth (2001). "Electrostatics and the gating pore of Shaker potassium channels." J Gen Physiol **117**(1): 69-89.

Isom, L. L., K. S. De Jongh, et al. (1992). "Primary structure and functional expression of the beta 1 subunit of the rat brain sodium channel." Science **256**(5058): 839-842.

Jiang, Y., V. Ruta, et al. (2003). "The principle of gating charge movement in a voltage-dependent K+ channel." Nature **423**(6935): 42-48.

Jo, S. and B. P. Bean (2011). "Inhibition of neuronal voltage-gated sodium channels by brilliant blue G." Mol Pharmacol **80**(2): 247-257.

Jones, D. K. and P. C. Ruben (2008). "Biophysical defects in voltage.gated sodium channels associated with long QT and Brugada syndromes." Channels (Austin) **2**(2): 70-80.

Jurkat-Rott, K., B. Holzherr, et al. (2010). "Sodium channelopathies of skeletal muscle result from gain or loss of function." Pflugers Arch **460**(2): 239-248.

Kirsch, G. E., M. Alam, et al. (1994). "Differential effects of sulfhydryl reagents on saxitoxin and tetrodotoxin block of voltage-dependent Na channels." Biophys J **67**(6): 2305-2315.

Kontis, K. J., A.Rounaghi, and A.L.Goldin. (1997). "Sodium channel activation gating is affected by substitutions of voltage sensor positive charges in all four domains." Journal of General Physiology **1997**: 10.

Kontis, K. J. and A. L. Goldin (1997). "Sodium channel inactivation is altered by substitution of voltage sensor positive charges." J Gen Physiol **110**(4): 403-413.

Kontis, K. J., A. Rounaghi, et al. (1997). "Sodium channel activation gating is affected by substitutions of voltage sensor positive charges in all four domains." J Gen Physiol **110**(4): 391-401.

Kontis, K. J. a. A. L. G. (1997). "Sodium channel inactivation is altered by substitution of voltage sensor positive charges." Journal of General Physiology **110**: 10.

Leffler, A., R. I. Herzog, et al. (2005). "Pharmacological properties of neuronal TTX-resistant sodium channels and the role of a critical serine pore residue." Pflugers Arch **451**(3): 454-463.

Liu, Y., M. Holmgren, et al. (1997). "Gated access to the pore of a voltage-dependent K+ channel." Neuron **19**(1): 175-184.

Liu, Y., M. E. Jurman, et al. (1996). "Dynamic rearrangement of the outer mouth of a K+ channel during gating." Neuron **16**(4): 859-867.

Long, S. B., E. B. Campbell, et al. (2005). "Crystal structure of a mammalian voltage-dependent Shaker family K+ channel." Science **309**(5736): 897-903.

Lopez-Barneo, J., T. Hoshi, et al. (1993). "Effects of external cations and mutations in the pore region on C-type inactivation of Shaker potassium channels." Receptors Channels **1**(1): 61-71.

Mannikko, R., S. Pandey, et al. (2005). "Hysteresis in the voltage dependence of HCN channels: conversion between two modes affects pacemaker properties." J Gen Physiol **125**(3): 305-326.

Mitchell, P. (1961). "Coupling of phosphorylation to electron and hydrogen transfer by a chemi-osmotic type of mechanism." Nature **191**: 144-148.

Miyamoto, K., T. Nakagawa, et al. (2001). "Solution structures of the cytoplasmic linkers between segments S4 and S5 (S4-S5) in domains III and IV of human brain sodium channels in SDS micelles." J Pept Res **58**(3): 193-203.

Noda, M., S. Shimizu, et al. (1984). "Primary structure of Electrophorus electricus sodium channel deduced from cDNA sequence." Nature **312**(5990): 121-127.

Olcese, R., R. Latorre, et al. (1997). "Correlation between charge movement and ionic current during slow inactivation in Shaker K+ channels." J Gen Physiol **110**(5): 579-589.

Ong, B. H., G. F. Tomaselli, et al. (2000). "A structural rearrangement in the sodium channel pore linked to slow inactivation and use dependence." J Gen Physiol **116**(5): 653-662.

Papadopoulos, V., P. Kamtchouing, et al. (1987). "Adult rat Sertoli cells secrete a factor or factors which modulate Leydig cell function." J Endocrinol **114**(3): 459-467.

Papazian, D. M., L. C. Timpe, et al. (1991). "Alteration of voltage-dependence of Shaker potassium channel by mutations in the S4 sequence." Nature **349**(6307): 305-310.

Payandeh, J., T. Scheuer, et al. (2011). "The crystal structure of a voltage-gated sodium channel." Nature **475**(7356): 353-358.

Perez-Garcia, M. T., N. Chiamvimonvat, et al. (1997). "Mechanisms of sodium/calcium selectivity in sodium channels probed by cysteine mutagenesis and sulfhydryl modification." Biophys J **72**(3): 989-996.

Piper, D. R., A. Varghese, et al. (2003). "Gating currents associated with intramembrane charge displacement in HERG potassium channels." Proc Natl Acad Sci U S A **100**(18): 10534-10539.

Satin, J., J. W. Kyle, et al. (1992). "A mutant of TTX-resistant cardiac sodium channels with TTX-sensitive properties." Science **256**(5060): 1202-1205.

Schauf, C. L., T. L. Pencek, et al. (1976). "Slow sodium inactivation in Myxicola axons. Evidence for a second inactive state." Biophys J **16**(7): 771-778.

Seoh, S. A., D. Sigg, et al. (1996). "Voltage-sensing residues in the S2 and S4 segments of the Shaker K+ channel." Neuron **16**(6): 1159-1167.

Sheets, M. F. and D. A. Hanck (1995). "Voltage-dependent open-state inactivation of cardiac sodium channels: gating current studies with Anthopleurin-A toxin." J Gen Physiol **106**(4): 617-640.

Sheets, M. F. and D. A. Hanck (2002). "The outermost lysine in the S4 of domain III contributes little to the gating charge in sodium channels." Biophys J **82**(6): 3048-3055.

Sheets, M. F., J. W. Kyle, et al. (2000). "The role of the putative inactivation lid in sodium channel gating current immobilization." J Gen Physiol **115**(5): 609-620.

Sheets, M. F., J. W. Kyle, et al. (1999). "The Na channel voltage sensor associated with inactivation is localized to the external charged residues of domain IV, S4." Biophys J **77**(2): 747-757.

Smith, M. R. and A. L. Goldin (1997). "Interaction between the sodium channel inactivation linker and domain III S4-S5." Biophys J **73**(4): 1885-1895.

Sokolov, S., T. Scheuer, et al. (2005). "Ion permeation through a voltage- sensitive gating pore in brain sodium channels having voltage sensor mutations." Neuron **47**(2): 183-189.

Sokolov, S., T. Scheuer, et al. (2007). "Gating pore current in an inherited ion channelopathy." Nature **446**(7131): 76-78.

Sokolov, S., T. Scheuer, et al. (2010). "Ion permeation and block of the gating pore in the voltage sensor of NaV1.4 channels with hypokalemic periodic paralysis mutations." J Gen Physiol **136**(2): 225-236.

Starace, D. M. and F. Bezanilla (2004). "A proton pore in a potassium channel voltage sensor reveals a focused electric field." Nature **427**(6974): 548-553.

Stefani E, B. F. (1998). "Cut-open oocyte voltage-clamp technique." Methods Enzymol. **293**: 18.

Struyk, A. F. and S. C. Cannon (2007). "A Na+ channel mutation linked to hypokalemic periodic paralysis exposes a proton-selective gating pore." J Gen Physiol **130**(1): 11-20.

Stühmer W, C. F., Suzuki H, Wang XD, Noda M, Yahagi N, Kubo H, Numa S. (1989). "Structural parts involved in activation and inactivation of the sodium channel." Nature **339**(6226): 6.

Tempel, B. L., D. M. Papazian, et al. (1987). "Sequence of a probable potassium channel component encoded at Shaker locus of Drosophila." Science **237**(4816): 770-775.

Thomsen, W. J. and W. A. Catterall (1989). "Localization of the receptor site for alpha-scorpion toxins by antibody mapping: implications for sodium channel topology." Proc Natl Acad Sci U S A **86**(24): 10161-10165.

Todt, H., S. C. Dudley, Jr., et al. (1999). "Ultra-slow inactivation in mu1 Na+ channels is produced by a structural rearrangement of the outer vestibule." Biophys J **76**(3): 1335-1345.

Townsend, C. and R. Horn (1997). "Effect of alkali metal cations on slow inactivation of cardiac Na+ channels." J Gen Physiol **110**(1): 23-33.

Tsushima, R. G., R. A. Li, et al. (1997). "P-loop flexibility in Na+ channel pores revealed by single- and double-cysteine replacements." J Gen Physiol **110**(1): 59-72.

Vilin, Y. Y., E. Fujimoto, et al. (2001). "A single residue differentiates between human cardiac and skeletal muscle Na+ channel slow inactivation." Biophys J **80**(5): 2221-2230.

Villalba-Galea, C. A., W. Sandtner, et al. (2008). "S4-based voltage sensors have three major conformations." Proc Natl Acad Sci U S A **105**(46): 17600-17607.

Wang, S. Y., K. Bonner, et al. (2003). "Tryptophan scanning of D1S6 and D4S6 C-termini in voltage-gated sodium channels." Biophys J **85**(2): 911-920.

Wang, Y., K. D. Park, et al. (2011). "Development and characterization of novel derivatives of the antiepileptic drug lacosamide that exhibit far greater enhancement in slow inactivation of voltage-gated sodium channels." ACS Chem Neurosci **2**(2): 90-106.

Wedekind, H., J. P. Smits, et al. (2001). "De novo mutation in the SCN5A gene associated with early onset of sudden infant death." Circulation **104**(10): 1158-1164.

Wei, J., D. W. Wang, et al. (1999). "Congenital long-QT syndrome caused by a novel mutation in a conserved acidic domain of the cardiac Na+ channel." Circulation **99**(24): 3165-3171.

West, J. W., D. E. Patton, et al. (1992). "A cluster of hydrophobic amino acid residues required for fast Na(+)-channel inactivation." Proc Natl Acad Sci U S A **89**(22): 10910-10914.

Wit, A. L., B. F. Hoffman, et al. (1972). "Slow conduction and reentry in the ventricular conducting system. I. Return extrasystole in canine Purkinje fibers." Circ Res **30**(1): 1-10.

Xiong, W., Y. Z. Farukhi, et al. (2006). "A conserved ring of charge in mammalian Na+ channels: a molecular regulator of the outer pore conformation during slow inactivation." J Physiol **576**(Pt 3): 739-754.

Xiong, W., R. A. Li, et al. (2003). "Molecular motions of the outer ring of charge of the sodium channel: do they couple to slow inactivation?" J Gen Physiol **122**(3): 323-332.

Yan, G. X. and C. Antzelevitch (1999). "Cellular basis for the Brugada syndrome and other mechanisms of arrhythmogenesis associated with ST-segment elevation." Circulation **100**(15): 1660-1666.

Yang, N., A. L. George, Jr., et al. (1996). "Molecular basis of charge movement in voltage-gated sodium channels." Neuron **16**(1): 113-122.

Zhang, M. M., P. Gruszczynski, et al. (2010). "Cooccupancy of the outer vestibule of voltage-gated sodium channels by micro-conotoxin KIIIA and saxitoxin or tetrodotoxin." J Neurophysiol **104**(1): 88-97.

Zhang, M. M., J. R. McArthur, et al. (2009). "Synergistic and antagonistic interactions between tetrodotoxin and mu-conotoxin in blocking voltage-gated sodium channels." Channels (Austin) **3**(1): 32-38.

Zimmer, T. and R. Surber (2008). "SCN5A channelopathies--an update on mutations and mechanisms." Prog Biophys Mol Biol **98**(2-3): 120-136.

Gating transitions in the selectivity filter region of a sodium channel are coupled to the domain IV voltage sensor

Deborah L. Capes[a,b], Manoel Arcisio-Miranda[a,c], Brian W. Jarecki[a], Robert J. French[d], and Baron Chanda[a,1]

[a]Department of Neuroscience, University of Wisconsin, Madison, WI 53706; [b]Molecular and Cellular Pharmacology Graduate Program, and [c]Department of Biophysics, Federal University of Sao Paulo, 04023-060, Sao Paulo, Brazil; and [d]Department of Physiology and Pharmacology, University of Calgary, Calgary, AB, Canada T2N 4N1

Edited by Richard W. Aldrich, University of Texas, Austin, TX, and approved January 5, 2012 (received for review September 22, 2011)

Voltage-dependent ion channels are crucial for generation and propagation of electrical activity in biological systems. The primary mechanism for voltage transduction in these proteins involves the movement of a voltage-sensing domain (D), which opens a gate located on the cytoplasmic side. A distinct conformational change in the selectivity filter near the extracellular side has been implicated in slow inactivation gating, which is important for spike frequency adaptation in neural circuits. However, it remains an open question whether gating transitions in the selectivity filter region are also actuated by voltage sensors. Here, we examine conformational coupling between each of the four voltage sensors and the outer pore of a eukaryotic voltage-dependent sodium channel. The voltage sensors of these sodium channels are not structurally symmetric and exhibit functional specialization. To track the conformational rearrangements of individual voltage-sensing domains, we recorded domain-specific gating pore currents. Our data show that, of the four voltage sensors, only the domain IV voltage sensor is coupled to the conformation of the selectivity filter region of the sodium channel. Trapping the outer pore in a particular conformation with a high-affinity toxin or disulphide crossbridge impedes the return of this voltage sensor to its resting conformation. Our findings directly establish that, in addition to the canonical electromechanical coupling between voltage sensor and inner pore gates of a sodium channel, gating transitions in the selectivity filter region are also coupled to the movement of a voltage sensor. Furthermore, our results also imply that the voltage sensor of domain IV is unique in this linkage and in the ability to initiate slow inactivation in sodium channels.

electrophysiology | Nav1.4 | outer pore conformation

Voltage-gated sodium channels, like the other constituents of the voltage-gated ion channel superfamily, undergo gating transitions that result in channel opening and inactivation. Structural studies mainly on potassium selective ion channels have established that the opening of the channel primarily involves splaying of the bundle crossing formed on the intracellular side by the S6 helices (1–3). C-type inactivation gating, which follows channel opening and is mechanistically distinct from fast N-type inactivation, involves conformational rearrangements in the selectivity filter region (4–8).

According to our current thinking, inactivation gating at the selectivity filter region arises as a result of structural changes that follow pore opening and are not due to the movement of voltage sensors (9–11). Indeed, gating currents, which are a measure of voltage-sensing charge movements, are recorded under conditions with altered C-type inactivation (12) or with blockers that interact intimately with groups at the ion binding site (13, 14). For instance, the gating currents in exemplar Shaker potassium channels are typically measured in the background of the W434F mutation which results in a permanently C-type inactivated channel (15, 16). Although it has been suggested that the slow C-type inactivation may be coupled to voltage sensor movement, the evidence to date has been indirect and somewhat confounding. Charge–voltage (Q–V) curves of Shaker potassium channel were found to undergo time and voltage-dependent shifts, which correlated with development of C-type inactivation (17). Signals from fluorescent probes attached to the S3–S4 loop of the Shaker potassium channel develop an additional component, which also correlates with C-type inactivation (18). However, this may not reflect coupling between voltage sensor and outer pore because these fluorescent probes are bulky and, in all likelihood, directly sense the conformation of the outer pore. Recent studies have suggested that the holding-potential–dependent shift in the Q–V curve is an intrinsic property of a voltage sensor and may not necessarily reflect coupling to the outer pore. Charge–voltage curves of an isolated voltage sensor lacking a pore domain (D) were found to exhibit these charge shifts ("mode shifts") upon changing the holding potential (19). Moreover, a noninactivating mutant of the human ether-a-go-go related gene (HERG) channel (20) and noninactivating hyperpolarization-activated cyclic nucleotide-gated (HCN) channels (21) both show holding-potential–dependent shifts in Q–V curves. Finally, this correlation between charge shift and C-type inactivation has been reexamined by other groups who have concluded that these two processes are not coupled in the Shaker potassium channel (22).

The goal of this study is to test whether, in a voltage-gated sodium channel, the outer pore conformation is energetically coupled to the movement of a voltage sensor. As in the tetrameric potassium channels, the voltage-gated sodium channels also have two gates that control ion flux through the central pore. Studies with accessory subunits (23, 24) and local anesthetics (25, 26) provide reassuring evidence that the primary pore gate is on the cytoplasmic side of the channel. The cytoplasmic region of the β4 subunit behaves as a classical open pore blocker (1). It blocks the conductance of the open pore in a state-dependent manner and prevents the deactivation of the sodium channel gates (23). The recently solved landmark structure of a prokaryotic sodium channel, NaVab also shows rather strikingly that the intracellular pore helices can gate the ion conducting pathway (27). Several groups have proposed that the selectivity filter region of the sodium channel is the site for a second gate, which is involved in slow and ultraslow inactivation gating (28–36). In many respects, slow inactivation gating in the sodium channels is similar to C-type inactivation (4, 5, 28, 34, 35). Although residues

Author contributions: D.L.C., M.A.-M., and B.C. designed research; D.L.C., M.A.-M., and B.W.J. performed research; R.J.F. contributed new reagents/analytic tools; D.L.C., M.A.-M., B.W.J., and B.C. analyzed data; and D.L.C. and B.C. wrote the paper.

The authors declare no conflict of interest.

This article is a PNAS Direct Submission.

[1]To whom correspondence should be addressed. E-mail: chanda@wisc.edu.

This article contains supporting information online at www.pnas.org/lookup/suppl/doi:10.1073/pnas.1115575109/-/DCSupplemental.

in the intracellular S6 segments of the sodium channels have also been implicated in slow inactivation (37, 38), recent evidence with disulphide crosslinking of paired substituted cysteines strongly suggests that the occlusion of outer pore is a critical determinant for slow inactivation (31, 32). Here, we examine the coupling between the individual voltage sensors of a sodium channel and conformational rearrangements in the selectivity filter region. Using disulphide crossbridge of pore residues and high-affinity toxins, we establish that modulation of the selectivity filter conformation specifically modifies the activation of the domain IV (DIV) voltage sensor, thus implying that these two processes are conformationally coupled.

Results and Discussion

Gating Pore Currents in Charge Neutralized Mutants. To monitor the conformation of individual voltage sensors, we generated a series of mutants in which the first two or three extracellular charges of one voltage sensor at a time were mutated to a glutamine (Fig. 1*A*). Design of these *charge neutralized* (CN) Nav1.4 mutants, e.g., domain I (DI-CN) was motivated in part by recent findings that mutation of specific charged residues in the S4 segments allows state-dependent ion flux through the voltage-sensing domains (39–42). These currents directly report the movement of voltage sensors and are referred to as gating pore currents (also omega currents) to distinguish them from the canonical ionic currents through the central pore.

Each of the CN mutants, when expressed in *Xenopus* oocytes, generate currents upon depolarization resembling the wild-type sodium currents (Fig. 1*B*) (43). Due to low expression as well as persistent outward leak, we used the DII-CN mutant in which only the first two charges are neutralized for the remainder of this study. In addition to typical sodium currents, we observe large hyperpolarization activated inward currents in all CN mutants (Fig. 2). The kinetics and voltage dependence of these currents are similar to the gating pore currents reported for domain II (41).

This approach of monitoring individual voltage sensors overcomes the limitations of using large spectroscopic probes to monitor local conformational dynamics (44, 45). The fluorescent probes attached to the voltage sensors are in close proximity to the outer pore (the top of S5 and S6 segments) and, therefore, one cannot unambiguously ascribe those signals to voltage sensor movements (18).

Effect of Pore Blocking Toxins on Gating Pore Currents. To probe the coupling between the selectivity filter and the voltage sensors, we first examined the effect of tetrodotoxin (TTX), a high-affinity sodium channel blocker, because it has been reported to inhibit sodium currents in a use-dependent manner (46, 47). In CN mutants, the currents elicited by depolarizing voltage steps were completely blocked by a saturating concentration of TTX (up to 1.1 μM) (Fig. S1). As expected, TTX does not block gating pore currents through the CN mutants (41, 42). Nonetheless, to our surprise, the gating pore currents through DIV-CN were significantly altered by TTX (Fig. 2). At −110 mV, the

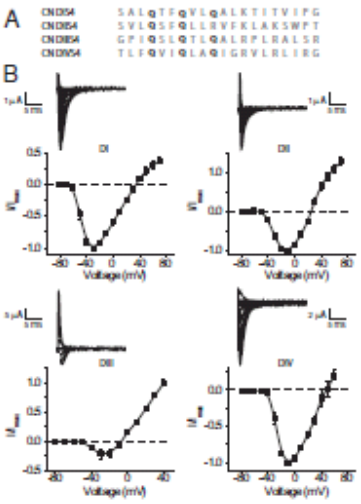

Fig. 1. Functionality of the charge-neutralized sodium channel mutants. (*A*) The sequence of the altered S4 segments of all four mutants. The sites that were mutated to glutamines are bold. (*B*) Current–voltage relationships for each of the mutants with a representative family of traces. Note that some of these current recordings were obtained in different ionic conditions (for details see *Methods*). Each graph represents the mean ± SE of at least three independent experiments. Also note that the ionic currents at more depolarized potentials are, in some cases, contaminated by gating currents.

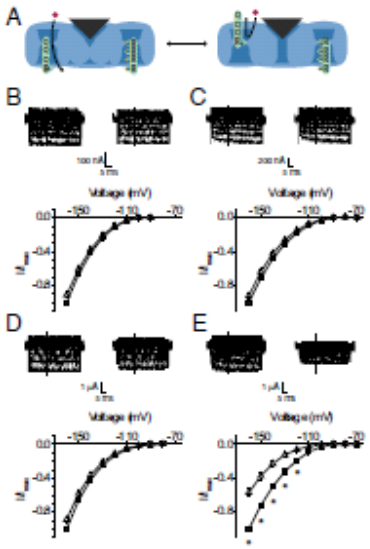

Fig. 2. Effect of TTX on gating pore currents through the individual voltage sensors. (*A*) Schematic diagram depicting the conformational processes that produce voltage-dependent gating pore currents. (*Left*) Channel where the main pore is closed and the voltage sensors are in a resting conformation. In this condition, the mutant voltage sensor is in a permissive position for gating pore currents. Currents through the central pore are blocked by a pore toxin. (*Right*) Channel with the voltage sensors in an activated conformation and the remaining charges in the mutant voltage sensor move into a position that blocks the flux of gating pore current. A family of gating pore currents before (*Left*, filled square) and after (*Right*, unfilled triangle) addition of TTX from the DI-CN (*B*), DII-CN (*C*), DIII-CN (*D*), and DIV-CN (*E*) mutants (*Upper*). Normalized current–voltage plots of the same (*Lower*). The currents at each voltage were measured at the end of 20 ms, marked as a dashed line. Each plot represents the mean ± SE of at least three independent experiments. *P value <0.05, statistical significance.

PHYSIOLOGY

magnitude of current was reduced by as much as 65%. Moreover, a further increase in toxin concentration (up to 10-fold) did not increase inhibition of gating pore currents, suggesting that this effect is saturated (Fig. S2). We can eliminate the possibility that the hyperpolarization activated currents through DIV-CN are due to ion flux through the central pore as opposed to being gating pore currents because the central pore currents remain completely blocked by TTX (Fig. S1). Therefore, we consider the possibility that TTX is somehow modifying the currents fluxing through gating pore within the DIV voltage sensor.

First, we examined the possibility that TTX binds directly to the voltage sensor in the DIV-CN mutant. We introduced a pore mutation at a site known to be critical for TTX binding (Y401S) in the background of the DIV-CN mutant. The Y401S mutation, located next to the selectivity determining DEKA (D400, E755, K1237, A1529) locus (48–52), yields a channel that is nearly insensitive to block by TTX (53, 54). In this background (Y401S DIV-CN), TTX had no effect on gating pore currents through the DIV voltage sensor (Fig. S3). Therefore, TTX likely influences the gating pore currents through the DIV voltage sensor by binding to the outer pore of the sodium channel.

Next, we considered the possibility that TTX interacts directly with the charged voltage sensor while being docked to its binding site in the outer pore. The highly charged pore blocking peptide, μ-conotoxin (μ-CTX), has been previously suggested to shift the voltage dependence of activation by a small degree by modifying the surface charge (55). Our prediction will be that μ-CTX, which has a nominal net charge of +6 at neutral pH, will have a much larger effect on gating pore currents if these interactions are determined solely by electrostatics (56). We observed that the saturating concentrations of μ-CTX cause a much smaller reduction (16% at most) in the DIV-CN gating pore currents (Fig. 3 and Fig. S1). These findings and others (57) support the notion that TTX perturbs the DIV voltage sensor through a mechanism that is unlikely to involve direct electrostatic interaction.

A plot of residual gating pore currents versus voltage reveals that μ-CTX inhibition of the gating pore currents is voltage independent, whereas TTX block is pronounced at depolarized potentials (Fig. S4). The voltage dependence of the block is not due to differences in voltage-dependent binding because these measurements were obtained at saturating concentrations of TTX (central pore currents remain fully blocked). Therefore, this voltage dependence reflects the effect of TTX on the gating transition of the voltage sensor and shows that TTX binding favors the activated state of the DIV voltage sensor.

TTX Modulates Off-Gating Currents. Whereas gating pore current data suggest that TTX specifically modulates the gating pore currents and by extension the voltage sensor movement, we sought to validate this observation independently. Alternate approaches to monitor conformational rearrangement of the voltage sensors involve measuring gating currents or fluorescence signals from site-specific probes. Gating currents are the most direct measure of voltage sensor movements but recording them in absence of pore blockers remains technically demanding.

To eliminate contamination due to ionic currents, we measured the off-gating currents in the wild-type channels after a depolarizing pulse sufficient to induce fast inactivation. Permeant ions in the external solution were substituted by *N*-methyl D-glucamine (NMG) to eliminate any ionic current contamination of tail currents. Robust nonlinear charge movements were recorded from the wild-type channel without pore blockers (Fig. S5) and, as expected, the charge–voltage curves obtained from these measurements were saturated at extreme potentials. A comparison of the off-gating currents before and after addition of saturating concentrations of TTX shows that the total off-gating charge is reduced by 24% (Fig. 4). Note that a substantial shift in the *Q–V* curve to a more hyperpolarized potential in the presence of TTX would result in subtraction of some of the nonlinear charge component and will be manifested as a reduced gating charge. As opposed to TTX, μ-CTX caused no reduction in the total gating charge, consistent with its effect on gating pore currents through the DIV voltage sensor (Fig. 4).

The above differences in perturbation of voltage sensor movements by the two toxins may reflect differences in their binding site or their state dependence. Remarkably, both TTX and μ-CTX can be simultaneously accommodated in the pore and, furthermore, TTX can be trapped in its binding site by μ-CTX (58, 59). The mutagenesis data also suggest that the critical residues implicated in TTX binding is in the narrow ion access pathway in the selectivity filter region (53, 54, 60). Because TTX causes a reduction in the total charge of the off-gating currents and influences the behavior of the DIV voltage sensor to a much greater extent than μ-CTX, we suggest that μ-CTX may be a more appropriate tool for collecting sodium channel gating currents. In summary, these gating current experiments establish that the TTX binding in the selectivity filter region of the sodium channel influences the movements of one or more voltage sensors of the sodium channel.

Cross-Bridging in the Selectivity Filter Affects the DIV Voltage Sensor. One possible explanation for such cross-talk is that the central pore toxins introduce a nonnative interaction that perturbs the conformation of the DIV voltage sensor. Alternatively, this long-range interaction may reflect an inherent allosteric coupling between the outer pore and this particular voltage sensor (61).

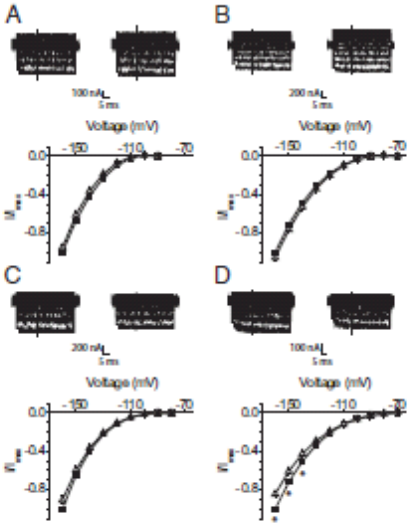

Fig. 3. Effect of μ-CTX on gating pore currents through the individual voltage sensors. A family of hyperpolarization activated currents before (Left; filled square) and after (Right; unfilled triangle) addition of μ-CTX from the DII-CN (*A*), DII-CN (*B*), DIII-CN (*C*), and DIV-CN (*D*) mutants (*Upper*). Normalized current-voltage plots of the same (*Lower*). Currents were recorded and normalized following the protocol described in *Methods*. Currents at each voltage were measured at the end of 20 ms, marked as a dashed line. Each plot represents the mean ± SE of at least three independent experiments. **P* value <0.05, statistical significance.

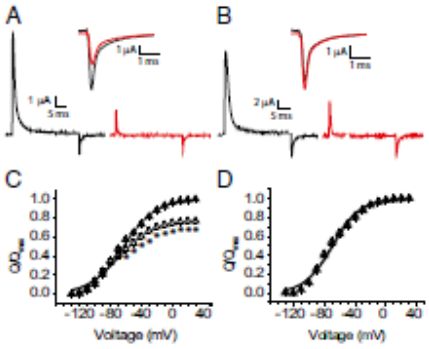

Fig. 4. Off-gating currents from the wild-type sodium channel in absence and presence of outer pore blockers. (*A*) Wild-type off-gating currents before (black trace) and after (red trace) TTX. (*Inset*) Off-gating current traces on an enlarged scale. (*B*) Wild-type off-gating currents before (black trace) and after (red trace) μ-CTX. (*Inset*) Off-gating current traces are shown enlarged. (*C*) Charge–voltage curves of the wild-type channel in the presence (filled triangle) and absence (unfilled triangle) of TTX. Each plot represents the mean ± SE of at least four independent experiments. See *Methods* for a description of the protocol. *$P < 0.01$, statistical significance. (*D*) Charge–voltage curves of the wild-type channel before (filled triangle) and after (unfilled triangle) block of sodium currents by μ-CTX, shown as in *C*.

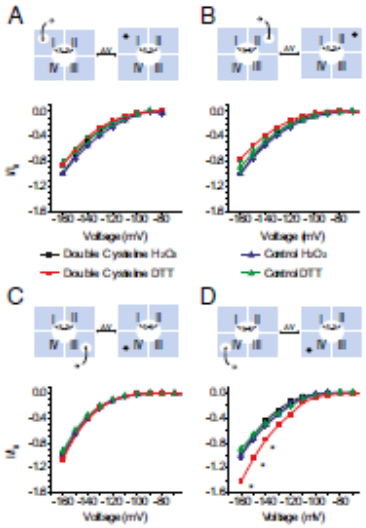

Fig. 5. Effect of disulphide cross-bridge formation in the outer pore of the sodium channel on gating pore currents through DI, DII, DIII, and DIV voltage sensors. Above each panel, a schematic diagram depicting gating pore currents through individual voltage sensors is shown. Upon depolarization, the gating pores in individual domains close, which allowed us to monitor the conformational movements of individual domains. In all cases, the pore is trapped in an inactivated conformation by disulphide cross-linking. (*A*) Normalized current-voltage plots of D400C/E755C DI-CN gating pore currents in H_2O_2 (black squares) and DTT (red squares) compared with the DI-CN control in H_2O_2 (blue triangles) and DTT (green triangles). (*B*) Normalized current–voltage plots of D400C/E755C DII-CN gating pore currents compared with those of DII-CN. Symbols are as in *A*. (*C*) Normalized current-voltage curves of D400C/E755C DIII-CN gating pore currents compared with the DIII-CN control. The symbols are the same as in *A*. (*D*) Normalized current-voltage curves of D400C/E755C DIV-CN gating pore currents compared with those of the DIV-CN control. Each plot represents the mean ± SE of at least three independent experiments. I_o refers to the H_2O_2 traces collected at −160 mV. Data were normalized to I_o for the controls and for the double cysteine mutants. *P value <0.03, statistical significance.

To discriminate between these two possible scenarios, we used the disulphide trapping method (62). Paired cysteine substitutions in the selectivity filter region of the sodium channel form a disulphide cross-bridge and high-affinity Cd^{2+} binding sites in a state-dependent manner (30–32, 63, 64). We hypothesize that disulphide cross-linking within the pore region may prevent relative structural rearrangements and reveal intrinsic conformational coupling between the pore and the voltage sensors.

We generated a double cysteine mutant (D400C/E755C) in the background of DI, DII, DIII, and DIV-CN. These two residues constitute part of the DEKA locus in the selectivity filter region of the sodium channel and spontaneously form a disulphide cross-bridge, resulting in block of sodium currents (63). Ion conduction recovers when this cross-bridge is broken under reducing conditions. In our case, we observe small sodium currents in oocytes expressing our mutants and these currents were abolished upon addition of 4 mM H_2O_2 (Fig. S6). Under reducing conditions (1 mm dithiothreitol, DTT), we recorded robust sodium currents upon depolarization, which indicated that the cysteine cross-bridge was broken. Comparison of gating pore currents through the D400C/E755C DI, DII, and DIII mutants in reducing and oxidizing conditions showed little change (Fig. 5 *A–C*, respectively), whereas the gating pore currents of D400C/E755C DIV-CN increased substantially in DTT (70% at −140 mV) (Fig. 5*D*). The effects of the disulfide bridge on the gating pore currents of DIV are not due to a direct effect of H_2O_2 or DTT because the reagents have no effect on channels lacking the D400C/E755C mutations (Fig. 5).

Conformational transitions in the selectivity filter region of the sodium channel have been implicated in slow and "ultraslow" inactivation (28–34). Our experiments directly demonstrate that the domain IV voltage sensor in the skeletal muscle sodium channel is coupled to conformational transitions in the selectivity filter region of the sodium channel. Although we cannot completely rule out the possibility that the other voltage sensors are also coupled to gating transitions in the outer pore, it is remarkable that perturbation studies have previously implicated S4-DIV as being involved in slow inactivation (61). We find that prolonged depolarizations that promote slow inactivation in sodium channels inhibit gating pore currents through the domain IV voltage sensor (Fig. S7). This correlation suggests that the movement of the DIV voltage sensor may be linked to entry into the slow inactivated state. However, we should note that the reduction in the DIV gating pore currents after long depolarizations could be due to an intrinsic voltage sensor mode shift as was observed in isolated voltage sensors (19).

Mutations in domain IV also specifically affect the binding of anticonvulsants to neuronal sodium channels (65). These drugs bind to the pore in an activity-dependent manner when applied to the external side but not to the internal side (66). Moreover, TTX, which binds close to putative selectivity filter of the sodium channel, is also known to block in a use-dependent manner (67, 68). These intriguing findings are consistent with the notion established herein that the domain IV voltage sensor and outer pore of the sodium channel are conformationally coupled. The present findings are in contrast to the prevalent view that movement of the voltage sensors is exclusively coupled to opening of cytoplasmic pore gates. Furthermore, our results provide an example in which this anomalous electromechanical coupling exists

PHYSIOLOGY

concurrently with canonical voltage sensor pore coupling. These mechanistic differences in coupling may underpin functional specialization of sodium channel domains (43, 69–72) and may be a universal feature of other nonsymmetric voltage-dependent ion channels.

Methods

Molecular Biology and Expression. Mutations were made using the QuikChange mutagenesis kit (Stratagene). cRNA was made using the mMessage mMachine T7 kit (Ambion) after digesting the plasmids containing the sodium channel gene with NotI enzyme. For heterologous expression, 50 nL of cRNA containing a mixture of α- and β1-subunit in 1:1 stoichiometry was injected into stage IV or V *Xenopus laevis* oocytes. After injection, the oocytes were kept at 18 °C in 1 × standard oocyte solution with Ca^{2+} and gentamicin for 2–5 d before recording.

Electrophysiology. Recordings were made using the cut-open oocyte voltage clamp configuration with CA-1B amplifier (Dagan) as described previously (73). Gating and ionic currents were sampled at 250 kHz with a Digidata 1400 interface (MDS Analytical Technologies) and low-pass filtered at 20 kHz. The oocytes were clamped at a holding potential of −80 mV for at least 5 min before recording. Current-voltage curves for DI, DIV-CN, and DIV-CN Y401S were obtained in 105 mM Na^+-Mes (methanesulfonic acid) external solution, whereas those for DII-CN and DIII-CN mutants were obtained in an external solution containing either 52.5 mM Na^+-Mes or 105 mM K^+-Mes, respectively. Following a 50-ms prepulse to −120 mV, the currents were elicited by test pulses ranging from −80 to +70 mV for a duration of 60 ms. Gating pore currents were recorded in 105 mM Na^+-Mes for both DI and DIV-CN, whereas the gating pore currents for DII-CN and DIII-CN were recorded in 105 mM K^+-Mes external solution with 10 mM Hepes and 2 mM $Ca(OH)_2$ at pH 7.4. Unless stated otherwise, these recordings used NMG-Mes internal solution with 105 mM NMG, 10 mM Hepes, and 2 mM EGTA at pH 7.4. Gating pore currents were elicited by test pulses from −160 to −70 mV for 60 ms following a 50-ms prepulse to −120 mV. The currents were normalized with respect to the maximum current measured before toxin, typically at −160 mV. Channels were blocked using 0.6–1.1 μM of TTX or 6–25.7 μM of μ-CTX in the external solutions. Gating pore currents were recorded without a P/4 subtraction protocol, which means that the activation kinetics were likely to be contaminated by capacity transients. Offline leak subtraction was used to eliminate the linear leak component in experiments where it was significant (74).

To record the off-gating currents, we applied a prepulse to +50 mV for 30 ms to inactivate the channels. This was followed by a test pulse to potentials ranging from −130 mV to +50 mV for 20-ms durations. These experiments were performed in NMG-Mes internal and external (105 mM NMG-Mes with 10 mM Hepes, and 2 mM $Ca(OH)_2$) solutions. To obtain gating currents in presence of toxin, 0.6–1.1 μM TTX or 6–25.7 μM μ-CTX was added to the external solution. At these concentrations, ionic currents were fully blocked. The charge–voltage curves for the off-gating currents were fit to a single Boltzmann equation: $Q/Q_{max}(V) = 1/(1 + \exp(-ze(V - V_{1/2})/kT))$ to estimate the $V_{1/2}$ (voltage for half-maximal activation) and z (valence) values. Linear capacity transients were eliminated by P/−4 subtraction at a holding potential of −130 mV.

For cross-linking experiments, the oocytes expressing mutants were treated with 2 mM H_2O_2 to maximize the disulfide formation. To measure currents under reducing conditions, 1 mM of freshly made DTT was added to the external solution containing 105 mM Na^+-Mes.

ACKNOWLEDGMENTS. We thank K. M. Schuldt for technical assistance with Na_V channel mutants and the members of the B.C. laboratory, Meyer Jackson, and Francisco Bezanilla for their valuable comments. This work was supported by National Institutes of Health training grants (to D.L.C. and B.W.J.), Grant R01-GM084140 (to B.C.), and the Shaw Scientist Award (to B.C.).

1. Armstrong CM (1966) Time course of TEA(+)-induced anomalous rectification in squid giant axons. *J Gen Physiol* 50:491–503.
2. Liu Y, Holmgren M, Jurman ME, Yellen G (1997) Gated access to the pore of a voltage-dependent K+ channel. *Neuron* 19:175–184.
3. Jiang Y, et al. (2002) The open pore conformation of potassium channels. *Nature* 417:523–526.
4. Liu Y, Jurman ME, Yellen G (1996) Dynamic rearrangement of the outer mouth of a K+ channel during gating. *Neuron* 16:859–867.
5. López-Barneo J, Hoshi T, Heinemann SH, Aldrich RW (1993) Effects of external cations and mutations in the pore region on C-type inactivation of Shaker potassium channels. *Receptors Channels* 1:61–71.
6. Cordero-Morales JF, et al. (2006) Molecular determinants of gating at the potassium-channel selectivity filter. *Nat Struct Mol Biol* 13:311–318.
7. Cordero-Morales JF, Cuello LG, Perozo E (2006) Voltage-dependent gating at the KcsA selectivity filter. *Nat Struct Mol Biol* 13:319–322.
8. Cuello LG, Jogini V, Cortes DM, Perozo E (2010) Structural mechanism of C-type inactivation in K(+) channels. *Nature* 466:203–208.
9. Panyi G, Deutsch C (2006) Cross talk between activation and slow inactivation gates of Shaker potassium channels. *J Gen Physiol* 128:547–559.
10. Panyi G, Deutsch C (2007) Probing the cavity of the slow inactivated conformation of shaker potassium channels. *J Gen Physiol* 129:403–418.
11. Cuello LG, et al. (2010) Structural basis for the coupling between activation and inactivation gates in K(+) channels. *Nature* 466:272–275.
12. Perozo EMR, MacKinnon R, Bezanilla F, Stefani E (1993) Gating currents from a nonconducting mutant reveal open-closed conformations in Shaker K+ channels. *Neuron* 11:353–358.
13. Armstrong CM, Bezanilla F (1974) Charge movement associated with the opening and closing of the activation gates of the Na channels. *J Gen Physiol* 63:533–552.
14. Heginbotham L, MacKinnon R (1992) The aromatic binding site for tetraethylammonium ion on potassium channels. *Neuron* 8:483–491.
15. Yang Y, Yan Y, Sigworth FJ (1997) How does the W434F mutation block current in Shaker potassium channels? *J Gen Physiol* 109:779–789.
16. Starkus JG, Kuschel L, Rayner MD, Heinemann SH (1998) Macroscopic Na+ currents in the "Nonconducting" Shaker potassium channel mutant W434F. *J Gen Physiol* 112:85–93.
17. Glauner K, Lerche H, Toro L, Bezanilla F, Stefani E (1997) Correlation between charge movement and ionic current during slow inactivation in Shaker K+ channels. *J Gen Physiol* 110:579–589.
18. Loots E, Isacoff EY (1998) Protein rearrangements underlying slow inactivation of the Shaker K+ channel. *J Gen Physiol* 112:377–389.
19. Villalba-Galea CA, Sandtner W, Starace DM, Bezanilla F (2008) S4-based voltage sensors have three major conformations. *Proc Natl Acad Sci USA* 105:17600–17607.
20. Piper DR, Varghese A, Sanguinetti MC, Tristani-Firouzi M (2003) Gating currents associated with intramembrane charge displacement in HERG potassium channels. *Proc Natl Acad Sci USA* 100:10534–10539.
21. Männikkö R, Pandey S, Larsson HP, Elinder F (2005) Hysteresis in the voltage dependence of HCN channels: Conversion between two modes affects pacemaker properties. *J Gen Physiol* 125:305–326.
22. Haddad GA, Blunck R (2011) Mode shift of the voltage sensors in Shaker K+ channels is caused by energetic coupling to the pore domain. *J Gen Physiol* 137:455–472.
23. Raman IM, Bean BP (2001) Inactivation and recovery of sodium currents in cerebellar Purkinje neurons: Evidence for two mechanisms. *Biophys J* 80:729–737.
24. Grieco TM, Malhotra JD, Chen C, Isom LL, Raman IM (2005) Open-channel block by the cytoplasmic tail of sodium channel beta4 as a mechanism for resurgent sodium current. *Neuron* 45:233–244.
25. Hille B (1977) Local anesthetics: Hydrophilic and hydrophobic pathways for the drug-receptor reaction. *J Gen Physiol* 69:497–515.
26. Wang SY, Mitchell J, Moczydlowski E, Wang GK (2004) Block of inactivation-deficient Na+ channels by local anesthetics in stably transfected mammalian cells: Evidence for drug binding along the activation pathway. *J Gen Physiol* 124:691–701.
27. Payandeh J, Scheuer T, Zheng N, Catterall WA (2011) The crystal structure of a voltage-gated sodium channel. *Nature* 475:353–358.
28. Balser JR, et al. (1996) External pore residue mediates slow inactivation in mu 1 rat skeletal muscle sodium channels. *J Physiol* 494:431–442.
29. Bénitah JP, Chen Z, Balser JR, Tomaselli GF, Marbán E (1999) Molecular dynamics of the sodium channel pore vary with gating: Interactions between P-segment motions and inactivation. *J Neurosci* 19:1577–1585.
30. Ong BH, Tomaselli GF, Balser JR (2000) A structural rearrangement in the sodium channel pore linked to slow inactivation and use dependence. *J Gen Physiol* 116:653–662.
31. Xiong W, et al. (2006) A conserved ring of charge in mammalian Na+ channels: A molecular regulator of the outer pore conformation during slow inactivation. *J Physiol* 576:739–754.
32. Xiong W, Li RA, Tian Y, Tomaselli GF (2003) Molecular motions of the outer ring of charge of the sodium channel: Do they couple to slow inactivation? *J Gen Physiol* 122:323–332.
33. Todt H, Dudley SC, Jr., Kyle JW, French RJ, Fozzard HA (1999) Ultra-slow inactivation in mu1 Na+ channels is produced by a structural rearrangement of the outer vestibule. *Biophys J* 76:1335–1345.
34. Townsend C, Horn R (1997) Effect of alkali metal cations on slow inactivation of cardiac Na+ channels. *J Gen Physiol* 110:23–33.
35. Vilin YY, Fujimoto E, Ruben PC (2001) A single residue differentiates between human cardiac and skeletal muscle Na+ channel slow inactivation. *Biophys J* 80:2221–2230.
36. Hilber K, et al. (2001) The selectivity filter of the voltage-gated sodium channel is involved in channel activation. *J Biol Chem* 276:27831–27839.
37. Vedantham V, Cannon SC (2000) Rapid and slow voltage-dependent conformational changes in segment IVS6 of voltage-gated Na(+) channels. *Biophys J* 78:2943–2958.
38. Struyk AF, Cannon SC (2002) Slow inactivation does not block the aqueous accessibility to the outer pore of voltage-gated Na channels. *J Gen Physiol* 120:509–516.
39. Starace DM, Bezanilla F (2004) A proton pore in a potassium channel voltage sensor reveals a focused electric field. *Nature* 427:548–553.

40. Tombola F, Pathak MM, Isacoff EY (2005) Voltage-sensing arginines in a potassium channel permeate and occlude cation-selective pores. *Neuron* 45:379–388.
41. Sokolov S, Scheuer T, Catterall WA (2005) Ion permeation through a voltage-sensitive gating pore in brain sodium channels having voltage sensor mutations. *Neuron* 47: 183–189.
42. Struyk AF, Cannon SC (2007) A Na+ channel mutation linked to hypokalemic periodic paralysis exposes a proton-selective gating pore. *J Gen Physiol* 130:1–20.
43. Chanda B, Bezanilla F (2002) Tracking voltage-dependent conformational changes in skeletal muscle sodium channel during activation. *J Gen Physiol* 120:629–645.
44. Horn R (2000) A new twist in the saga of charge movement in voltage-dependent ion channels. *Neuron* 25:511–514.
45. Cha A, Bezanilla F (1998) Structural implications of fluorescence quenching in the Shaker K+ channel. *J Gen Physiol* 112:391–408.
46. Patton DE, Goldin AL (1991) A voltage-dependent gating transition induces use-dependent block by tetrodotoxin of rat IIA sodium channels expressed in Xenopus oocytes. *Neuron* 7:637–647.
47. Heggenes ST, Starkus JG (1986) Saxitoxin and tetrodotoxin. Electrostatic effects on sodium channel gating current in crayfish axons. *Biophys J* 49:629–643.
48. Heinemann SH, Terlau H, Stühmer W, Imoto K, Numa S (1992) Calcium channel characteristics conferred on the sodium channel by single mutations. *Nature* 356: 441–443.
49. Favre I, Moczydlowski E, Schild L (1996) On the structural basis for ionic selectivity among Na+, K+, and Ca2+ in the voltage-gated sodium channel. *Biophys J* 71: 3110–3125.
50. Chiamvimonvat N, Pérez-Garcia MT, Ranjan R, Marban E, Tomaselli GF (1996) Depth asymmetries of the pore-lining segments of the Na+ channel revealed by cysteine mutagenesis. *Neuron* 16:1037–1047.
51. Pérez-Garcia MT, et al. (1997) Mechanisms of sodium/calcium selectivity in sodium channels probed by cysteine mutagenesis and sulfhydryl modification. *Biophys J* 72: 989–996.
52. Huang CJ, Favre I, Moczydlowski E (2000) Permeation of large tetra-alkylammonium cations through mutant and wild-type voltage-gated sodium channels as revealed by relief of block at high voltage. *J Gen Physiol* 115:435–454.
53. Backx PH, Yue DT, Lawrence JH, Marban E, Tomaselli GF (1992) Molecular localization of an ion-binding site within the pore of mammalian sodium channels. *Science* 257: 248–251.
54. Satin J, et al. (1992) A mutant of TTX-resistant cardiac sodium channels with TTX-sensitive properties. *Science* 256:1202–1205.
55. French RJ, et al. (1996) Interactions between a pore-blocking peptide and the voltage sensor of the sodium channel: An electrostatic approach to channel geometry. *Neuron* 16:407–413.
56. Moczydlowski E, Olivera BM, Gray WR, Strichartz GR (1986) Discrimination of muscle and neuronal Na-channel subtypes by binding competition between [3H]saxitoxin and mu-conotoxins. *Proc Natl Acad Sci USA* 83:5321–5325.
57. Moczydlowski E, Garber SS, Miller C (1984) Batrachotoxin-activated Na+ channels in planar lipid bilayers. Competition of tetrodotoxin block by Na+. *J Gen Physiol* 84: 665–686.
58. Zhang MM, et al. (2009) Synergistic and antagonistic interactions between tetrodotoxin and mu-conotoxin in blocking voltage-gated sodium channels. *Channels (Austin)* 3:32–38.
59. Zhang MM, et al. (2010) Cooccupancy of the outer vestibule of voltage-gated sodium channels by micro-conotoxin KIIIA and saxitoxin or tetrodotoxin. *J Neurophysiol* 104: 88–97.
60. Leffler A, Herzog RI, Dib-Hajj SD, Waxman SG, Cummins TR (2005) Pharmacological properties of neuronal TTX-resistant sodium channels and the role of a critical serine pore residue. *Pflugers Arch* 451:454–463.
61. Mitrovic N, George AL, Jr., Horn R (2000) Role of domain 4 in sodium channel slow inactivation. *J Gen Physiol* 115:707–718.
62. Falke JJ, Koshland DE, Jr. (1987) Global flexibility in a sensory receptor: A site-directed cross-linking approach. *Science* 237:1596–1600.
63. Bénitah JP, et al. (1997) Molecular motions within the pore of voltage-dependent sodium channels. *Biophys J* 73:603–613.
64. Tsushima RG, Li RA, Backx PH (1997) P-loop flexibility in Na+ channel pores revealed by single- and double-cysteine replacements. *J Gen Physiol* 110:59–72.
65. Yang YC, Hsieh JY, Kuo CC (2009) The external pore loop interacts with S6 and S3-S4 linker in domain 4 to assume an essential role in gating control and anticonvulsant action in the Na(+) channel. *J Gen Physiol* 134:95–113.
66. Kuo CC (1998) A common anticonvulsant binding site for phenytoin, carbamazepine, and lamotrigine in neuronal Na+ channels. *Mol Pharmacol* 54:712–721.
67. Cohen CJ, Bean BP, Colatsky TJ, Tsien RW (1981) Tetrodotoxin block of sodium channels in rabbit Purkinje fibers. Interactions between toxin binding and channel gating. *J Gen Physiol* 78:383–411.
68. Gonoi T, Sherman SJ, Catterall WA (1985) Voltage clamp analysis of tetrodotoxin-sensitive and -insensitive sodium channels in rat muscle cells developing in vitro. *J Neurosci* 5:2559–2564.
69. Bosmans F, Martin-Eauclaire MF, Swartz KJ (2008) Deconstructing voltage sensor function and pharmacology in sodium channels. *Nature* 456:202–208.
70. Horn R, Ding S, Gruber HJ (2000) Immobilizing the moving parts of voltage-gated ion channels. *J Gen Physiol* 116:461–476.
71. Sheets MF, Kyle JW, Kallen RG, Hanck DA (1999) The Na channel voltage sensor associated with inactivation is localized to the external charged residues of domain IV, S4. *Biophys J* 77:747–757.
72. Yang N, Horn R (1995) Evidence for voltage-dependent S4 movement in sodium channels. *Neuron* 15:213–218.
73. Taglialatela M, Toro L, Stefani E (1992) Novel voltage clamp to record small, fast currents from ion channels expressed in Xenopus oocytes. *Biophys J* 61:78–82.
74. Sokolov S, Scheuer T, Catterall WA (2010) Ion permeation and block of the gating pore in the voltage sensor of NaV1.4 channels with hypokalemic periodic paralysis mutations. *J Gen Physiol* 136:225–236.

Supporting Information

Capes et al. 10.1073/pnas.1115575109

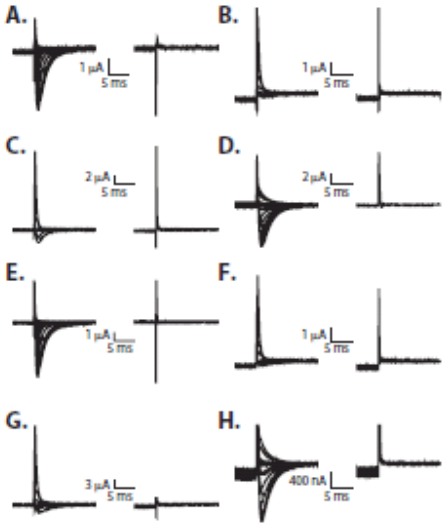

Fig. S1. Block of main pore currents by saturating concentrations of TTX or μ-CTX in the charge neutralized sodium channel mutants. Family of ionic currents elicited by depolarization before (*Left*) and after (*Right*) addition of TTX for DI-CN (*A*), DII-CN (*B*), DIII-CN (*C*), and DIV-CN (*D*). Family of ionic currents elicited by depolarization before (*Left*) and after (*Right*) addition of μ-CTX for DI-CN (*E*), DII-CN (*F*), DIII-CN (*G*), and DIV-CN (*H*). DI-CN and DIV-CN were recorded in the presence of 105 mM Na^+-Mes external solution, whereas DII-CN and DIII-CN were obtained in presence of K^+-Mes external solution. Pulse protocol is the same as reported in *Methods*.

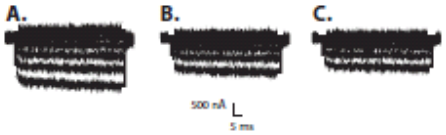

Fig. S2. Effect of increasing concentrations of TTX on DIV-CN gating pore currents. Family of DIV-CN gating pore currents before TTX addition (*A*), in 1 μM TTX (*B*), and in 10 μM TTX (*C*). Gating pore currents were recorded in the presence of 105 mM Na^+-Mes external solution. Pulse protocol is the same as reported in *Methods*.

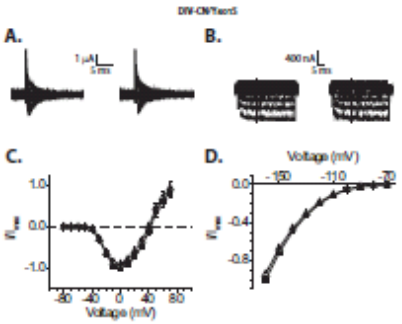

Fig. S3. TTX does not inhibit gating pore currents of the DIV-CN/Y401S mutant. (*A*) Family of DIV-CN/Y401S traces shown before (*Left*) and after (*Right*) TTX application. (*B*) Family of gating pore currents before (*Left*) and after (*Right*) addition of TTX from the DIV-CN/Y401S mutant. (*C*) Current–voltage (*I-V*) relationship of the DIV-CN/Y401S mutant in absence (unfilled triangle) and presence (filled square) of TTX. Voltage protocol is the same as in *Methods*. Data were collected in the presence of 105 mM Na^+-Mes external solution. (*D*) Normalized current-voltage plots of the gating pore currents from the DIV-CN/Y401S mutant before (filled square) and after (unfilled triangle) addition of TTX. Currents were recorded in the presence of 105 mM Na^+-Mes external solution using voltage protocols described in *Methods*. Currents were normalized to the maximum current measured before toxin, typically at −160 mV. Currents at each voltage were measured at the end of 20 ms, marked as a dashed line (*B*). Each current-voltage plot represents the mean ± SE of four experiments.

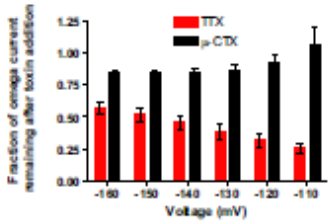

Fig. S4. Voltage dependence of TTX and μ-CTX inhibition of DIV gating pore currents. Plot of the fraction of DIV hyperpolarization-activated current remaining after toxin addition versus voltage. Each graph represents the mean ± SE of five independent experiments. Fraction of gating pore current remaining after toxin addition was calculated by dividing the currents obtained after toxin addition by the currents obtained before toxin was added (following normalization).

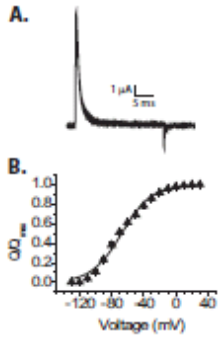

Fig. S5. (*A*) Wild-type off-gating currents in the absence of pore blocker. Voltage protocol is the same as in *Methods*. (*B*) Wild-type charge–voltage plots in the absence of pore blocker. Each plot represents the mean ± SE of 11 independent experiments.

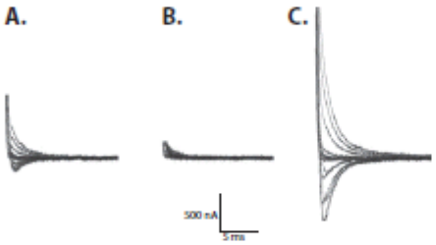

Fig. S6. Representative sodium current traces under varying redox conditions in D400C/E755C DIV-CN. Family of ionic currents from oocytes expressing the D400C/E755C DIV-CN mutant (*A*), in presence of 2 mM H_2O_2 (*B*), and upon addition of 1 mM DTT after washout of H_2O_2 (*C*). All traces were collected from the same oocyte in presence of 105 mM Na^+-Mes external solution using a voltage protocol listed in *Methods*.

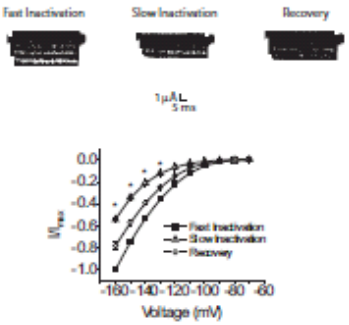

Fig. S7. Effect of cumulative slow inactivation on the DIV-CN gating pore currents. Family of gating pore currents (*Above*) is shown after fast inactivation, after a 30-s cumulative slow inactivation protocol, and after a 10-min recovery at −80 mV. Normalized current-voltage plots of the DIV-CN gating pore currents (*Below*) before slow inactivation (filled squares), after a 30-s cumulative slow inactivation protocol (unfilled triangles), and after a 10-min recovery at −80 mV (unfilled circles). The channels were pulsed from −120 mV to −10 mV for 20 ms to measure the ionic current and then a pulse train from −160–60 mV for 60 ms was collected before returning to −120 mV for 20 ms. Our cumulative inactivation protocol was modified from protocols used by Cummins and Sigworth and Townsend and Horn (1, 2). For the 30-s cumulative slow inactivation protocol, the oocytes were held at −10 mV for 30 s before beginning the protocol described above and were also held at −10 mV for 30 s in between every voltage step. Each plot represents the mean ± SE of six independent experiments. Statistical significance from the gating pore currents collected after fast inactivation, $*P < 0.02$.

1. Cummins TR, Sigworth FJ (1996) Impaired slow inactivation in mutant sodium channels. *Biophys J* 71:227–236.
2. Townsend C, Horn R (1997) Effect of alkali metal cations on slow inactivation of cardiac Na+ channels. *J Gen Physiol* 110:23–33.

In preparation:

Pore opening is not concerted in a eukaryotic voltage-gated sodium channel.

Marcel P. Goldschen-Ohm[1], Deborah Capes[1], Kevin Oelstrom[1], Baron Chanda[1]

[1]University of Wisconsin, Madison, WI, Dept. of Neuroscience

Number of words in 1st paragraph:	278
Number of words in remainder of text:	3,143
Number of words in Methods Summary:	182
Number of words in online Methods:	1,075
Number of References:	59
Number of Figures:	5
Number of Pages:	24

Voltage-gated ion channels are important for electrical and chemical signaling pathways in a variety of excitable cells [1,2]. In outwardly rectifying potassium channels, depolarization initiates conformational changes in four identical voltage-sensing domains, which culminate in a single-step concerted opening of the pore [3,4,5,6,7,8]. This final all-or-none transition ensures that the conductance of biological membranes is steeply voltage-dependent. However, both eukaryotic voltage-gated sodium and calcium channels lack the symmetry of exemplar potassium channels. Indeed, conformational changes in the domain IV voltage-sensor of sodium channels lag those in the other three domains, and have also been linked to inactivation [9,10,11,12]. Nonetheless, it remains unclear whether the central pore in the sodium channel opens in a single concerted step. Development of well-constrained kinetic models of sodium channel activation has been hindered by the presence of fast inactivation which typically masks all but the first few events [13,14,15]. In this study, we combined single channel recordings, cysteine accessibility, and fluorescence measurements from site specific probes to study the activation gating in an inactivation deficient mutant Nav1.4-L435W/L437C/A438W (WCW) [16]. We observed three distinct conductance levels whose kinetics are correlated with either macroscopic activation or inactivation in wild type channels. A comparison of the relative time and voltage-dependent kinetics of individual domain movements with various conductance levels shows that rearrangements of domain IV underlie formation of a distinct pore conformation preceding inactivation. Our experiments reveal that, contrary to gating models of potassium channels, the pore opening in sodium channels involves multiple non-concerted transitions which are driven by asymmetric movements of voltage-sensors. These findings shed new light on the effects of disease causing mutations at distal sites on inactivation gating in voltage-gated sodium channels [17,18,19].

Voltage-gated ion channels are biological equivalents of a transistor and, much like the semiconductor devices, they are crucial for propagating and amplifying electrical signals [20]. One of the hallmarks of these ion channels is that their conductance is very voltage-dependent, more so than the silicon based counterparts. These channel proteins are made up of a central ion conducting pore and four discrete voltage-sensing domains, each of which contributes to approximately three gating charges, Although, the voltage-sensing domains can activate independently, the final pore opening transition is concerted which ensures that these channels open in an all-or-none manner. Much of our present knowledge about the gating mechanisms of this family of ion channels comes from studies on voltage-dependent potassium channels which are made up of four identical subunits. Eukaryotic voltage-gated sodium and calcium channels lack this structural symmetry and this, therefore, raises questions about the conserved nature of the gating transitions in these ion channels.

A complicating factor in studies of sodium channel gating is that they rapidly inactivate after opening, which allows the membrane to reset for the next signal. Similar to the N-terminal domain of Shaker potassium channels [21,22], inactivation of eukaryotic voltage-gated sodium channel involves an occlusion of the pore by an intracellular hydrophobic segment [23,24]. However, disease causing mutations throughout the channel affect fast inactivation, suggesting that this process is intimately coupled to more global conformational changes

[11,25,26,17,27,19,28]. In particular, studies with fluorescent probes [9], gating modifier toxins [29], and paddle chimeras [10] imply that whereas domains I-III are primarily involved in activation, domain IV has a distinct role in inactivation. These and mutagenesis studies [27,11,30,31,32] have led to the notion that domain IV is unique, and apparently couples activation to inactivation in sodium channels. However, the mechanism underlying this relationship between domain IV movement, channel opening, and inactivation is not understood.

Development of quantitative models of sodium channel activation has been hindered by inactivation, which occurs at a similar voltage range and contributes to the shaping of both macroscopic current rise and decay [13,14]. Therefore, removing inactivation represents an attractive approach to study the complete activation process in isolation, and may also reveal slower or less frequent aspects of channel gating. This approach has been used to successfully develop detailed quantitative models of Shaker potassium channel activation [5,33,34,35,46].

However, studies of inactivation deficient sodium channel preparations have yet to reveal a consistent picture of the activation process. For example, whether or not removing inactivation reveals a prolonged activation time course appears to depend on the particular preparation used and the choice of compound for disrupting inactivation [36,37,38,15]. Unfortunately, interpretation of these studies is complicated by potentially heterogeneous channel populations, and possible secondary effects of compounds whose mechanism for impairing inactivation is not entirely clear. Both of these complications make it difficult to be certain that a channel population has been uniformly modified.

In contrast to the potentially heterogeneous effects of exogenously applied compounds, genetic mutations are an attractive method for applying a specific and uniform local perturbation. The triplet mutations I1488Q/F1489Q/M1490Q (QQQ) in the domain III-IV linker [23], or L435W/L437C/A438W (WCW) in the domain I S6 segment [16], each largely remove fast inactivation in vertebrate voltage-gated sodium channels, possibly by disrupting the putative inactivation particle or its docking site, respectively. However, whereas the QQQ mutant does not express well in heterologous systems, the WCW mutant expresses reasonably well for the recording of single channels, gating currents, and fluorescence from site-specific probes. This ability to study a single inactivation deficient mutant using a variety of biophysical methods is an enormous advantage for developing a comprehensive view of sodium channel gating.

Consistent with a lack of fast inactivation, single Nav1.4-WCW channels (9 patches) opened repeatedly throughout 200-400 ms depolarizing voltage steps from -60 to 0 mV (Fig. 1a). In contrast, single Nav1.4 channels (6 patches) opened 1.5 ± 0.2 times at all voltages tested before entering an absorbing closed state which we attributed to inactivation. Currents obtained by averaging single channel records were reflective of macroscopic whole cell current responses, suggesting that the observed single channel activity is representative of these channel's behavior (Fig. 1b; Supplementary Fig. 1).

Immediately apparent in Nav1.4-WCW single channel records is the presence of multiple conductance levels, with subconductances at approximately 1/3 (S1) and 2/3 (S2) of the fully open (O) level (Fig. 1a). Based on the frequent occurrence of events that within our resolution appear to transition directly between closed and

fully open states (C ↔ O), or skip an intermediate level such as C ↔ S2 or O ↔ S1, and the similarity of the conductance in O (17.5 ± 1.4 pS) to that of Nav1.4 (17.1 ± 1.4 pS), we conclude that these events represent subconductances in a single channel. The alternative, that the three conductance levels reflect the coincidental opening of one to three low-conductance channels in the patch, would require a mechanism for cooperativity between channels to account for the frequent simultaneous opening and closing of two or three channels (within our resolution, channels appeared to open directly to the fully open state about 50% of the time at all voltages tested). Nav1.4 channels also exhibited a single subconductance at approximately 1/2 of the main conductance level (Supplementary Fig. 2a). However, the subconductance in Nav1.4 occurred only infrequently, possibly because rapid inactivation limits the opportunity to visit a subconducting state, and thus precluded a more detailed kinetic analysis. The presence of subconductances in Nav1.4-WCW is consistent with the frequent observation of subconductances upon removal of inactivation in both sodium and potassium channels [39,39,5,40,41,42 43], as well as observations of subconductances in wild type channels [43,44].

To address the kinetics of individual conductance levels in Nav1.4-WCW, we idealized single channel records using the segmental k-means (SKM) algorithm in the QUB software suite [45] allowing for two subconducting states (Supplementary Fig. 2b; see methods). The presence of a single channel was determined by a lack of any visible stacked openings above the fully open level. Given their high probability of being open at -20 and 0 mV, this approach is a robust method for detecting patches containing single Nav1.4-WCW channels. The idealized conductance levels were representative of Gaussian fits to single channel amplitude distributions (Fig. 1c; Supplementary Fig. 3). Each conductance level displayed a linear current-voltage relation (Fig. 1d), with slopes which were, for Nav1.4-WCW: S1 = 6.8 ± 0.9 pS, S2 = 12.5 ± 1.3 pS, O = 17.5 ± 1.4 pS; and for Nav1.4: 17.1 ± 1.4 pS, and similar reversal potentials (Nav1.4-WCW: S1 = 34.2 ± 9.9 mV, S2 = 36.3 ± 8.9 mV, O = 36.6 ± 6.3 mV; Nav1.4: 43.4 ± 5.8 mV) (Fig. 1e). However, reversal potentials obtained from the extrapolation of linear fits as shown in figure 1d are unlikely to detect less than 2 fold changes in Na^+:K^+ permeability as observed for subconductances in Shaker potassium channels. Similar conductance levels were also observed during deactivation of single Nav1.4-WCW channels (Supplementary Fig. 4). We note that the S2 conductance level often exhibited more noise than other levels, giving rise to the possibility that S2 may reflect the filtering of a rapid flicker such as C ↔ O or S1 ↔ O (Supplementary Fig. 5).

The time to first opening after application of a depolarizing voltage step was highly voltage dependent for each individual conductance level, with more depolarized potentials eliciting channel opening faster on average than more hyperpolarized potentials (Fig. 2a). Although the latencies to O and S2 were similar, on average the first event in S2 occurred slightly later than that in O, consistent with the idea that activation preferentially involves transitions from C → O → S2. In contrast, latency to S1 was much longer than that for S2 and O. However, the voltage dependence of the weighted time constant from bi-exponential fits to the cumulative probability of having first opened was similar for each conductance level, suggesting that the set of closed states that is traversed in the activation pathway prior to reaching each of the conducting states all have

a similar voltage dependence (Supplementary Fig. 6). The probability of observing a null sweep (i.e. no visible channel activity during the 200 ms pulse) was also voltage dependent, decreasing from about 80% at -60 mV to 30% at 0 mV.

A comparison with Nav1.4 shows that following the onset of a voltage step to 0 mV, the probability of having first opened rises with a similar time course for both Nav1.4 and Nav1.4-WCW up to the time of peak current in Nav1.4 (Fig. 2b). This suggests that the rate constants for activation which define the rising phase of currents in Nav1.4 are not different in Nav1.4-WCW. However, whereas Nav1.4 activation saturated within 10-20 ms at 0 mV, Nav1.4-WCW channels continued to open for the first time much later into the voltage step. For Nav1.4, these late openings are likely masked by inactivation from closed states prior to opening (i.e. if the channel has not opened within approximately 20 ms of the depolarization it is likely to already be inactivated). Thus, removing closed state inactivation in Nav1.4-WCW (Supplementary Fig. 1) reveals a prolonged activation time course. Such late channel activation was also observed previously for other inactivation deficient preparations including N1662A, another mutation that may reside within the inactivation gate [30], and after treatment with NBA [46].

Thus, although the time to peak current is prolonged in Nav1.4-WCW as compared to Nav1.4 (Fig. 1b), the opening latency of single channels reveals that this is not due to slower activation rates, but reflects a prolonged activation time course resulting in a larger peak open probability (Fig. 2c). Indeed, upon scaling the average current responses for Nav1.4 and Nav1.4-WCW to their relative maximal open probabilities, we find that their rising phases up to the time to peak for Nav1.4 are indistinguishable. The peak open probabilities we observed here are similar to previous reports of single Nav1.4 and other inactivation deficient sodium channel preparations [37,46,47]. These data suggest that the activation process in Nav1.4 lasts much longer than the time to peak, where it is occluded by rapid inactivation. Furthermore, figure 2c illustrates how fast inactivation can play a major role in shaping the rising phase of macroscopic currents [13,14,15].

Apparent dwell times in subconductance levels were often long-lived as compared to open times for Nav1.4, and the lifetime in O and S2 increased with depolarization (Supplementary Fig. 7; Supplementary Table 1), similar to previous observations of inactivation deficient sodium channel preparations [46,41,48,47]. Increasing depolarization also reduced the frequency and duration of closed times, which likely reflect the movement of the voltage sensors.

The average probability in each conductance level (P_{S1}, P_{S2}, P_O) was computed from the idealized records for every time point (Fig. 3a). P_O increased rapidly early on during activation, whereas P_{S1} and P_{S2} increased more slowly. At 0 mV, P_O even exhibits a peak and subsequent slow decay. This slow decay could reflect either a small contamination in the observed activation process from slow inactivation, or a transition from O → S1/S2. In the latter case, we would predict that after opening, P_O should decay with similar kinetics to a rise in P_{S1} or P_{S2}. To test this, we computed the conditional probability in each conductance level (CP_{S1}, CP_{S2}, CP_O) by averaging the probability at every time point after aligning each sweep to the time of first opening to any level (Fig. 3b). After first opening, CP_O decays with a similar time course to a rise in CP_{S2},

suggesting that the pore preferentially adopts a fully open conformation first in the activation pathway, followed by a rearrangement associated with the S2 subconductance. In contrast, CP_{S1} does not show any obvious correlation with respect to the time of initial channel opening. Thus, S1 may represent a pore conformation off the main activation pathway.

An examination of the kinetics of individual conductance levels in single molecules shows that the time course of the rise and subsequent decay (inactivation) in the open probability of Nav1.4 corresponds nearly exactly to the rate of entry into the O and S2 conductance levels in Nav1.4-WCW, respectively (Fig. 4a). However, unlike the inactivated state in Nav1.4, the S2 state is not absorbing, and therefore we do not observe a substantial decrease in P_O with time (i.e. channels reach an apparent equilibrium between O and S2).

Given that the domain IV voltage sensor has been implicated as having a unique role in inactivation [9], we asked whether or not the movement of specific voltage sensors could underlie the different conductance levels. To test this, we measured fluorescence signals from fluorophores attached to individual voltage sensors in Nav1.4 during depolarizing voltage steps (Supplementary Fig. 8). A comparison of the kinetics of P_O and P_{S2} with the relative time courses of fluorescent responses from individual voltage sensors shows that domain I-III voltage sensors track entry into O, whereas the domain IV voltage sensor tracks entry into S2 (Fig. 4b; Supplementary Fig. 9). This suggests that the fully open conductance level O reflects channel opening upon activation of voltage sensors in domains I-III, whereas the S2 subconductance level reflects a conformational state associated with inactivation and movement of the domain IV voltage sensor.

Functionally, inactivation reflects entry into an absorbing closed state. Structurally, this is manifested as an occlusion of the pore upon binding of an intracellular hydrophobic "particle" [23,49,50]. This idea is supported by cysteine accessibility studies which show that cysteines introduced in sites such as F1579C become inaccessible during inactivation, but are orders of magnitude more accessible either prior to or upon removal of inactivation [51]. Given the correlation between the time course of S2 and wild type inactivation, we were interested in testing whether the subconductances observed here might simply reflect a weakly conducting form of inactivated state, where the inactivation particle still binds, but only partially occludes the pore. In this case, we predict that the bound inactivation particle should still pose a significant barrier to accessibility of larger reagents such as MTSET for sites normally hidden during inactivation.

To test this, we examined the accessibility of an introduced pore cysteine (F1579C), which in a wild type background shows no reactivity to internal MTSET while inactivated, but whose reactivity is increased to up to 50 $M^{-1}s^{-1}$ upon impairing inactivation by changing the stimulus frequency and duration, or with a peptide toxin [51]. To avoid contamination from modification of L437C in WCW, we mutated position 437 to serine, hereafter referred to as WSW (L435W/L437S/A438W). Both Nav1.4-WSW and Nav1.4-WSW-F1579C severely disrupted fast inactivation similar to Nav1.4-WCW, suggesting that these mutations did not alter the overall behavior of the WCW mutant (Supplementary Fig. 10). Exposure of Nav1.4-WSW-F1579C to 250 μM internal MTSET at 0 mV conferred a gradual reduction in peak current amplitude with a second order rate constant for modification of 5,360 ± 180 $M^{-1}s^{-1}$ (2 oocytes), whereas no apparent modification of Nav1.4-WSW was

observed (three oocytes) (Supplementary Fig. 10). Taken together, substantially increased reactivity of the F1579C position in the WSW background shows that these sites are not protected, and is consistent with the idea that at least structurally these channels are unlike inactivated states. Thus, the subconductances observed here reflect distinct conformations of the open pore as opposed to conducting forms of the inactivated state.

The simplest model that can qualitatively account for our single channel, fluorescence, and pore accessibility observations requires that channel gating involve a conducting conformation of the pore distinct from that of the fully open state, which directly precedes fast inactivation (Fig. 5). We posit that in wild type channels inactivation occurs rapidly from the S2 state, such that subconductances are rarely observed, but which are revealed upon destabilization of the inactivated state. In this model, the S2 conductance arises either from the S2 state itself, or from a rapid flicker between S2 and inactivated states. In either case, the rate limiting step to inactivation in wild type channels is the formation of the S2 pore. Therefore, we propose that Nav1.4 inactivation involves activation of the domain IV voltage sensor, which promotes a rearrangement of the pore to a conformation to which the inactivation particle readily binds.

The existence of a distinct pre-inactivated pore conformation can explain how both microscopic activation and inactivation rates are rapid while the apparent time course of macroscopic current inactivation is slow, as the latter primarily reflects the rate of entry into S2. Therefore DIV mutations which disrupt the stability of the S2 state without necessarily affecting the initial activation process or the inactivation particle can produce defects in inactivation gating [17]. The formation of S2 state also offers a potential explanation for why some inactivation impaired preparations reveal a prolonged activation time course [37,15], whereas others appear not to [36,38]. For example, a perturbation that specifically destabilizes the inactivated state will uncover the S2 conductance, thereby giving rise to a prolonged increase in channel open probability. In contrast, inhibiting entry into the S2 state will also effectively remove inactivation without exhibiting this additional conductance or a prolonged activation time course. Thus, prior apparently conflicting results may reflect differential effects between various inactivation disrupting perturbations that either inhibit formation of the pore conformation preceding inactivation or binding of the inactivation particle itself. In addition, preferential binding of anesthetics such as lidocaine to the S2 pore conformation may explain apparently conflicting observations regarding the affinity of these drugs for open versus inactivated states [52,53]. Interestingly, a recent crystal structure of a prokaryotic voltage-gated sodium channel shows that these channels can adopt an asymmetric pore conformation, although its relation to functional inactivation is not entirely clear [54].

The occurrence of a second open pore conformation immediately preceding pore block by an accessory beta2 subunit has also been observed in large conductance calcium and voltage activated (BK) channels [55]. However, the second open state in the symmetric BK channel has not been associated with the movement of an individual voltage sensor. The subconductances reported here also differ from those observed upon removal of inactivation in Shaker potassium channels, in that they are both long lived and correlated with activation of the domain IV voltage sensor specifically. In contrast, Shaker's activation coupled

subconductances reflect very brief intermediates, consistent with the primarily concerted motion of four highly coupled units, although it remains unclear whether these subconductances directly correspond to the activation of individual voltage-sensing segments [42]. Thus, a fundamental difference between pore opening in eukaryotic voltage-gated sodium and potassium channels is that for sodium channels the asymmetric movement of the domain IV voltage sensor confers a non-concerted, two step pore opening process which directly couples movement of the domain IV voltage sensor to fast inactivation. By rapidly occluding the second open pore conformation, fast inactivation essentially converts an intrinsically non-concerted two step pore opening process to one that behaves functionally as a single pore opening transition.

Methods Summary

Single channel recordings were acquired from inside-out patches excised from HEK-293 cells expressing either Nav1.4 or Nav1.4-WCW channels at 10ºC. Silguard coated quartz pipettes (10-15 MΩ tip resistance) and custom RF shielding were used for low noise recordings. Currents were sampled at 100-250 kHz and low-pass filtered at 10 kHz. For analysis of single channel records, currents were digitally filtered at 2 kHz and resampled at 5 kHz. Idealized records containing four conductance levels (C, S1, S2, O) were generated using the segmental k-means (SKM) algorithm in the QUB software suite [45]. For the selected 2 kHz filter cutoff, the SKM algorithm generated consistent sets of dwell times for simulated data across the range of signal to noise representative for our current recordings from -60 to 0 mV. Fluorescence from TMRM labeled channels was recorded from a modified cut-open oocyte setup as described by Muroi and Chanda [56]. Accessibility of Nav1.4-WSW and Nav1.4-WSW-F1579C to internal MTSET (freshly dissolved and kept on ice prior to each experiment) was assayed from inside-out patches excised from Xenopus oocytes after mechanical removal of the viteline layer.

References

1. Hodgkin, A. L. & Huxley, A. F., A quantitative description of membrane current and its application to conduction and excitation in nerve. *J. Physiol.* **117**, 500-544 (1952).

2. Catterall, W. A., Ion Channel Voltage Sensors: Structure, Function, and Pathophysiology. *Neuron* **67**, 915–928 (2010).

3. Zagotta, W. N. & Aldrich, R. W., Voltage-dependent gating of Shaker A-type potassium channels in Drosophila muscle. *J. Gen. Physiol.* **95**, 29-60 (1990).

4. Schoppa, N. E. & Sigworth, F. J., Activation of Shaker potassium channels. III. An activation gating model for wild-type and V2 mutant channels. *J. Gen. Physiol.* **111**, 313-342 (1998).

5. Hoshi, T., Zagotta, W. N. & Aldrich, R. W., Shaker potassium channel gating. I: Transitions near the open state. *J. Gen. Physiol.* **103**, 249-278 (1994).

6. Bezanilla, F., Perozo, E. & Stefani, E., Gating of Shaker K+ channels: II. The components of gating currents and a model of channel activation. *Biophys. J.*, 1011-1021 (1994).

7. Ledwell, J. L. & Aldrich, R. W., Mutations in the S4 region isolate the final voltage-dependent cooperative step in potassium channel activation. *J. Gen. Physiol.* **113**, 389-414 (1999).

8. Smith-Maxwell, C. J., Ledwell, J. L. & Aldrich, R. W., Role of the S4 in cooperativity of voltage-dependent potassium channel activation. *J. Gen. Physiol.* **111**, 399-420 (1998).

9. Chanda, B. & Bezanilla, F., Tracking voltage-dependent conformational changes in skeletal muscle sodium channel during activation. *J. Gen. Physiol.* **120**, 629-645 (2002).

10. Bosmans, F., Martin-Eauclaire, M. F. & Swartz, K. J., Deconstructing voltage sensor function and pharmacology in sodium channels. *Nature*, 202-208 (2008).

11. Chen, L. Q., Santarelli, V., Horn, R. & Kallen, R. G., A unique role for the S4 segment of domain 4 in the inactivation of sodium channels. *J. Gen. Physiol.*, 549-556 (1996).

12. Sheets, M. F. & Hanck, D. A., Voltage-dependent open-state inactivation of cardiac sodium channels: gating current studies with Anthopleurin-A toxin. *J. Gen. Physiol.* **106**, 617-640 (1995).

13. Aldrich, R. W., Corey, D. P. & Stevens, C. F., A reinterpretation of mammalian sodium channel gating based on single channel recording. *Nature* **306**, 436-441 (1983).

14. Aldrich, R. W. & Stevens, C. F., Voltage-dependent gating of single sodium channels from mammalian neuroblastoma cells. *J. Neurosci.* **7**, 418-431 (1987).

15. Gonoi, T. & Hille, B., Gating of Na channels. Inactivation modifiers discriminate among models. *J. Gen. Physiol.* **89**, 253-274 (1987).

16. Wang, S. Y., Bonner, K., Russell, C. & Wang, G. K., Tryptophan scanning of D1S6 and D4S6 C-termini in voltage-gated

sodium channels. *Biophys. J.* **85**, 911-920 (2003).

17. Jurkat-Rott, K., Holzherr, B., Fauler, M. & Lehmann-Horn, F., Sodium channelopathies of skeletal muscle result from gain or loss of function. *Pflugers Arch.* **460**, 239-248 (2010).

18. Jurkat-Rott, K. *et al.*, Voltage-sensor sodium channel mutations cause hypokalemic periodic paralysis type 2 by enhanced inactivation and reduced current. *PNAS* **97**, 9549-9554 (2000).

19. Wagner, S. *et al.*, A novel sodium channel mutation causing a hyperkalemic paralytic and paramyotonic syndrome with variable clinical expressivity. *Neurology* **49**, 1018-1025 (1997).

20. Sigworth, F. J., Structural biology: Life's transistors. *Nature* **423**, 21-22 (2003).

21. Armstrong, C. M. & Bezanilla, F., Inactivation of the sodium channel. II. Gating current experiments. *J. Gen. Physiol.* **70**, 567-590 (1977).

22. Hoshi, T., Zagotta, W. N. & Aldrich, R. W., Biophysical and molecular mechanisms of Shaker potassium channel inactivation. *Science* **250**, 533-538 (1990).

23. West, J. W. *et al.*, A cluster of hydrophobic amino acid residues required for fast Na(+)-channel inactivation. *PNAS* **89**, 10910-10914 (1992).

24. Eaholtz, G., Scheuer, T. & Catterall, W. A., Restoration of inactivation and block of open sodium channels by an inactivation gate peptide. *Neuron* **12**, 1041-1048 (1994).

25. Kontis, K. J. & Goldin, A. L., Sodium channel inactivation is altered by substitution of voltage sensor positive charges. *J. Gen. Physiol.*, 403-413 (1997).

26. Motoike, H. K. *et al.*, The Na+ channel inactivation gate is a molecular complex: a novel role of the COOH-terminal domain. *J. Gen. Physiol.* **123**, 155-165 (2004).

27. Chahine, M. *et al.*, Sodium channel mutations in paramyotonia congenita uncouple inactivation from activation. *Neuron*, 281-294 (1994).

28. Kuo, C. C. & Bean, B. P., Na+ channels must deactivate to recover from inactivation. *Neuron* **12**, 819-829 (1994).

29. Sheets, M. F., Kyle, J. W., Kallen, R. G. & Hanck, D. A., The Na channel voltage sensor associated with inactivation is localized to the external charged residues of domain IV, S4. *Biophys. J.*, 747-757 (1999).

30. McPhee, J. C., Ragsdale, D. S., Scheuer, T. & Catterall, W. A., A critical role for the S4-S5 intracellular loop in domain IV of the sodium channel alpha-subunit in fast inactivation. *J. Biol. Chem.* **273**, 1121-1129 (1998).

31. Lerche, H. *et al.*, Role in fast inactivation of the IV/S4-S5 loop of the human muscle Na+ channel probed by cysteine mutagenesis. *J. Physiol.* **505**, 345-352 (1997).

32. Mitrovic, N. *et al.*, Role in fast inactivation of conserved amino acids in the IV/S4-S5 loop of the human muscle Na+

channel. *Neurosci Lett.* **214**, 9-12 (1996).

33. Zagotta, W. N., Hoshi, T., Dittman, J. & Aldrich, R. W., Shaker potassium channel gating. II: Transitions in the activation pathway. *J. Gen. Physiol.* **103**, 279-319 (1994).

34. Zagotta, W. N., Hoshi, T. & Aldrich, R. W., Shaker potassium channel gating. III: Evaluation of kinetic models for activation. *J. Gen. Physiol.* **103**, 321-362 (1994).

35. Schoppa, N. E. & Sigworth, F. J., Activation of shaker potassium channels. I. Characterization of voltage-dependent transitions. *J. Gen. Physiol.* **111**, 271-294 (1998).

36. Armstrong, C. M., Bezanilla, F. & Rojas, E., Destruction of sodium conductance inactivation in squid axons perfused with pronase. *J. Gen. Physiol.* **62**, 375-391 (1973).

37. Patlak, J. & Horn, R., Effect of N-bromoacetamide on single sodium channel currents in excised membrane patches. *J. Gen. Physiol.* **79**, 333-351 (1982).

38. Wang, G. K., Brodwick, M. S. & Eaton, D. C., Removal of sodium channel inactivation in squid axon by the oxidant chloramine-T. *J. Gen. Physiol.* **86**, 289-302 (1985).

39. Chinn, K. & Narahashi, T., Temperature-dependent subconducting states and kinetics of deltamethrin-modified sodium channels of neuroblastoma cells. *Pflugers Arch.* **413**, 571-579 (1989).

40. Nagy, K., Subconductance states of single sodium channels modified by chloramine-T and sea anemone toxin in neuroblastoma cells. *Eur. Biophys. J.* **15**, 129-132 (1987).

41. Kohlhardt, M., Fröbe, U. & Herzig, J. W., Properties of normal and non-inactivating single cardiac Na+ channels. *Proc. R. Soc. Lond. B Biol. Sci.* **232**, 71-93 (1987).

42. Zheng, J. & Sigworth, F. J., Selectivity changes during activation of mutant Shaker potassium channels. *J. Gen. Physiol.* **110**, 101-117 (1997).

43. Patlak, J. B., Sodium channel subconductance levels measured with a new variance-mean analysis. *J. Gen. Physiol.* **92**, 413-430 (1988).

44. Zheng, J., Vankataramanan, L. & Sigworth, F. J., Hidden Markov model analysis of intermediate gating steps associated with the pore gate of shaker potassium channels. *J. Gen. Physiol.* **118**, 547-564 (2001).

45. Qin, F., Restoration of single-channel currents using the segmental k-means method based on hidden Markov modeling. *Biophys. J.* **86**, 1488-1501 (2004).

46. Horn, R., Vandenberg, C. A. & Lange, K., Statistical analysis of single sodium channels. Effects of N-bromoacetamide. *Biophys. J.* **45**, 323-335 (1984).

47. Lawrence, J. H. *et al.*, Single-channel analysis of inactivation-defective rat skeletal muscle sodium channels containing the F1304Q mutation. *Biophys. J.* **71**, 1285-1294 (1996).

48. Grant, A. O., Chandra, R., Keller, C., Carboni, M. & Starmer, C. F., Block of wild-type and inactivation-deficient cardiac sodium channels IFM/QQQ stably expressed in mammalian cells. *Biophys. J.* **79**, 3019-3035 (2000).

49. Vedantham, V. & Cannon, S. C., Slow inactivation does not affect movement of the fast inactivation gate in voltage-gated Na+ channels. *J. Gen. Physiol.* **111**, 83-93 (1998).

50. Kellenberger, S., Scheuer, T. & Catterall, W. A., Movement of the Na+ channel inactivation gate during inactivation. *J. Biol. Chem.* **271**, 30971-30979 (1996).

51. Sunami, A. *et al.*, Accessibility of mid-segment domain IV S6 residues of the voltage gated Na+ channel to methanethiosulfonate reagents. *J. Physiol.* **561**, 403-413 (2004).

52. Bennett, P. B., Valenzuela, C., Chen, L. Q. & Kallen, R. G., On the molecular nature of the Lidocaine receptor of cardiac Na+ channels - Modification of block by alterations in the α-subunit III-IV interdomain. *Circ. Res.* **77**, 584-592 (1995).

53. Wang, S. Y., Mitchell, J., Moczydlowski, E. & Wang, G. K., Block of inactivation-deficient Na+ channels by local anesthetics in stably transfected mammalian cells: evidence for drug binding along the activation pathway. *J. Gen. Physiol.* **124**, 691-701 (2004).

54. Payandeh, J., Gamal El-Din, T. M., Scheuer, T., Zheng, N. & Catterall, W. A., Crystal structure of a voltage-gated sodium channel in two potentially inactivated states. *Nature* **0**, 1-6 (2012).

55. Benzinger, G. R., Xia, X. M. & Lingle, C. J., Direct observation of a preinactivated, open state in BK channels with beta2 subunits. *J. Gen. Physiol.*, 119-131 (2006).

56. Muroi, Y. & Chanda, B., Local anesthetics disrupt energetic coupling between the voltage-sensing segments of a sodium channel. *J. Gen. Physiol.* **133**, 1-15 (2009).

57. Irvine, L. A., Jafri, M. S. & Winslow, R. L., Cardiac sodium channel Markov model with temperature dependence and recovery from inactivation. *Biophys. J.* **76**, 1868-1885 (1999).

58. Levis, R. A. & Rae, J. L., The use of quartz patch pipettes for low noise single channel recording. *Biophys. J.* **65**, 1666-1677 (1993).

59. Colquhoun, D. & Sigworth, F. J., in *Single-Channel Recording*, edited by Sakmann, B. & Neher, E. (Plenum Press, New York, 1995), pp. 589-633.

Supplementary Information is linked to the online version of the paper at www.nature.com/nature.

Acknowledgments This work was supported by research grants from NIH GM084140-01 and Shaw Scientist Award to B.C. and American Heart Association (Midwest Affiliate) Postdoctoral Fellowship 12POST9440021 to M.P.G. We thank Dr. Ging Kuo Wang and Dr. Sho-Ya Wang for their gift of a HEK-293 cell line stably expressing the rat Nav1.4-WCW construct, and Dr. Meyer Jackson for the use of his quartz electrode puller.

Author Contributions M.P.G. and B.C. conceived the study and wrote the manuscript. M.P.G. designed and performed single channel and macroscopic experiments, and analyzed all of the data. D.C. performed single channel experiments. K.O. performed cysteine accessibility experiments. B.C. supervised the project.

Author Information Reprints and permissions information is available at www.nature.com/reprints. The authors declare no competing financial interests. Correspondence and requests for materials should be addressed to B.C. (chanda@wisc.edu).

Figure 1. Multiple conductance levels during gating of single inactivation deficient Nav1.4-WCW channels. (a) Single channel records in response to 200 ms depolarizing pulses from -60 to 0 mV (-120 mV holding) for Nav1.4 (left, only first 100 ms shown) and Nav1.4-WCW (right) channels at 10°C (filtered at 1 kHz for display). Dashed lines indicate observed conductance levels (C = closed, S1, S2, O; openings are downward). (b) Macroscopic responses obtained by averaging single channel records. (c) Single channel amplitude distributions from all points in a single channel patch at -40 mV (see Supplemental Fig. 3 for amplitude distributions at other voltages) after discarding points adjacent to changes in amplitude in the idealized record. Smooth dashed lines are individual Gaussian fits to each conductance level, and the smooth solid line is their sum. (d) Current-voltage relation for each conductance level and its linear fit. The main conductance level for Nav1.4 (squares) nearly overlaps that of Nav1.4-WCW (circles). Data between -120 and -80 mV is from deactivation to the indicated potential (Supplemental Fig. 4). (e) Summary of the conductance (top) and reversal potential (V_{rev}, bottom) for each conductance level from individual patches.

Figure 2. Activation latency and open probability for Nav1.4 and Nav1.4-WCW. (a) Cumulative probability of first opening to each individual conductance level during activation from -60 to 0 mV (maximum probability increases with voltage). The reduction of the maximum from unity reflects the probability of observing a null sweep with no channel activity. (b) A comparison of the cumulative probability of first opening for Nav1.4 and Nav1.4-WCW during the first 20 ms of activation at 0 mV. Smooth lines are bi-exponential fits. (c) Comparison of the average single channel response scaled to the observed peak open probability during activation at 0 mV for Nav1.4 (solid red) and Nav1.4-WCW (cyan). The response for Nav1.4 is also shown after normalizing to the peak response for Nav1.4-WCW (dotted red).

Figure 3. Kinetics of individual conductance levels. (a) Average probability at every time point for each conducting state from idealized records (dots, only first 100 ms shown), and fits to the equation $\Sigma_i A_i [1 - exp(-t/\tau_i)]$ (lines, see Supplemental Table 2). The first 40 ms period is shown on the right after normalizing the fits to illustrate the relative kinetics of the initial rise in probability for each level. (b) Average conditional probability at every time point after aligning the idealized records so that the first event in each sweep occurs at time zero (dots), and fits to the equation $\Sigma_i A_i exp(-t/\tau_i)$ + constant (lines, see Supplemental Table 2).

Figure 4. Individual conductance levels are correlated with the movement of specific voltage sensing domains. (a) Average single channel open probability for Nav1.4 during activation at 0 mV (black) overlaid with the probability for Nav1.4-WCW to be either fully open (P_O, blue dots) or in a state associated with the S2 subconductance (P_{S2}, magenta dots). P_{S2} is shown inverted and scaled to illustrate its similar time course to that of Nav1.4 macroscopic inactivation. (b) P_O and P_{S2} are shown as in *a* overlaid with fluorescence signals from fluorophores attached to individual voltage sensors from domains I-IV in Nav1.4. See Supplementary figure 9 for time constants at all voltages tested. Because fluorescence signals were prohibitively difficult to

reliably obtain below room temperature, these signals were uniformly scaled in time to account for the different temperatures at which the single channel (10°C) and fluorescence (room temp.) was obtained (see methods). We note, however, that the 5-fold scaling employed here is consistent with both the observed temperature dependence of sodium channel current kinetics [57], and the observation that domains I-III track macroscopic current activation [9].

Figure 5. A simple cartoon depicting the preferential sequence of events during Nav1.4-WCW channel activation. The closed to open transition represents all of the steps from resting to activated, and the closed to S2 transition reflects inactivation from closed states. In this model, the S2 state represents a distinct conformation of the open pore which precedes inactivation. In wild type channels, inactivation occurs sufficiently rapidly from the S2 state so that it is rarely observed. For simplicity, the S1 subconductance is not included here, but this conductance may potentially be represented as a parallel set of states to indicate an independent allosteric conformation of the channel.

Methods

Constructs. The inactivation deficient rat skeletal muscle clone L435W/L437C/A438W was gifted by Dr. Ging Kuo Wang and Dr. Sho-Ya Wang. This triple mutant was recloned in the rat Nav1.4 background with multiple silent mutations to facilitate cloning as first described in Muroi and Chanda [56], as well as an additional silent mutation at N434 to remove a *MfeI* cut site introduced by the L453W mutation. The mutation C437S was introduced in the WCW background with the QUICKCHANGE mutagenesis kit (Stratagene, CA) to obtain the WSW construct, and subcloned into pBSTA for expression in Xenopus oocytes. Mutations were verified by sequencing the entire cloning cassette from enzyme cut sites *MfeI* to *BsiWI*. The mutation F1579C was gifted by Dorothy Hanck, and subcloned into Nav1.4-WSW using enzyme cut sites *XbaI* and *BspEI*.

Heterologous expression in HEK-293 cells and oocytes. HEK-293 cells (ATCC) were cultured in a 37ºC, 5% CO_2 incubator using MEM supplemented with 10% fetal bovine serum, 100 U.I./mL Penicillin, 100 µg/mL Streptomycin, 1x sodium pyruvate and 1x nonessential amino acids (Invitrogen). Cells were transfected with 1-2 µg rat Nav1.4 or rat Nav1.4-L435W/L437C/A438W cDNA in the pBudCE4.1 vector (gift from Dr. David Wagner) using Lipofectamine LTX (Invitrogen). Recordings were made 24-72 hours after transfection. Recordings were also made from a HEK-293 cell line stably expressing the rat Nav1.4-L435W/L437C/A438W construct [53]. The media for the stable line was supplemented with 200 µg/mL Geneticin (G418, Invitrogen) to maintain a selective pressure for cells expressing the mutant construct. No qualitative differences were observed in either macroscopic or single channel behavior between channels expressed in the stable line and the transiently transfected mutant. For cysteine accessibility studies, the α-subunit (Nav1.4-WSW and Nav1.4-WSW-F1579C) and β1-subunit cDNAs were transcribed using the mMessage mMachine Kit (Ambion Inc., Austin, TX), and their RNAs injected into defolliculated *Xenopus* oocytes in a ~1:1 molar ratio.

Electrophysiology. Single channel data was acquired from inside-out patches excised from HEK-293 cells using an Axon Digidata 1400 digitizer and Axon 200B amplifier (MDS Analytical Technologies) with AxoGraph software (AxoGraph Scientific, Sydney, AU). Recordings were sampled at 100-250 kHz and low-pass filtered at 10 kHz. The pipette/extracellular solution was (in mM): 140 NaCl, 0.5 $CaCl_2$, 10 HEPES, pH 7.4, and the bath/intracellular solution was (in mM): 100 CsF, 30 KCl, 10 EGTA, 10 HEPES, pH 7.4. Quartz pipettes (Sutter QF-150-75) coated with Silguard (Dow Corning Corp., Midland, MI) and having a tip resistance of 10-15 MΩ were used for low noise recordings [58], and additionally a custom RF shield made from tin foil was placed around the recording chamber. The bath temperature was held at 10 ± 1ºC with a low noise peltier driven temperature controlled chamber (QE-1HC, CL-100 and TCM-1, Warner Instruments, LLC, Hamden, CT). For whole cell recordings we used boroscilicate pipets (World Precision Instruments, Inc., Sarasota, FL) with a tip resistance of about 2 MΩ. Whole cell series resistance compensation was usually 90%.

Single channel analysis. Single channel records were digitally filtered at f_c = 2 kHz and resampled at 5 kHz for analysis. The rise time of the filter T_r was estimated as $T_r = 0.3 / f_c$ = 150 μs, and the dead time T_d was set to 2.5 sample points (T_d = 500 μs) [59]. For Nav1.4-WCW channels, idealized records containing four conductance levels (closed, open, and two subconductances) were generated using the segmental k-means (SKM) algorithm in the QUB software suite [45]. For Nav1.4 channels, idealized records were obtained using SKM with two conductance levels (closed, open), and similar results were obtained with a half amplitude threshold crossing. Because the fast component in some of the observed dwell time distributions for Nav1.4-WCW approached the limits in our ability to idealize an event, it is likely that the single channel records contain brief events that were not resolved in this analysis. Thus, the reported apparent dwell times may reflect the time spent not in a single state, but a set of states (e.g. a conducting state and a brief unresolved closed state). However, the average time dependent probability was insensitive to the omission of brief events, and thus is representative of the channel behavior.

We tested for artifacts in the voltage dependence of the dwell times at each conductance level due to the idealization by taking idealized records at -40 and -60 mV where our signal to noise is greatest and rescaling them and adding noise to simulate the same records at -20 and 0 mV. At a filter cutoff of 2 kHz this method gave similar dwell time distributions at all signal to noise ratios reflecting our recorded data between -60 and 0 mV, whereas filtering at higher bandwidths such as 5 kHz resulted in erroneous voltage dependent dwell times for the same record at different signal to noise levels.

Fluorescence. Optical signals were recorded from a modified cut-open oocyte setup after labeling with 10 μM tetramethylrhodamine (TMR) maleimide (TMRM; Invitrogen) as described by Muroi and Chanda [56]. Cysteines were introduced in individual voltage sensors at the sames sites used previously by Chanda and Bezanilla [9]. Fluorescence was recorded at room temperature, as fluorescent responses at colder temperatures were quenched and lacked sufficient signal to noise to extract reliable kinetics. One possibility for reduced signal to noise is that the solubility of oxygen, which is a potent quencher of fluorescence, increases at lower temperatures. To account for the temperature dependence of sodium channel kinetics [57], fluorescence responses were uniformly scaled in time by a factor of 5 in order to compare them to the single channel kinetics observed at 10ºC. The scaling factor was chosen so as to maintain the correlation between the activation of domains I-III and the macroscopic current rise for Nav1.4 [9], and is consistent with the temperature dependence of these channels [57].

Cysteine accessibility. Accessibility to internally perfused MTSET was examined in inside-out patches from Xenopus oocytes 4-5 days post-injection after mechanical removal of the viteline layer. The pipette/extracellular solution was (in mM): 115 NaCl, 5 KCl, 2 $CaCl_2$, 10 HEPES, pH 7.2, and the bath/intracellular solution was (in mM): 100 K-Aspartate, 20 NaCl, 2.5 $MgCl_2$, 2 EGTA, 10 HEPES, pH 7.2. Fresh MTSET was dissolved in the bath solution and kept on ice prior to each experiment. A single exponential

was fit to the reaction time course of peak current vs. cumulative MTSET exposure time at 0 mV. Dividing the reciprocal of the rate constant by the concentration of MTSET yielded the apparent second order rate constant for modification.

Figure 1

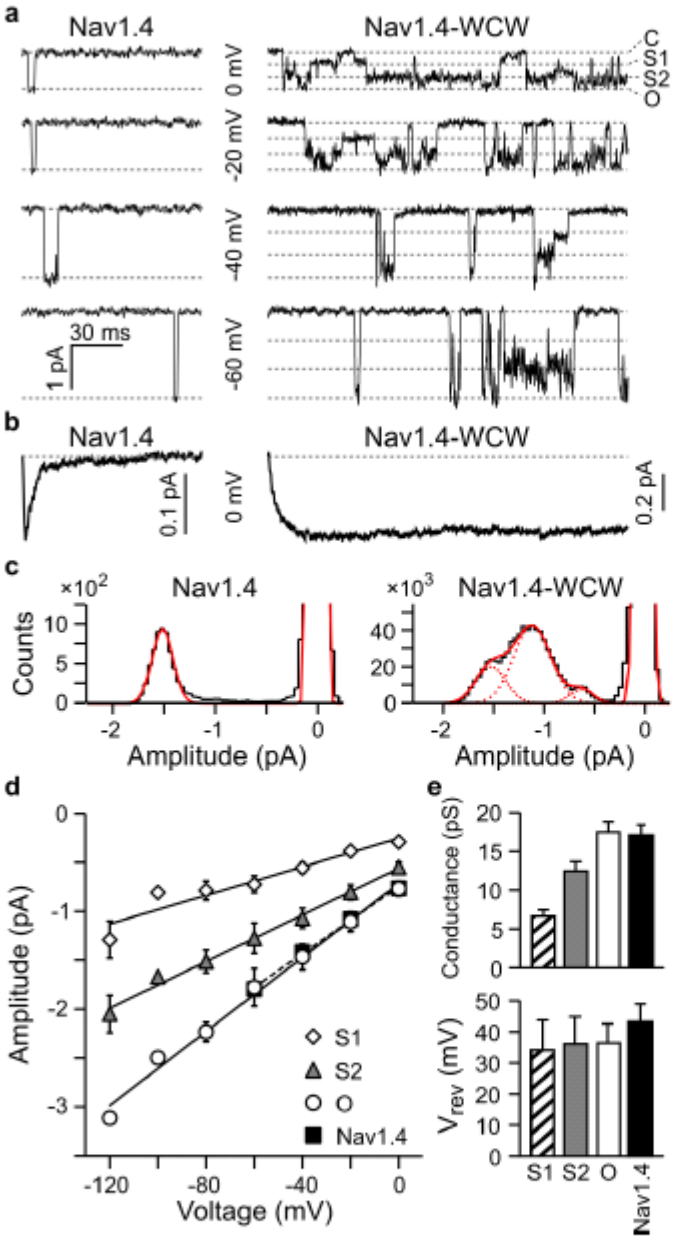
a
Nav1.4
Nav1.4-WCW
C
S1
S2
O
0 mV
-20 mV
-40 mV
-60 mV
30 ms
1 pA
b
Nav1.4
Nav1.4-WCW
0.1 pA
0 mV
0.2 pA
c
×10²
Nav1.4
×10³
Nav1.4-WCW
Counts
Amplitude (pA)
Amplitude (pA)
d
Amplitude (pA)
S1
S2
O
Nav1.4
Voltage (mV)
e
Conductance (pS)
V_rev (mV)
S1 S2 O Nav1.4

Figure 2

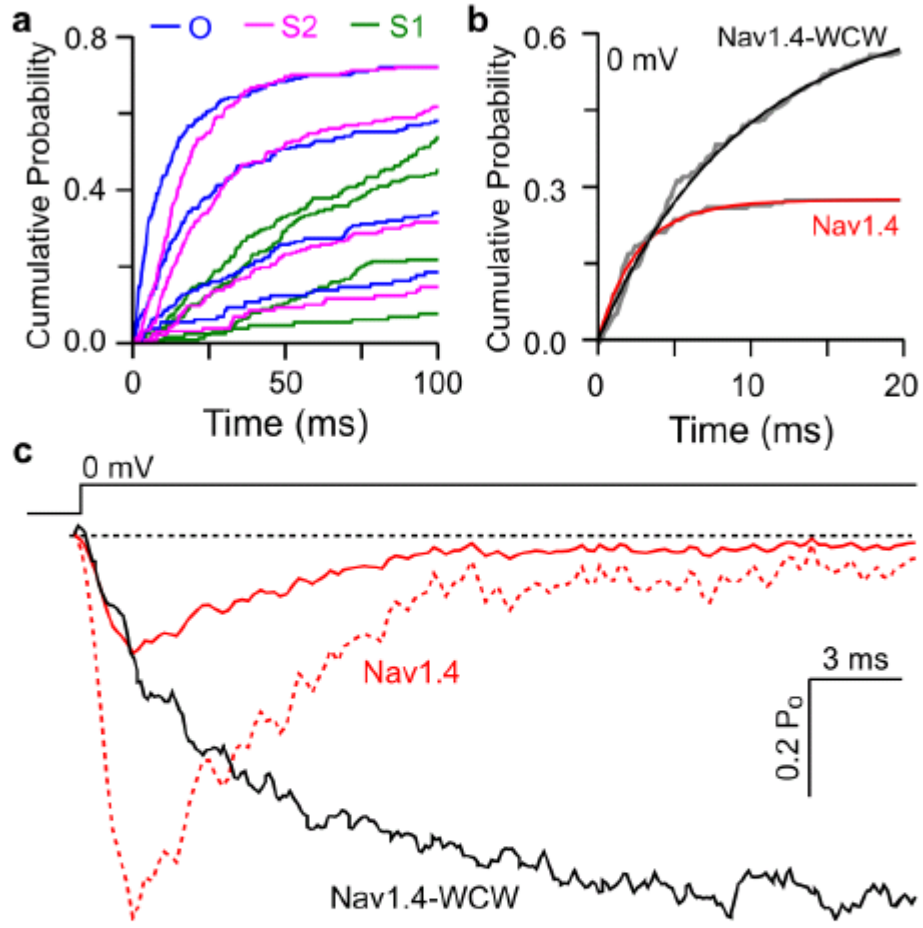
a
O
S2
S1
Cumulative Probability
0.8
0.4
0.0
0
50
100
Time (ms)
b
0.6
0.3
0.0
0 mV
Nav1.4-WCW
Nav1.4
Cumulative Probability
0
10
20
Time (ms)
c
0 mV
Nav1.4
3 ms
0.2 Po
Nav1.4-WCW

Figure 3

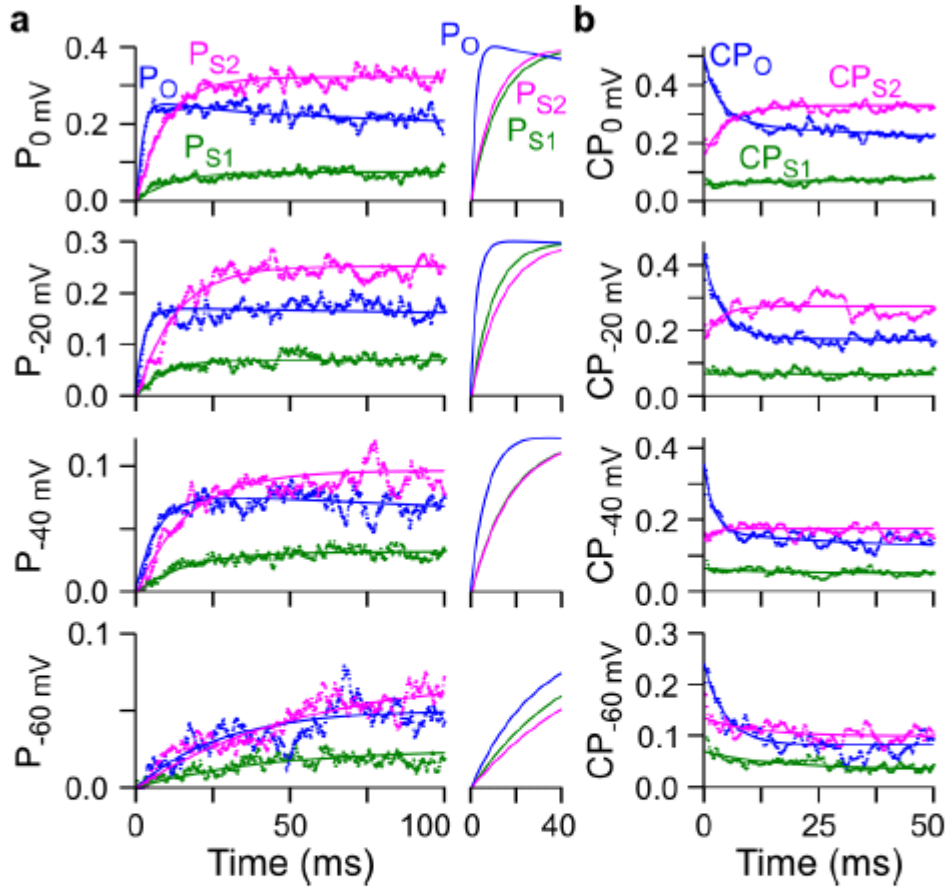
a
b
P0 mV
P-20 mV
P-40 mV
P-60 mV
CP0 mV
CP-20 mV
CP-40 mV
CP-60 mV
PO
PS2
PS1
CPO
CPS2
CPS1
Time (ms)
Time (ms)

Figure 4

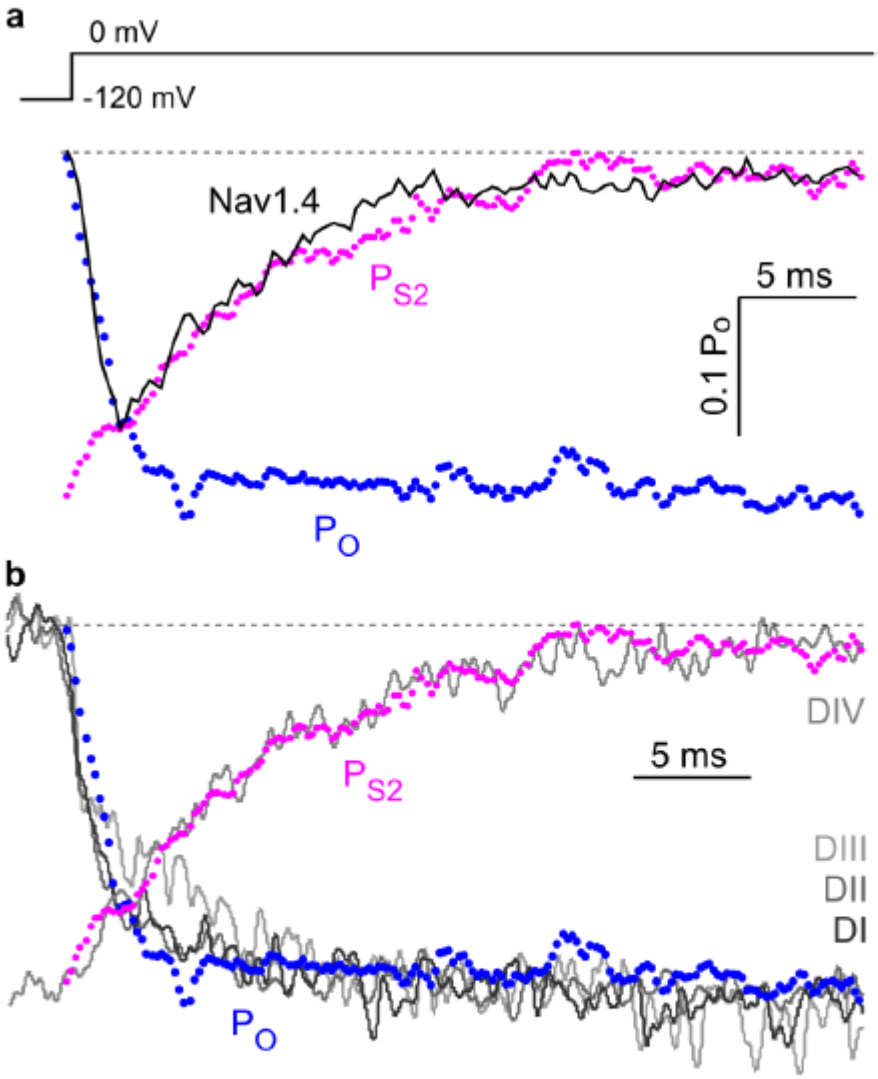

Figure 5

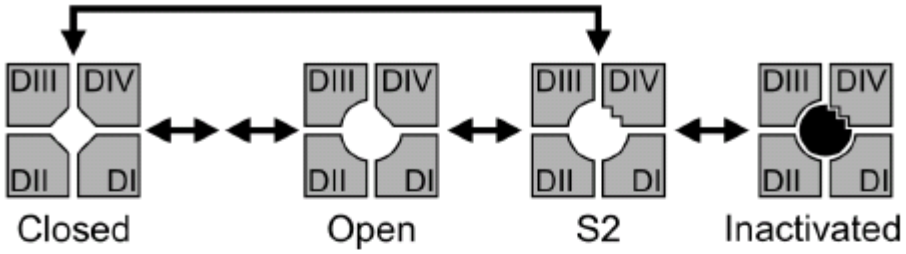

Supplementary Information for:

Pore opening is not concerted in a eukaryotic voltage-gated sodium channel.

In Nature

Marcel P. Goldschen-Ohm[1], Debbie Capes[1], Kevin Oelstrom[1], Baron Chanda[1]
[1]University of Wisconsin, Madison, WI, Dept. of Neuroscience

Fast inactivation of voltage gated sodium channels is critical for normal signaling between excitable cells. However, rapid accumulation of channels in non-conducting inactivated states typically occludes all but the first few events during channel activation as assayed by current through the pore. Thus, removing inactivation should reveal both the time course of the activation process as well as less frequent intrinsic gating properties of the pore. Therefore, we explored the single channel behavior of the fast inactivation deficient skeletal muscle sodium channel mutant Nav1.4-WCW [1].

Subconductances have been observed in single sodium channel records from neuroblastoma cells, rat cardiomyocytes and dissociated mouse muscle cells after treatment with compounds that disrupt inactivation such as chloramine-T, sea anemone toxin ATX-II or DPI 201-106 [2,3,4,5,6]. Infrequent subconductances have also been observed in these preparations without drug treatment, suggesting that subconductances are an intrinsic aspect of native sodium channel gating that is revealed upon removal of inactivation [7,8,4,5]. Removing inactivation in Shaker potassium channels also reveals two subconductances [9,10]. However, in contrast to the very brief activation coupled subconductances reflecting intermediates between closed and fully open states in Shaker [11], the subconductances reported here for Nav1.4-WCW are both long lived and preferentially visited following channel opening to the fully open level.

The WCW mutations severely impair fast inactivation. Responses to depolarizing voltage steps were recorded from wild type rat Nav1.4 and rat Nav1.4-L435W/L437C/A438W (WCW) channels expressed in HEK-293 cells. Nav1.4-WCW expressed robustly, having capacitance normalized whole cell currents that were 3-fold larger than for Nav1.4 (two tailed unpaired t-Test, $P < 0.001$, $n = 8$ and 5). Nav1.4 currents inactivated nearly completely within 5-10 ms, whereas Nav1.4-WCW failed to show appreciable inactivation over the 20 ms test pulse (Supplementary Fig. 1a, c). Nav1.4-WCW right-shifted the conductance-voltage (G-V) relation as compared to Nav1.4 by 8 mV (Supplementary Fig. 1b). The voltage at which the conductance was half maximal ($V_{1/2}$) and the effective charge (z) from single Boltzmann fits to the G-V from individual cells were, for Nav1.4 (mean ± s.e.m.): $V_{1/2} = -32.6 \pm 1.9$ mV, $z = 3.8 \pm 0.4$ e^-, $n = 5$; and for Nav1.4-WCW: $V_{1/2} = -24.9 \pm 0.8$ mV, $z = 4.7 \pm 0.2$ e^-, $n = 8$. This shift was not due to a change in reversal potential (Nav1.4: $V_{rev} = 59.4 \pm 3.9$ mV; Nav1.4-WCW: $V_{rev} = 56.2 \pm 3.0$ mV), which suggests that the mutations do not affect the relative permeabilities of Na^+ versus K^+. These results are consistent with previous reports regarding whole cell voltage dependent currents from the rat Nav1.4-WCW construct [1].

As channels progress from closed to open to inactivated states, a right shift in the G-V with no change in the rate constants of activation (main text Fig. 2) suggests that Nav1.4-WCW speeds at least one backward rate along the deactivation pathway from open to closed states. This is consistent with the idea that one of the deactivation steps involves pushing the inactivation particle out of its docking site, the energetic cost of which is absent for Nav1.4-WCW [12]. In other words, removal of energetic stabilization of the open state by binding of the inactivation particle may account for the rightward shift in the conductance voltage curves. Consistent with such an idea, the QQQ mutations right shift the G-V by 5 mV [13], and another mutation in the putative docking site for the inactivation particle, N1662A, also gives rise to late channel activation and right shifts the G-V by 10 mV [14]. We note, however, that interpretation of this shift in the G-V is somewhat complicated due to the fact that whereas the peak conductance for Nav1.4-WCW is a steady state measure (ignoring slow inactivation), the peak response for Nav1.4 is not at equilibrium.

Nav1.4-WCW channels do not inactivate from closed states. Although the WCW mutations severely impair fast inactivation, slow inactivation persists in this channel [1], which becomes apparent during longer 1 s depolarizing voltage steps. The fraction of available (i.e. non-slow inactivated) channels at the end of a 1 s voltage step between -80 and 0 mV was assayed with a 20 ms test pulse to -20 mV (Supplementary Fig. 1f). Notably, the onset of slow inactivation coincided almost exactly with the onset of channel activation during the 1 s preconditioning pulse (Supplementary Fig. 1g). These data are consistent with previous results from Wang and colleagues [1,15], and show that Nav1.4-WCW channels do not inactivate at potentials too hyperpolarized to elicit channel activation. In contrast, sodium channels have been shown to be able to inactivate from closed states prior to channel opening [16]. The coincidental removal of both fast inactivation following channel opening and inactivation from closed states prior to channel opening by the WCW mutations suggests that the same fundamental mechanism may underlie these two processes.

Nav1.4-WCW single channel deactivation. Deactivation of single Nav1.4-WCW channels was assayed upon repolarization following a 40 ms activating voltage step to 50 mV. Both subconductances observed during channel activation were also apparent during deactivation (Supplementary Fig. 4a). The rate of decay of the probability in each conductance level increased with increasing hyperpolarization from -80 to -100 mV, as expected if part of the deactivation process involves the return of the voltage sensing charges to their resting conformations (Supplementary Fig. 4b). At both -80 and -100 mV, the probability of being fully open decayed rapidly as compared to the probability of being in a subconducting state. However, the single channel records clearly show that channels can close directly from any conductance level.

The S2 subconductance may reflect the filtering of a rapid flicker. Nav1.4-WCW channel activity associated with the S2 subconductance level often contained excess noise as compared to activity at the other apparent conductance levels. This excess noise could reflect the presence of multiple closely spaced conductance states or result from the filtering of a rapid flicker between the fully open and either closed or S1 conductance. The amplitude distributions resulting from the filtering of a rapid flicker between two states should take the form of a beta distribution, the shape of which will depend on the transition rates between the states [17]. Thus, to examine this possibility, we fit amplitude histograms from sojourns to the S2 level with beta distributions to estimate the rate of flicker. Beta distribution fits were nearly indistinguishable from Gaussian fits, with the former slightly overestimating the low end of the amplitude distribution, and the latter slightly underestimating the high end (Supplementary Fig. 5a). Thus, we cannot conclusively determine from these data whether or not S2 results from a rapid flicker. If S2 does represent a rapid flicker between open and either closed or S1 subconducting states, then the rate of flicker as estimated from fitting the amplitude histograms with beta distributions show very little voltage dependence (Supplementary Fig. 5b).

Voltage dependence of apparent dwell times in individual conductance levels. Nav1.4-WCW dwell time distributions for each conductance level were fit with sums of exponentials by maximizing their log likelihood [18] (Supplementary Fig. 7a, Supplementary Table 1). Closed time distributions indicate the presence of at least three closed states, whereas dwell times in the fully open level were well described by a single open state. Both subconductances were fit with two exponential components. However, the fast component was not well resolved, and is likely contaminated by rapid events such as C → O → C with a very short duration in O, which due to filtering appears to be a brief sojourn to S1 or S2. Thus, we took the longer time constant as representative for the dwells in S1 and S2. Bursting activity was defined as groups of openings separated by closures shorter than 5 ms. Burst length distributions exhibited at least two components consistent with the observation of two apparent long lived closed states. The bursting behavior of Nav1.4-WCW channels indicates that the open channel can transiently visit an unstable closed state similar to that observed upon removal of inactivation in Shaker potassium channels [9].

After first opening, most of the voltage dependence during Nav1.4-WCW channel activation could be attributed to the long closures between openings which decreased in frequency and duration with increasing depolarization. Given the similar steep voltage dependence for the first latencies, it is possible that these long closures reflect a return to voltage dependent closed states along the activation pathway. Although burst lengths were also very voltage dependent, this largely reflects the voltage dependence of the longer closures that separated bursts. Dwell times in S1 were not very voltage dependent, whereas openings to S2 and O increased slightly in duration with increasing depolarization. Nav1.4 open times were also well described by a

single exponential component with very little voltage dependence. Although open times for Nav1.4 were similar in duration to dwells in O for Nav1.4-WCW, ignoring changes in conductance level, Nav1.4-WCW channel openings lasted on average 2-3 time longer than those in Nav1.4.

Thus, Nav1.4-WCW channel openings are comprised of visits to a fully open state O that is similar in duration to the open state in Nav1.4 channels as well as prolonged dwells in subconducting states that contribute to an overall longer and voltage dependent open dwell time as compared to Nav1.4, akin to observations in other inactivation deficient preparations [19,4,20,21], as well as during infrequent bursting activity of cortical neurons [22]. In addition, the channel exhibits bursting activity giving rise to prolonged periods of high open probability. The large voltage dependence of the long lived closures separating bursts is consistent with the idea that these closures reflect the transition of one or more voltage sensors between activated and resting conformations. The larger voltage dependence of the closed states as compared to the open states might be expected if pore closure requires the return of only a single voltage sensor, whereas opening requires multiple voltage sensors to be activated.

Supplementary Figure 1

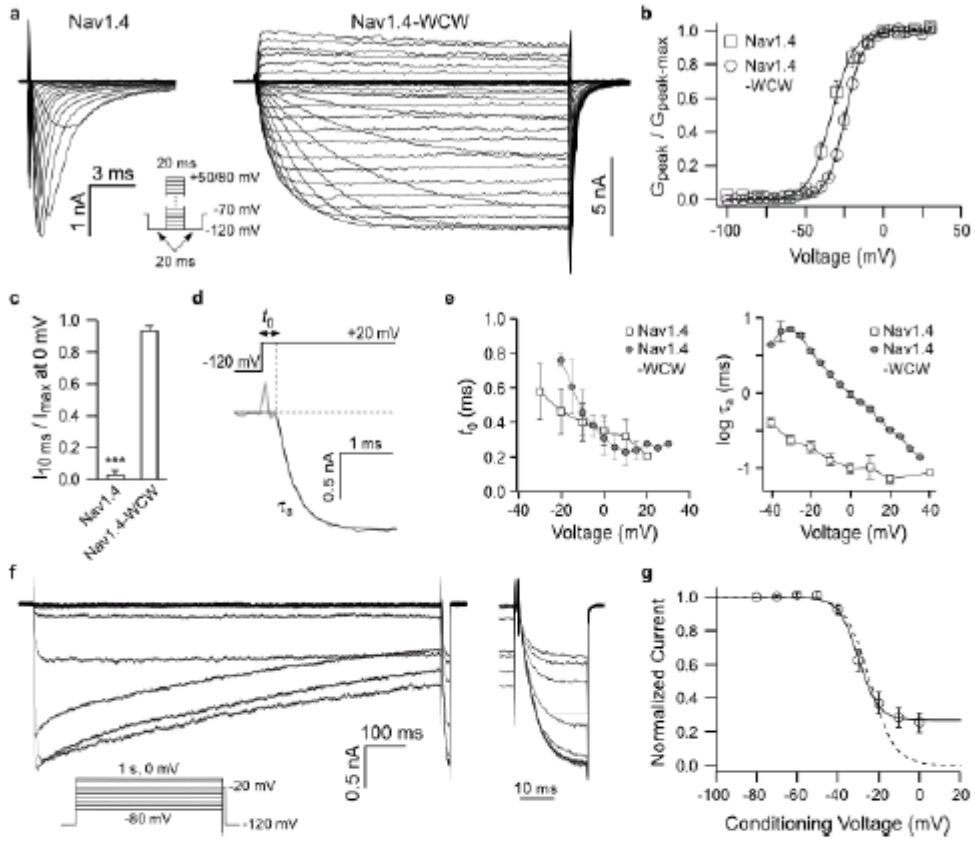

Supplementary Figure 1. Nav1.4-WCW severely disrupts fast inactivation and eliminates inactivation from closed states. (a) Whole cell current responses to 20 ms depolarizing voltage steps for rat Nav1.4 (left, only 10 ms shown) and rat Nav1.4-WCW (right) channels at room temperature. Cells were held at -70 mV and hyperpolarized to -120 mV for 20 ms prior to and following a 20 ms depolarizing pulse from -120 mV to +50 mV (Nav1.4) or +80 mV (Nav1.4-WCW) in 5-10 mV steps (see inset). (b) Normalized peak conductance-voltage relation from recordings such as those shown in *A* (mean ± s.e.m.). The $V_{1/2}$ and charge (*z*) for single Boltzmann fits to the mean were for Nav1.4: $V_{1/2}$ = -33.3 mV, *z* = 3.4 e^-, and for Nav1.4-WCW: $V_{1/2}$ = -24.4 mV, *z* = 4.2 e^-. (c) Summary of the fraction of the peak current remaining after 10 ms for Nav1.4 and Nav1.4-WCW. (d) The time course of current activation from the time at which the current was equal to half of the peak response up until the peak was fit to the equation I_{peak} (1 - exp(-(*t* - t_0) / τ_a)), where I_{peak} is the peak current, *t* is time, t_0 is the time of current onset which was allowed to lag the onset of the voltage step, and τ_a is the time constant of current activation. Example trace is for Nav1.4-WCW. (e) Voltage dependence of activation from fits as described in *d* (mean ± s.e.m.). Although t_0 is contaminated by the time required to charge the cell membrane, the similar delay for both constructs suggests that any differences in the time to current onset between Nav1.4 and Nav1.4-WCW must be less than t_0. (f) Nav1.4-WCW whole cell current responses to a steady-state inactivation protocol consisting of a 20 ms test pulse to -20 mV after a 1 s preconditioning pulse from -80 to 0 mV at room temperature. Holding potential was -120 mV and a 1 ms hyperpolarizing pulse to -140 mV preceded each test pulse. Responses to the test pulse are shown on an expanded time scale to the right. (g) The normalized peak current response during the test pulse is plotted against the voltage during the preconditioning pulse for five cells (open circles, mean ± s.e.m., n = 5). The conductance-voltage relation for

Nav1.4-WCW from *b* is shown inverted for comparison (dashed line). The peak response versus preconditioning voltage relation was fit with a single Boltzmann plus an added constant ($V_{1/2}$ = -29.9 mV, z = 4.9 e^-, constant = 0.27).

Supplementary Figure 2

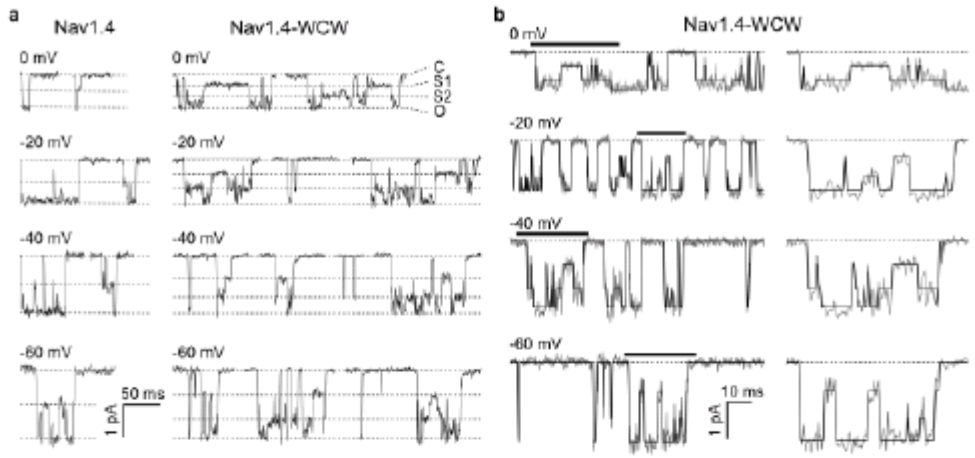

Supplementary Figure 2. Subconductances in Nav1.4 and Nav1.4-WCW channels. (a) Examples of subconductance events for Nav1.4 (left) and Nav1.4-WCW (right) channels during activation from -60 to 0 mV (dashed lines indicate observed conductance levels including the closed channel baseline, openings are downward). Responses were filtered at 1 kHz for display. (b) Example idealizations (solid black) of single Nav1.4-WCW channel activation records (gray, filtered at 2 kHz) including two subconductance levels obtained using the segmental k-means method in QUB [23] (see methods). The portion of each trace indicated by a black bar is shown on an expanded timescale to the right.

Supplementary Figure 3

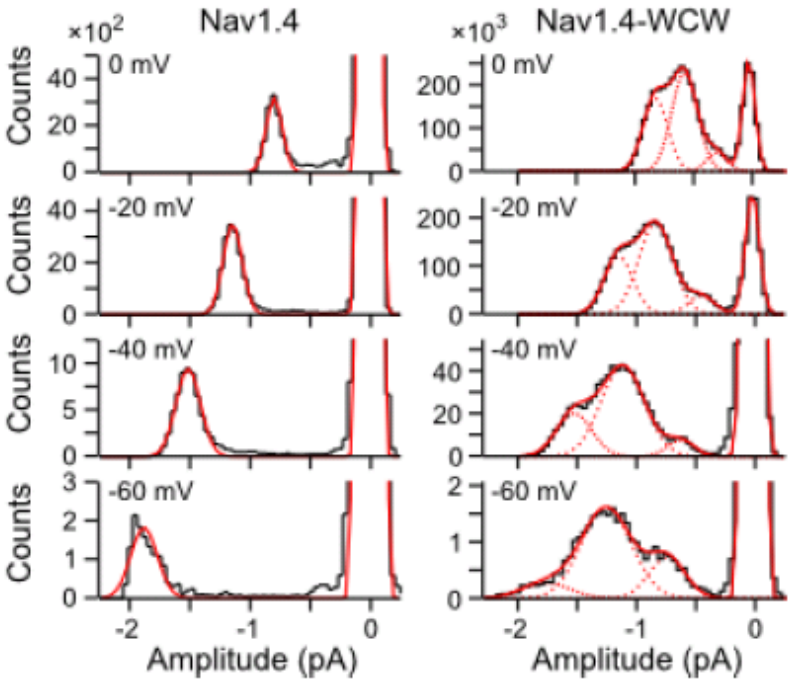

Supplementary Figure 3. Voltage dependence of individual conductance levels. Single channel amplitude distributions for Nav1.4 (left) and Nav1.4-WCW (right) channels. Histograms were obtained from all points in a single channel patch after discarding points adjacent to changes in amplitude in the idealized record to remove artifacts due to filtering. Red dashed lines are individual Gaussian fits to each conductance level, and the solid red line is their sum.

Supplementary Figure 4

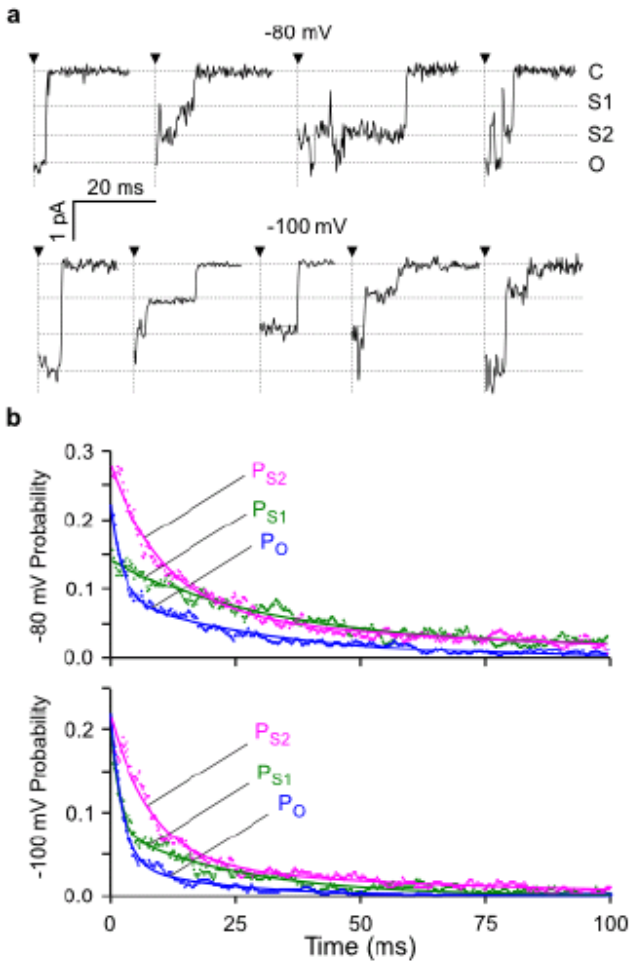

Supplementary Figure 4. Nav1.4-WCW single channel deactivation. (a) Deactivation of single Nav1.4-WCW channels at -80 and -100 mV following a 40 ms depolarizing pulse to 50 mV from a holding potential of -120 mV. Black arrows and vertical dashed lines indicate the onset of deactivation at the end of the activating pulse. Horizontal dashed lines illustrate the observed conductance levels. (b) The time dependent probability in each conductance level obtained from the idealized records (dots). Smooth lines are fits to the equation $\Sigma_i A_i \exp(-t/\tau_i)$, where A_i and τ_i are the amplitudes and time constants of an exponential decay (S1 at -80 mV: τ_1 = 32.4 ms, A_1 = 0.14; S2 at -80 mV: τ_1 = 10.7 ms, τ_2 = 89.5 ms, A_1 = 0.21, A_2 = 0.07; O at -80 mV: τ_1 = 2.4 ms, τ_2 = 34.0 ms, A_1 = 0.14, A_2 = 0.09; S1 at -100 mV: τ_1 = 1.7 ms, τ_2 = 25.4 ms, A_1 = 0.12, A_2 = 0.08; S2 at -100 mV: τ_1 = 8.3 ms, τ_2 = 66.2 ms, A_1 = 0.18, A_2 = 0.04; O at -100 mV: τ_1 = 2.4 ms, τ_2 = 22.5 ms, A_1 = 0.19, A_2 = 0.04).

Supplementary Figure 5

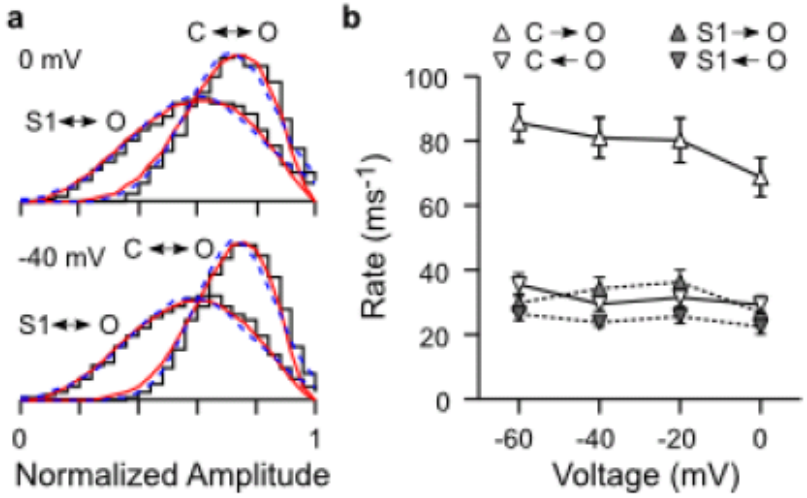

Supplementary Figure 5. Flicker analysis of a Nav1.4-WCW subconductance level. (a) Nav1.4-WCW amplitude histograms from channel activity during events at the S2 subconductance level after normalizing to the range [C = 0, O = 1] (C ↔ O) or [S1 = 0, O = 1] (S1 ↔ O). The first and last data points in each event were discarded to remove artifacts introduced by the filtering of the event onset and offset transitions. Histograms were fit with a beta distribution (solid red) or a Gaussian (dashed blue). (b) Mean ± s.e.m. across patches for the potential rate of flicker between either C and O or S1 and O estimated from beta distribution fits to the amplitude histograms as described by Yellen [17].

Supplementary Figure 6

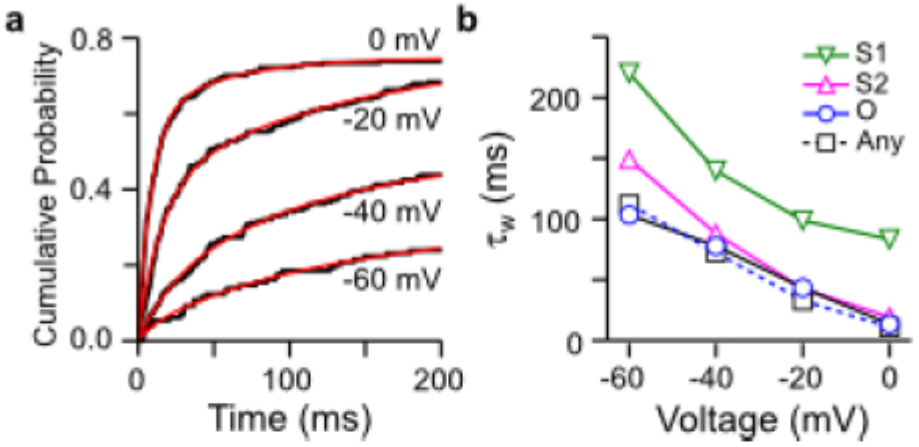

Supplementary Figure 6. Voltage dependence of latency to first opening for Nav1.4-WCW. (a) Cumulative probability that a Nav1.4-WCW channel has first opened to any conductance level during 200 ms depolarizing voltage steps from -60 to 0 mV (-120 mV holding potential). Smooth red lines are fits to the equation $\Sigma_{i=1,2} A_i [1 - exp(-t/\tau_i)]$, where A_i and τ_i are the amplitudes and time constants of a biexponential rise (0 mV: τ_1 = 8.6 ms, τ_2 = 49.6 ms, A_1 = 0.57, A_2 = 0.17; -20 mV: τ_1 = 15.4 ms, τ_2 = 140.4 ms, A_1 = 0.40, A_2 = 0.36; -40 mV: τ_1 = 23.8 ms, τ_2 = 118.9 ms, A_1 = 0.13, A_2 = 0.37; -60 mV: τ_1 = 12.8 ms, τ_2 = 129.1 ms, A_1 = 0.03, A_2 = 0.27). The reduction of the maximum from unity reflects the probability of observing a null sweep with no channel activity. (b) Summary of the weighted time constants from bi-exponential fits as shown in *a* for each individual conductance level.

Supplementary Figure 7

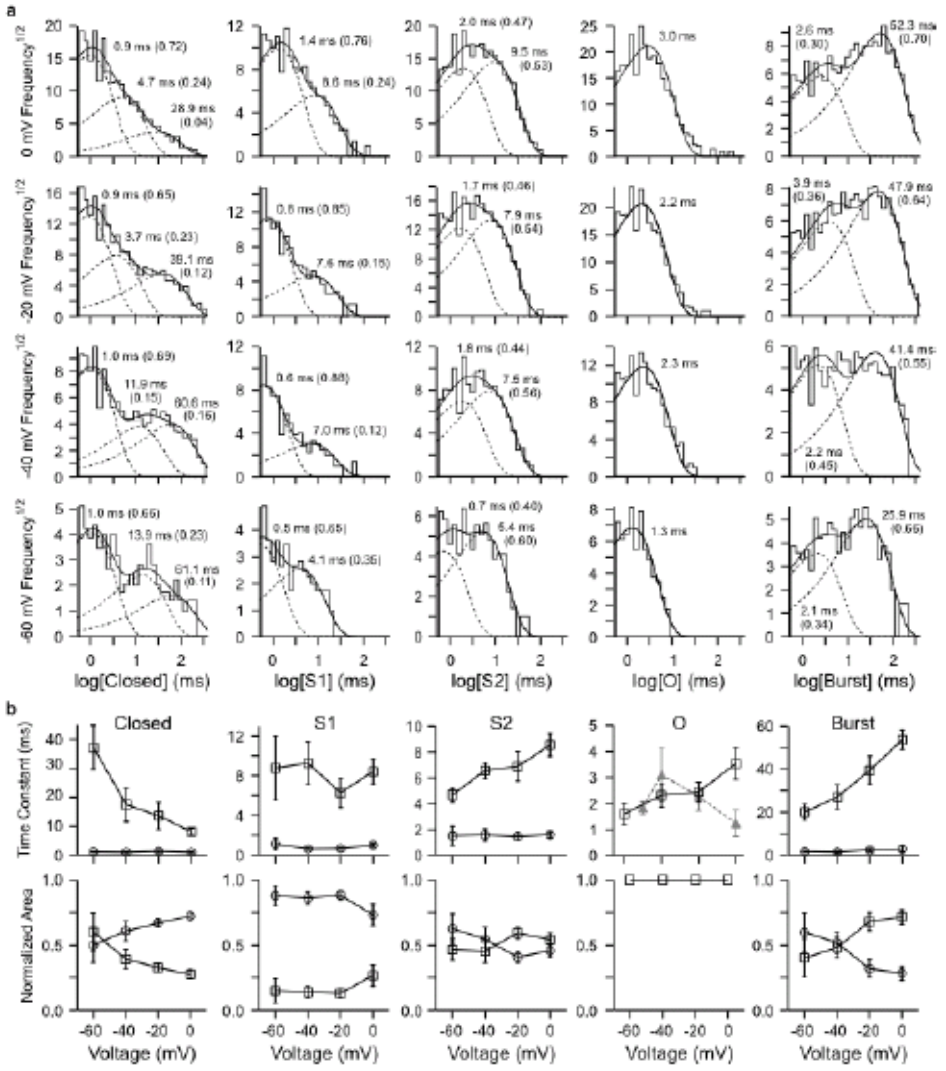

Supplementary Figure 7. Voltage dependence of apparent dwell times in individual conductance levels during Nav1.4-WCW activation. (a) Dwell time distributions from idealized records for each conductance level excluding events shorter than 0.5 ms. Smooth curves are the maximum log likelihood fit [18] for 1-3 exponential components (dashed lines are individual components and the solid line is their sum). Time constants (and relative areas) for each component are shown. (b) Mean ± s.e.m. from maximal likelihood fits to dwell time distributions for individual patches as shown in *a*. The time constant (and relative area) of the fast (circles) and slow* (squares) components are shown. *For the closed times the slow component is the sum of the two longest closed times weighted by their individual areas (and the sum of their areas). Open times from single exponential maximum log likelihood fits to Nav1.4 are shown as gray triangles for comparison.

Supplementary Figure 8

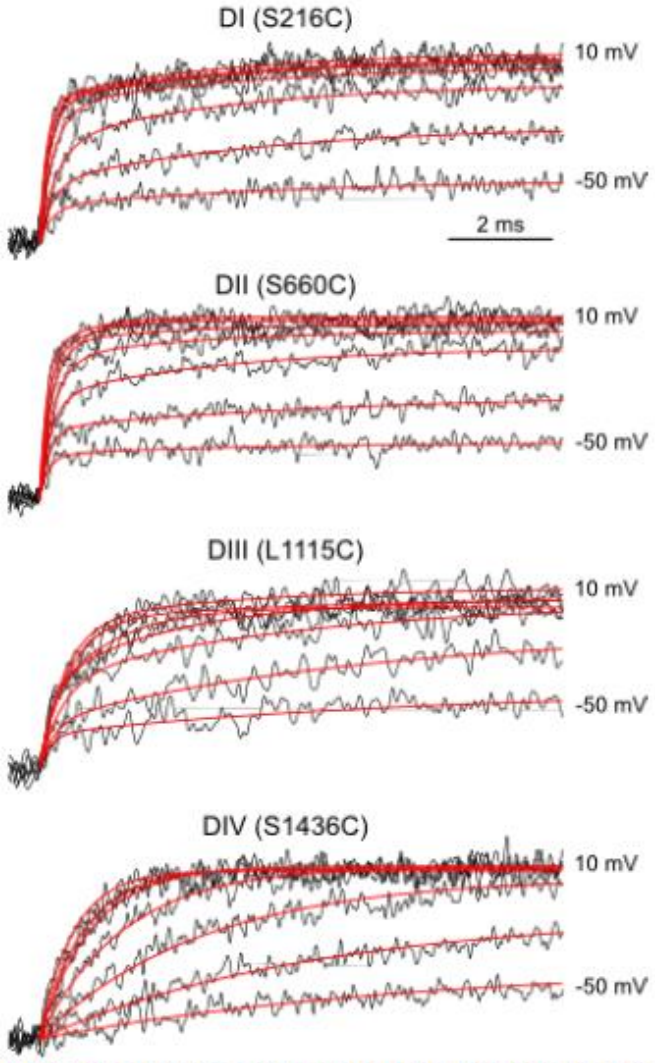

Supplemental Figure 8. Kinetics of fluorescent responses from fluorophores attached to introduced cysteines in each individual voltage sensor track entry into conductance levels O and S2. Fluorescent responses from site specific fluorophores in each voltage sensor [24] during voltage steps from -50 to 10 mV from a holding potential of -130 mV. Kinetics were determined from biexponential fits (red) to fluorescence signals (black), with the exception of domain IV, which was fit with a monoexponential.

Supplementary Figure 9

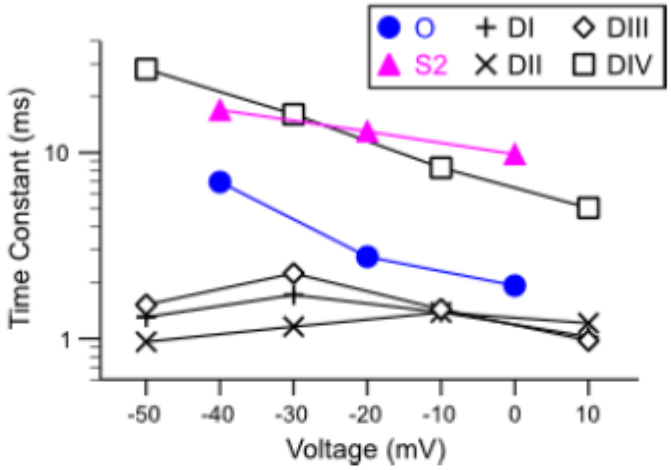

Supplementary Figure 9. Summary of the voltage dependence of the time constants for entry into the S2 and O conductance levels (main text Fig. 3), and the fast time constant from exponential fits to the fluorescence responses from individual voltage sensing domains (Supplementary Fig. 8), after scaling the fluorescence in time by a factor of 5 to account for the temperature difference between the fluorescence and single channel observations (see methods).

Supplementary Figure 10

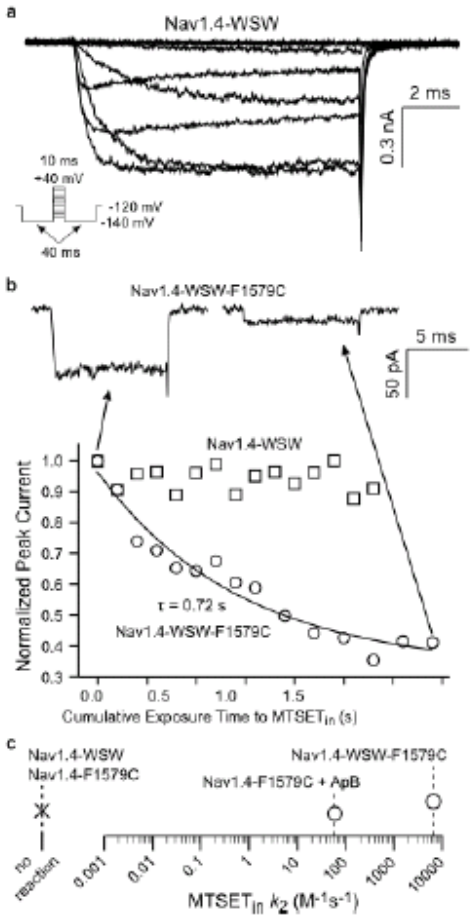

Supplementary Figure 10. The pore of Nav1.4-WSW is fully accessible to internal MTSET. (a) Current responses to 10 ms voltage steps from -120 to 40 mV (20 mV steps) from a holding potential of -140 mV (see inset) from Nav1.4-WSW channels in inside-out patches excised from Xenopus oocytes. (b) The time course of the reduction in peak current for Nav1.4-WSW and Nav1.4-WSW-F1579C with respect to the cumulative exposure time to internal MTSET at 0 mV. Protocol involved a 10 s period at a holding potential of -120 mV, followed by a 100 ms pulse to 0 mV to allow MTSET modification in the open state, another 10 s at -120 mV, and a 10 ms test pulse to 0 mV from which the peak response was obtained. This cycle was repeated as necessary to obtain the reaction rate. Inside-out patches were bathed in 250 μM MTSET during the entire experiment. Current responses for Nav1.4-WSW-F1579C prior to and after 1.7 s of exposure to internal MTSET at 0 mV are shown. (c) Second order reaction rate of internal MTSET with F1579C in Nav1.4-WSW is plotted along with the reported reaction rate for F1579C in Nav1.4 before and after disruption of fast inactivation with anthropleurin B (ApB) for comparison [25].

Supplementary Table 1. Time constants τ_i (and normalized areas A_i) from maximum log likelihood exponential fits to dwell time distributions [18] in individual conductance levels during Nav1.4-WCW activation (mean ± SEM; 9 patches).

	Voltage (mV)	τ_1 (ms)	τ_2 (ms)	A_1
Closed*	0	1.0 ± 0.1	8.1 ± 1.2	0.72 ± 0.03
	-20	1.3 ± 0.4	13.6 ± 4.6	0.67 ± 0.03
	-40	1.0 ± 0.1	17.5 ± 5.9	0.61 ± 0.07
	-60	1.1 ± 0.1	37.2 ± 7.7	0.50 ± 0.13
Burst	0	3.0 ± 1.5	53.6 ± 4.5	0.28 ± 0.06
	-20	2.5 ± 0.7	39.3 ± 6.7	0.32 ± 0.07
	-40	1.5 ± 0.4	27.1 ± 5.6	0.52 ± 0.08
	-60	1.7 ± 0.3	20.0 ± 3.7	0.60 ± 0.15
S1	0	1.0 ± 0.2	8.4 ± 1.3	0.73 ± 0.08
	-20	0.7 ± 0.1	6.3 ± 1.5	0.88 ± 0.03
	-40	0.7 ± 0.1	9.3 ± 2.2	0.86 ± 0.05
	-60	1.1 ± 0.6	8.8 ± 3.2	0.88 ± 0.08
S2	0	1.6 ± 0.2	8.5 ± 0.9	0.46 ± 0.05
	-20	1.4 ± 0.3	6.9 ± 1.1	0.41 ± 0.04
	-40	1.6 ± 0.5	6.5 ± 0.6	0.55 ± 0.09
	-60	1.5 ± 0.7	4.7 ± 0.6	0.63 ± 0.11
Open	0	3.5 ± 0.6	n/a	1.0
	-20	2.4 ± 0.4	n/a	1.0
	-40	2.3 ± 0.5	n/a	1.0
	-60	1.6 ± 0.4	n/a	1.0
Open (Nav1.4)	0	1.2 ± 0.5	n/a	1.0
	-20	2.3 ± 0.5	n/a	1.0
	-40	3.1 ± 1.0	n/a	1.0
	-50	1.8 ± 0.2	n/a	1.0

* The closed channel slow time constants (τ_2) are the weighted average of the two slowest components from a three component fit to the closed dwell time distributions.

Supplementary Table 2. Fast time constants τ_1 (and amplitudes A_1) from mono- or bi-exponential fits to the kinetics of the time dependent probability in each individual conductance level (P_x was fit with the equation $\Sigma_i A_i [1 - exp(-t/\tau_i)]$) and the conditional probability after first opening (CP_x was fit with the equation $\Sigma_i A_i exp(-t/\tau_i) + C$) (see main text Fig. 3).

	Voltage (mV)	A_1	τ_1 (ms)	C
P_O	0	0.26	1.9	n/a
	-20	0.17	2.7	n/a
	-40	0.07	6.7	n/a
	-60	0.05	27.5	n/a
P_{S2}	0	0.32	9.4	n/a
	-20	0.25	12.4	n/a
	-40	0.09	16.1	n/a
	-60	0.07	53.8	n/a
P_{S1}	0	0.08	11.2	n/a
	-20	0.07	8.9	n/a
	-40	0.03	15.5	n/a
	-60	0.02	41.5	n/a
CP_O	0	0.22	3.3	0.19
	-20	0.25	3.8	0.18
	-40	0.19	2.2	0.1
	-60	0.16	4.7	0.08
CP_{S2}	0	0.17	5.0	0.33
	-20	0.1	3.2	0.28
	-40	0.03	2.0	0.18
	-60	0.04	10.7	0.1
CP_{S1}	0	0.02	35.5	0.08
	-20	n/a*	n/a*	0.07
	-40	0.01	11.4	0.05
	-50	0.03	16.1	0.03

* Could not be distinguished from a horizontal line.

Supplementary References

1. Wang, S. Y., Bonner, K., Russell, C. & Wang, G. K., Tryptophan scanning of D1S6 and D4S6 C-termini in voltage-gated sodium channels. *Biophys. J.* **85**, 911-920 (2003).

2. Chinn, K. & Narahashi, T., Temperature-dependent subconducting states and kinetics of deltamethrin-modified sodium channels of neuroblastoma cells. *Pflugers Arch.* **413**, 571-579 (1989).

3. Nagy, K., Subconductance states of single sodium channels modified by chloramine-T and sea anemone toxin in neuroblastoma cells. *Eur. Biophys. J.* **15**, 129-132 (1987).

4. Kohlhardt, M., Fröbe, U. & Herzig, J. W., Properties of normal and non-inactivating single cardiac Na+ channels. *Proc. R. Soc. Lond. B Biol. Sci.* **232**, 71-93 (1987).

5. Patlak, J. B., Sodium channel subconductance levels measured with a new variance-mean analysis. *J. Gen. Physiol.* **92**, 413-430 (1988).

6. Chinn, K. & Narahashi, T., Stabilization of sodium channel states by deltamethrin in mouse neuroblastoma cells. *J. Physiol.* **380**, 191-207 (1986).

7. Cachelin, A. B., De Peyer, J. E., Kokubun, S. & Reuter, H., Sodium channels in cultured cardiac cells. *J. Physiol.* **340**, 389-401 (1983).

8. Nagy, K., Kiss, T. & Hof, D., Single Na channels in mouse neuroblastoma cell membrane. Indications for two open states. *Pflugers Arch.* **399**, 302-308 (1983).

9. Hoshi, T., Zagotta, W. N. & Aldrich, R. W., Shaker potassium channel gating. I: Transitions near the open state. *J. Gen. Physiol.* **103**, 249-278 (1994).

10. Schoppa, N. E. & Sigworth, F. J., Activation of Shaker potassium channels. II. Kinetics of the V2 mutant channel. *J. Gen. Physiol.* **111**, 295-311 (1998).

11. Zheng, J. & Sigworth, F. J., Selectivity changes during activation of mutant Shaker potassium channels. *J. Gen. Physiol.* **110**, 101-117 (1997).

12. Kuo, C. C. & Bean, B. P., Na+ channels must deactivate to recover from inactivation. *Neuron* **12**, 819-829 (1994).

13. West, J. W. *et al.*, A cluster of hydrophobic amino acid residues required for fast Na(+)-channel inactivation. *PNAS* **89**, 10910-10914 (1992).

14. McPhee, J. C., Ragsdale, D. S., Scheuer, T. & Catterall, W. A., A critical role for the S4-S5 intracellular loop in domain IV of the sodium channel alpha-subunit in fast inactivation. *J. Biol. Chem.* **273**, 1121-1129 (1998).

15. Wang, S. Y., Mitchell, J., Moczydlowski, E. & Wang, G. K., Block of inactivation-deficient Na+ channels by local anesthetics in stably transfected mammalian cells: evidence for drug binding along the activation pathway. *J. Gen. Physiol.* **124**, 691-701 (2004).

16. Horn, R., Patlak, J. & Stevens, C. F., Sodium channels need not open before they inactivate. *Nature* **291**, 426-427 (1981).

17. Yellen, G., Ionic permeation and blockade in Ca2+-activated K+ channels of bovine chromaffin cells. *J. Gen. Physiol.* **84**, 157-186 (1984).

18. Colquhoun, D. & Sigworth, F. J., in *Single-Channel Recording*, edited by Sakmann, B. & Neher, E. (Plenum Press, New York, 1995), pp. 589-633.

19. Horn, R., Vandenberg, C. A. & Lange, K., Statistical analysis of single sodium channels. Effects of N-bromoacetamide. *Biophys. J.* **45**, 323-335 (1984).

20. Lawrence, J. H. *et al.*, Single-channel analysis of inactivation-defective rat skeletal muscle sodium channels containing the F1304Q mutation. *Biophys. J.* **71**, 1285-1294 (1996).

21. Grant, A. O., Chandra, R., Keller, C., Carboni, M. & Starmer, C. F., Block of wild-type and inactivation-deficient cardiac sodium channels IFM/QQQ stably expressed in mammalian cells. *Biophys. J.* **79**, 3019-3035 (2000).

22. Magistretti, J. & Alonso, A., Fine gating properties of channels responsible for persistent sodium current generation in entorhinal cortex neurons. *J. Gen. Physiol.* **120**, 855-873 (2002).

23. Qin, F., Restoration of single-channel currents using the segmental k-means method based on hidden Markov modeling. *Biophys. J.* **86**, 1488-1501 (2004).

24. Chanda, B. & Bezanilla, F., Tracking voltage-dependent conformational changes in skeletal muscle sodium channel during activation. *J. Gen. Physiol.* **120**, 629-645 (2002).

25. Sunami, A. *et al.*, Accessibility of mid-segment domain IV S6 residues of the voltage gated Na+ channel to methanethiosulfonate reagents. *J. Physiol.* **561**, 403-413 (2004).